NISTIR 6230

Liquefaction Evaluation of Densified Sand at Approach to Pier 1 on Treasure Island, California, Using SASW Method

Building and Fire Research Laboratory
Gaithersburg, MD 20899

United States Department of Commerce
Technology Administration
National Institute of Standards and Technology

NISTIR 6230

Liquefaction Evaluation of Densified Sand at Approach to Pier 1 on Treasure Island, California, Using SASW Method

Ronald D. Andrus,[1] Kenneth H. Stokoe, II,[2] Riley M. Chung,[1] and James A. Bay[3]

[1]Building and Fire Research Laboratory
National Institute of Standards and Technology
Gaithersburg, MD 20899

[2]Department of Civil Engineering
The University of Texas at Austin
Austin, TX 78712

[3]Department of Civil and Environmental Engineering
Utah State University
Logan, UT 84322

October 1998
Building and Fire Research Laboratory
National Institute of Standards and Technology
Gaithersburg, MD 20899

U.S. Department of Commerce
William M. Daley, *Secretary*

Technology Administration
Gary R. Bachula, *Under Secretary for Technology*

National Institute of Standards and Technology
Raymond G. Kammer, *Director*

ABSTRACT

Areas of improved and unimproved soil near berthing Pier 1 at Treasure Island, California, were investigated by the Spectral-Analysis-of-Surface-Waves (SASW) test. The upper 12 m of sand fill beneath the approach to the pier had been densified by a vibrating probe technique in 1985. The area of improved soil, which is 23 m wide and 93 m long, performed well during the 1989 Loma Prieta earthquake (M_w = 7.0), while sinkholes, sand boils and cracks formed in the adjacent unimproved areas. SASW tests were conducted on a 240-m-long alignment that extended across the area of improved soil using a seismic vibrator as the principal source with receiver spacings from 7.6 m to 76 m. Average shear wave velocities determined for the densified and undensified sand fill below the water table were 192 m/s and 167 m/s, respectively. Two simplified analytical procedures based on shear wave velocity correctly predict no liquefaction for the densified sand, and marginal liquefaction for the undensified sand. Although less conservative, liquefaction assessment procedures based on the SPT and CPT provide similar predictions.

KEYWORDS: building technology; SASW test; seismic testing; shear wave velocity; soil improvement, soil liquefaction; surface waves

ACKNOWLEDGMENTS

The authors gratefully acknowledge the assistance of Richard Faris, Naval Facilities Engineering Command, San Bruno, Calif., for scheduling the SASW tests and supplying site information. Michael Bennett of the United States Geological Survey kindly provided photographs of the liquefaction features that occurred in the area during the 1989 Loma Prieta earthquake. Gerald Manning of Foundation Constructors, Inc. graciously provided information on the vibrating probe technique used to improved the soil near Pier 1.

The help of graduate research assistants from The University of Texas at Austin is also greatly appreciated. Brent Rosenblad assisted with field work, and Sung-Ho Joh assisted with initial data reduction.

Soheil Nazarian of The University of Texas at El Paso served as the outside reader for this report. His review comments are greatly appreciated.

Finally, the authors express their thanks to the staff of the Structures Division at the National Institute of Standards and Technology. Steve Johnson assisted with setting up of the workstation used to run the SASW data analysis programs at NIST. Shirley Taylor assisted with travel arrangements for field testing. Michael Riley and Nicholas Carino also reviewed this report, and provided many helpful suggestions.

TABLE OF CONTENTS

CHAPTER 1
INTRODUCTION 1
1.1 BACKGROUND 1
1.1.1 Treasure Island 2
1.2 PURPOSE 3
1.3 OVERVIEW OF REPORT 3

CHAPTER 2
SPECTRAL-ANALYSIS-OF-SURFACE-WAVES TEST 5
2.1 INTRODUCTION 5
2.2 FIELD TEST PROCEDURE 6
2.3 EXPERIMENTAL DISPERSION CURVE FORMATION 10
2.4 SHEAR WAVE VELOCITY PROFILE DETERMINATION 10
2.5 SASW PROCEDURE FOR THIS STUDY 13
2.6 LIMITATIONS 14

CHAPTER 3
INVESTIGATION AND LIQUEFACTION ANALYSIS AT THE APPROACH TO PIER SITE 17
3.1 INTRODUCTION 17
3.2 SUBSURFACE CONDITIONS 17
3.2.1 Vibrating Probe Technique 21
3.3 LIQUEFACTION EFFECTS 24
3.4 SASW TEST RESULTS 30
3.5 LIQUEFACTION ANALYSIS USING SIMPLIFIED PROCEDURES 39
3.5.1 Liquefaction Assessment Based on V_{S1} and CSR 39
3.5.2 Liquefaction Assessment Based on V_S and a_{max} 42
3.5.3 Liquefaction Assessment Based on $(N_1)_{60}$ and CSR 43
3.5.4 Liquefaction Assessment Based on q_{c1N} and CSR 45

CHAPTER 4
SUMMARY AND CONCLUSIONS 47
4.1 SUMMARY 47
4.2 RECOMMENDATIONS FOR FUTURE STUDY 47

APPENDIX A
SHEAR WAVE VELOCITY PROFILES BASED ON SASW TESTS AT APPROACH TO PIER SITE ON TREASURE ISLAND, CALIFORNIA 49

APPENDIX B
DISPERSION CURVES FOR SASW TESTS AT APPROACH TO PIER SITE ON TREASURE ISLAND, CALIFORNIA 57

REFERENCES 71

CHAPTER 1

INTRODUCTION

1.1 BACKGROUND

Liquefaction of loosely deposited granular soils is a major cause of damage in earthquakes. Delineation of weak soil layers and prediction of their liquefaction potential are key inputs in the engineering design of new and retrofitted structures. This information is also essential for reliable estimation of economic losses during future earthquakes. When projects extend for great distances, such as lifelines and large building complexes, cost-effective evaluations of extensive areas are required. Screening techniques based on geology, hydrology, and soil conditions show promise for identifying areas requiring more rigorous analyses. However, even these areas requiring further analyses can be quite large.

One promising technique for spatially evaluating the liquefaction susceptibility of granular soils is the Spectral-Analysis-of-Surface-Waves (SASW) test. This test is an *in situ* seismic method for determining small-strain shear wave velocity, V_S, profiles of soil deposits and pavements (Stokoe and Nazarian, 1985; Stokoe et al., 1988a; Gucunski and Woods, 1991; Stokoe et al., 1994). The SASW test does not require boreholes, and has the advantage of providing broad areal coverage. Testing can be performed at sites where minimal disturbance is required and when soils are difficult to sample. The use of V_S as an index of liquefaction potential is justified since both V_S and liquefaction are influenced by many of the same factors (e.g., void ratio, effective confining pressure, stress history, and geologic age). Thus, the SASW test is well suited for profiling large areas with the objective of developing two- and three-dimensional V_S images of the subsurface.

In March 1996, SASW tests were conducted across an area of densified sand at Treasure Island, California. The site, called the Approach to Pier site, is located on the south-eastern corner of the island, as shown in Fig. 1.1. The principal objective of the tests was to evaluate the ability of the SASW method to rapidly delineate stratigraphy and assess liquefaction resistance over a significant lateral extent. A partial summary of the test results, as well as liquefaction assessment, is published in a conference paper by Andrus et al. (1998). This report presents a complete discussion of the test procedures, analyses, and results.

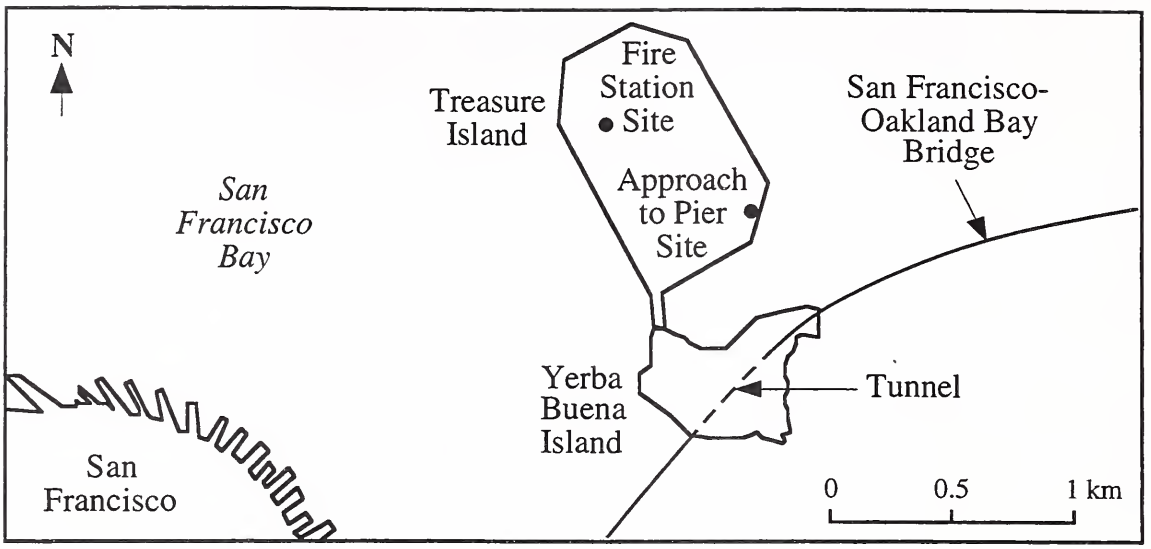

Fig. 1.1 - San Francisco Bay Showing Locations of the Approach to Pier and Fire Station Sites at Treasure Island.

1.1.1 Treasure Island

Treasure Island is a man-made island constructed in 1936-37. It was formed by hydraulic filling behind a perimeter rock dike. The perimeter dike served to contain the hydraulic fill, and was raised in sections over the previously placed fill. Currently, the island is owned by the U.S. Navy. Plans to transfer ownership of the island to the City of San Francisco are underway.

Treasure Island was classified as a level I national geotechnical experimentation site at a workshop sponsored by the National Science Foundation and Federal Highway Administration (Benoît and de Alba, 1991). Level 1 sites are those sites that have significant national importance, long-term accessibility, and good documentation. Only three sites were classified as level I sites at the workshop. (The other two sites are located at Texas A&M University.) The purpose of national geotechnical experimentation sites is to provide the geotechnical engineering community a system of well-documented sites for research and development.

Much of the work to date at Treasure Island centers around a full-scale ground response experiment (de Alba et al., 1994; de Alba and Faris, 1996a). Six accelerometers and eight piezometers are operating at various elevations near the fire station (see Fig. 1.1). Inclinometer casings are in place at the fire station and at two locations along the perimeter of the island, including the Approach to Pier site.

1.2 PURPOSE

Standard procedures for conducting the SASW test have not been developed. The purposes of this report is to outline a procedure for conducting the SASW test to delineate weak soil layers and assess liquefaction susceptibility at sites that extend for great distances. It is hoped that this document will aid the engineer in planning and conducting field liquefaction investigations using the SASW test, as well as contribute to the development of standard test procedures.

1.3 OVERVIEW OF REPORT

Following this introduction, in Chapter 2, the SASW field testing procedure and data analysis are reviewed, and methods used in this study are described. The field investigations and liquefaction analysis at the Approach to Pier site are discussed in Chapter 3. Chapter 4 provides a summary of conclusions as well as remarks about additional needed research.

CHAPTER 2

SPECTRAL-ANALYSIS-OF-SURFACE-WAVE TEST

2.1 INTRODUCTION

The Spectral-Analysis-of-Surface-Waves (SASW) test is an *in situ* seismic method for determining shear wave velocity profiles of soil deposits and pavements (Stokoe and Nazarian, 1985; Stokoe et al., 1988; Gucunski and Woods, 1991; Stokoe et al., 1994). The SASW test is based on the principle that high-frequency (short-wavelength) surface waves propagate only in the near-surface layers, and low-frequency (long-wavelength) surface waves propagate through the near-surface layers and deeper layers, as illustrated in Fig. 2.1. Thus, if stiffness varies with depth, surface waves of different frequencies will propagate at different velocities.

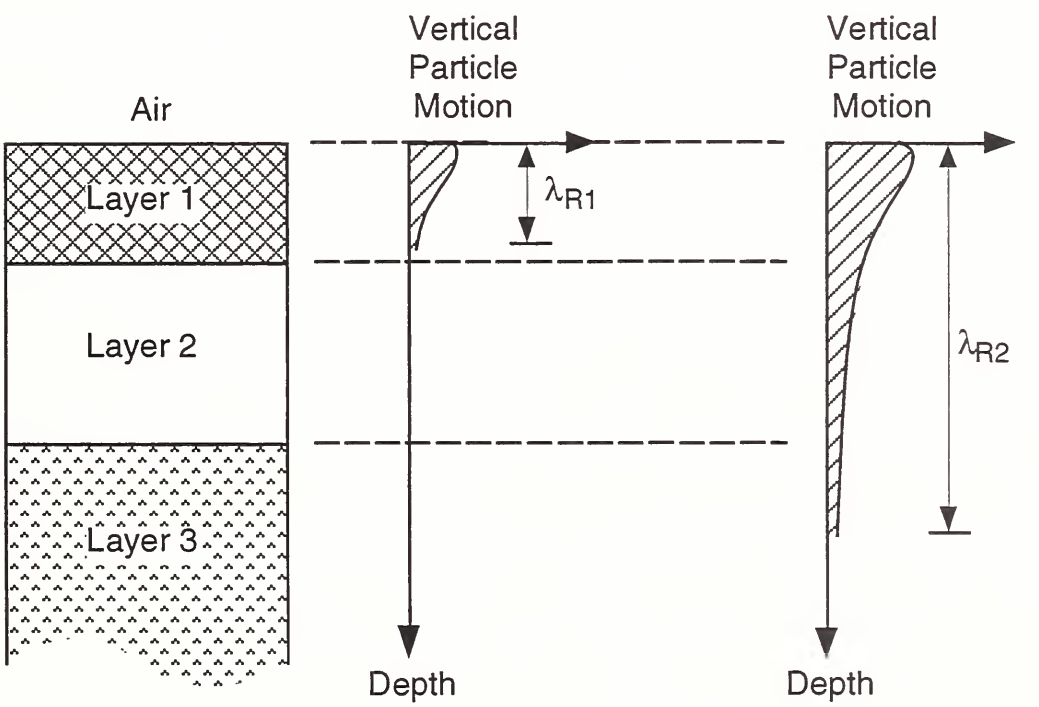

Fig. 2.1 - Approximate Distribution of Vertical Particle Motion with Depth for Two Surface Waves of Different Wavelengths (after Rix and Stokoe, 1989).

Surface waves have been used to study soils and pavements since the late 1940s. As reviewed in Roësset et al. (1991), the early studies generally consisted of steady-state harmonic vertical excitation using heavy shakers, progressive movement of receivers to determine the resulting surface wave wavelength, and analysis by simple empirical rules. This method is known as the steady-state Rayleigh wave technique. It did not gain wide acceptance because field equipment was bulky, test procedures were cumbersome, and only simple sites could be correctly determined because of the empirically-based analysis. During the last two decades, the method has been greatly improved with the development of personal computers, digital signal analyzers, simplified test procedures to obtain velocity measurements at several wavelengths with one receiver setup, large mobile shakers, and accurate computer models which provide extensive analysis procedures. These new techniques are collectively known as the SASW test.

The SASW test consists of three phases: (1) field testing, (2) data reduction and formation of the experimental surface wave dispersion curve (known as the "signature" of the site), and (3) inversion of the experimental dispersion curve to obtain the shear wave velocity profile.

2.2 FIELD TEST PROCEDURE

The basic configuration of source, receivers, and recording equipment in the SASW test is shown in Fig. 2.2. Two vertical receivers are placed on the ground surface a distance D apart. Surface waves are generated by a source, in line with the two receivers, at a distance D away from the near receiver. The source can be some type of vertical impact, a frequency sweep, or a random vibration. A FFT signal analyzer, or other appropriate device, is used to record the two receiver signals, and then transform them into the frequency domain. From the two frequency-domain records, the coherence and the phase of the cross-power spectrum are computed. These four records are saved on a floppy diskette or a hard-drive for later analysis.

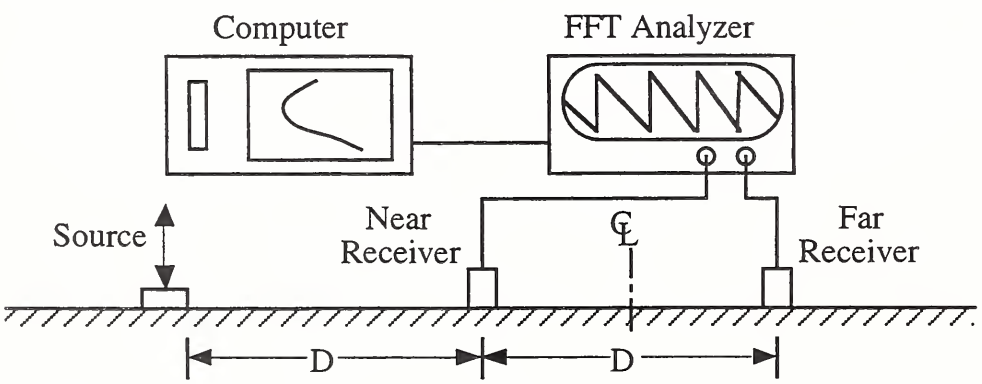

Fig. 2.2 - General SASW Field Testing Configuration.

A typical set of SASW records from testing performed in this study using a seismic vibrator is presented in Fig. 2.3. The phase of the cross-power spectrum (Fig. 2.3a) represents the phase difference between signals measured at the receivers as a function of frequency. It is from the phase of the cross-power spectrum that travel times are calculated for each frequency, as explained in Section 2.3. The coherence function (Fig. 2.3b), ranging between 0 and 1 for two or more averages, gives a general indication of the quality of the two signals. A coherence value near one indicates a very high signal-to-noise ratio, and good quality data. On the other hand, a coherence value near zero indicates a low signal-to-noise ratio, and likely poor quality data. The auto-power spectra (Figs. 2.3c and 2.3d) represent the distribution of relative energy at each frequency, and are a function of the source and ground characteristics. A constant auto-power spectrum (Fig. 2.3c between frequencies of about 5 Hz and 40 Hz) indicates constant relative energy. Variations between auto-power spectra for Receivers 1 and 2 (Figs. 2.3c and 2.3d) are a result of ground characteristics.

According to Richart et al. (1970), about two-thirds of the energy generated by a vertical source on a uniform half-space is transformed into surface waves, while the other third is transformed into body waves (compression and shear waves). In addition, body waves at the surface have lower amplitudes than body waves in the half-space. Body waves also exhibit geometrical attenuation in a uniform half-space at a rate of d^{-2} (where d is distance away from source), whereas surface waves geometrically decay at a much slower rate of $d^{-0.5}$ in the half-space. For the wavelengths of interest, which are short relative to the long travel distances, it is reasonable to assume that the body wave energy is generally insignificant compared to the surface wave energy. Thus, the records shown in Fig. 2.3 can be considered to be mainly measures of the surface or Rayleigh wave energy.

Various source-receiver setups and instrumentation requirements for SASW testing are reviewed in Gucunski and Woods (1991). The preferred source-receiver setup is illustrated in Fig. 2.4a. In this setup, called the *common receivers midpoint geometry*, receivers are placed equal distance (D/2) from a fixed centerline. Testing is performed with the source on both sides of the receiver array to compensate for effects of dipping layers and any phase shifts due to receivers and instrumentation (Nazarian et al., 1983). Testing is repeated at different values of D to obtained data over the desired range of wavelengths. Unfortunately, the common receivers midpoint geometry is not practical for automation and testing of large areas.

A source-receiver setup more appropriate for automation is illustrated in Fig. 2.4b. In this setup, called the *common source geometry*, the source location is fixed and the receiver centerline location is varied. Testing is performed with the source on only one side of the receiver array. Hiltunen and Woods (1990) obtained nearly identical results from tests on pavements using the two geometries. Nazarian et al. (1995) developed a trailer-mounted array of receivers and source in the common source geometry for testing pavements. In their trailer-mounted system, the receivers are mechanically lowered onto the pavement surface, and then raised before moving to the next test location. Moving source-receiver systems for generating continuous shear wave velocity profiles, rather than profile at discrete locations, are currently under development at The University of Texas at Austin.

a. Phase of the Cross Power Spectrum

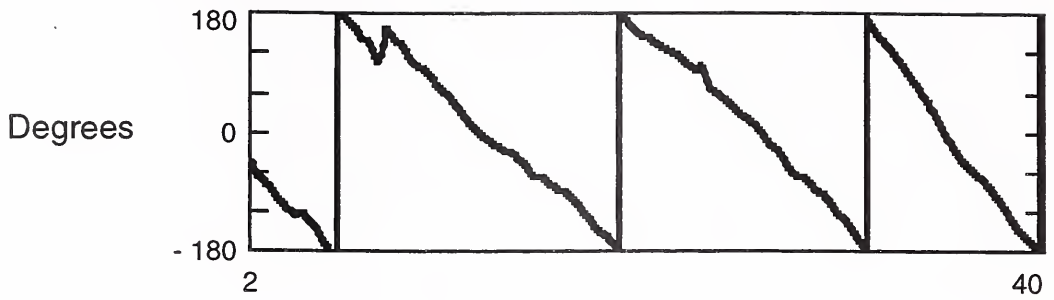

b. Coherence Function

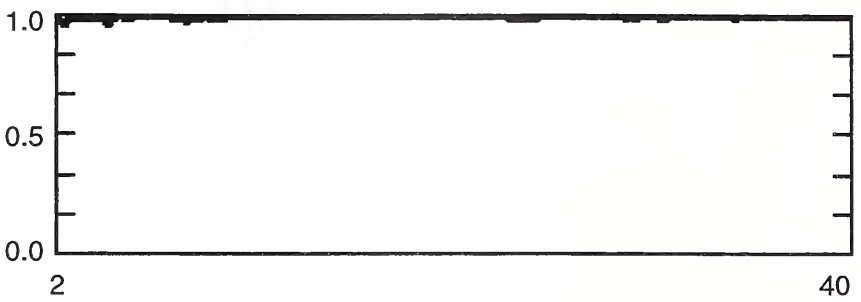

c. Receiver 1 Auto Power Spectrum

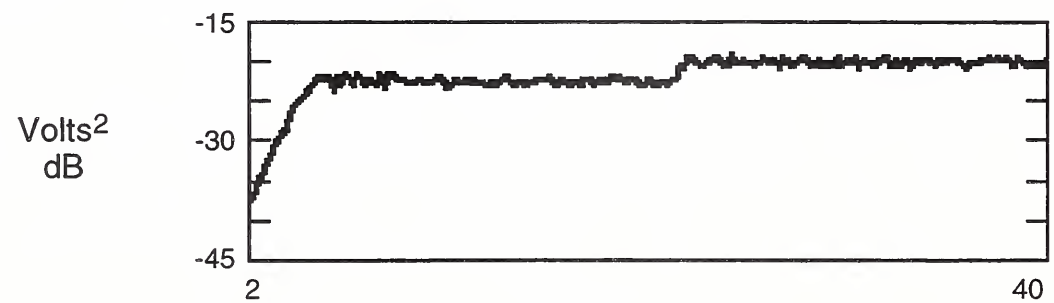

d. Receiver 2 Auto Power Spectrum

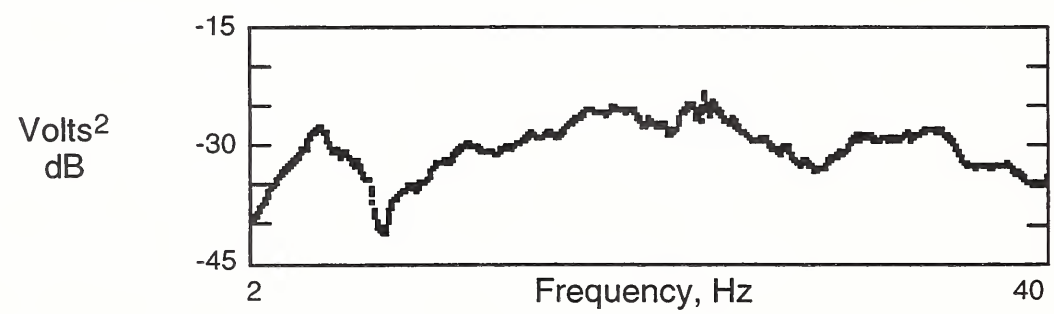

Fig. 2.3 - Typical Record Set Obtained During SASW Testing Using a Seismic Vibrator as the Source at the Approach to Pier Site; Array SA-6, Receiver Spacing = 15.2 m.

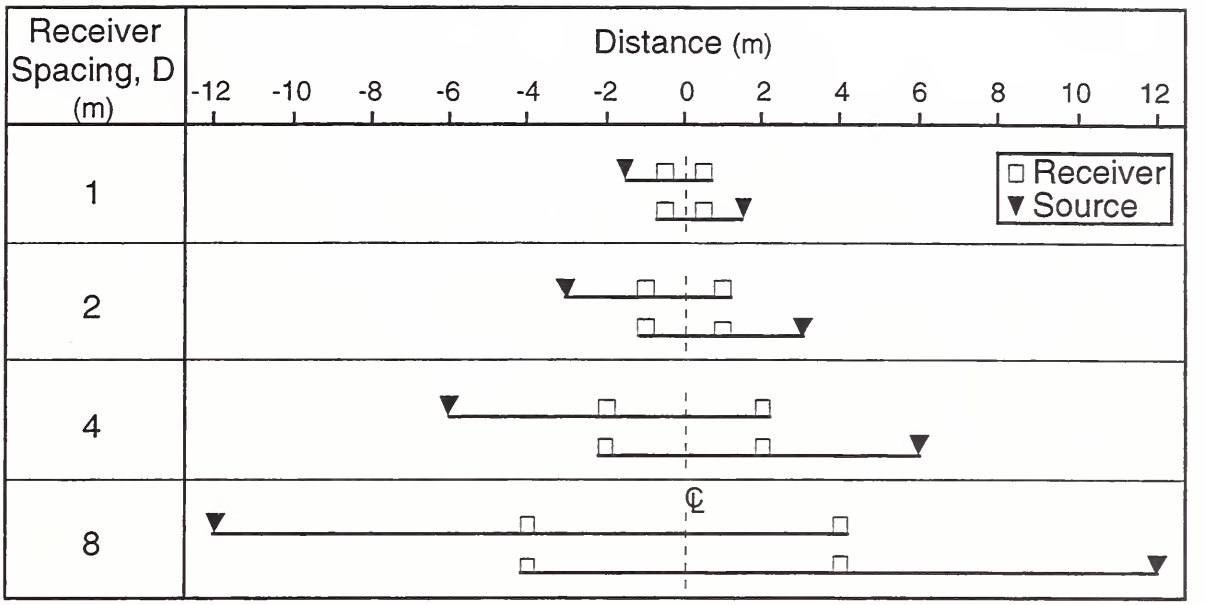

(a) Common Receivers Midpoint Geometry

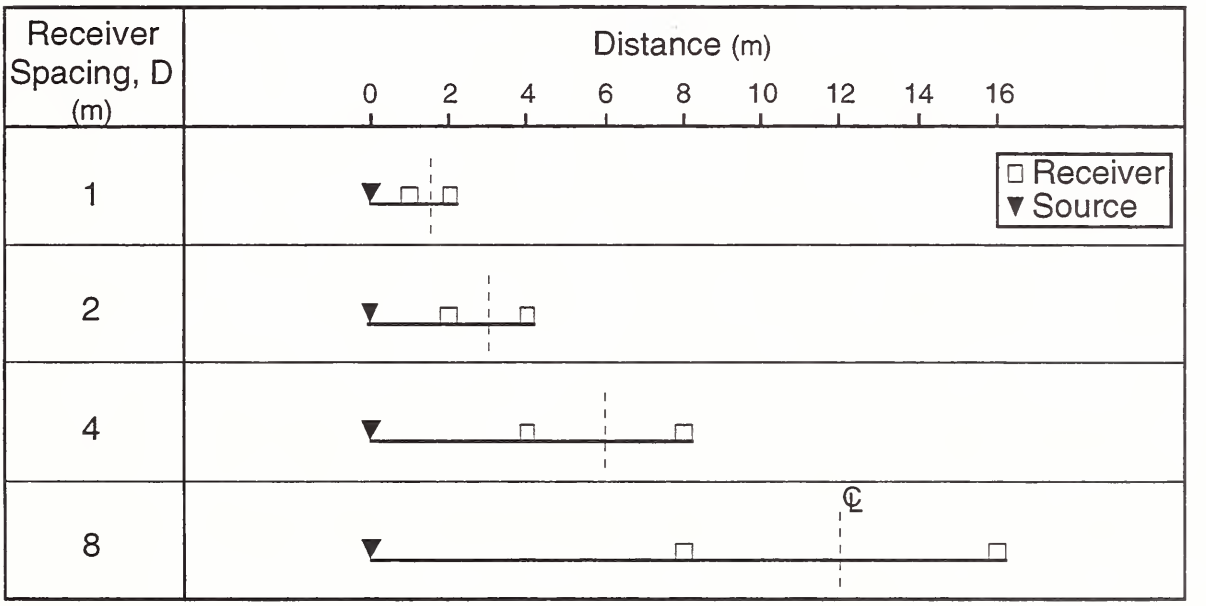

(b) Common Source Geometry

Fig. 2.4 - Two Source-Receiver Setups Used in SASW Testing (after Heiesy, 1981).

2.3 EXPERIMENTAL DISPERSION CURVE FORMATION

The cross-power spectrum is defined as taking the Fourier Transform of two signals separately and multiplying the results together. From the phase of the cross-power spectrum, a travel time, t, between receivers is obtained for each frequency by:

$$t = \Phi / (2 \pi f) \tag{2.1}$$

where Φ = phase difference in radians, and f = frequency in Hz. A Rayleigh wave phase velocity, V_R, is then calculated using:

$$V_R = D / t \tag{2.2}$$

The corresponding wavelength, λ_R, is then determined from:

$$\lambda_R = V_R / f \tag{2.3}$$

These calculations are repeated for each frequency where the data quality is good. From the results at all receiver spacings, a plot of V_R versus λ_R is assembled. This plot is called the *experimental dispersion curve*. This curve represents the "surface wave signature" of the site and is the culmination of the field measurements. A sample experimental dispersion curve is shown in Fig. 2.5.

2.4 SHEAR WAVE VELOCITY PROFILE DETERMINATION

A shear wave velocity, V_S, profile for each test array is obtained through an iterative process of matching the experimental dispersion curve to theoretical dispersion curves. To begin this iterative process, called *forward modeling*, initial properties (shear and compression wave velocities and densities) and layer thicknesses are assumed. Next, a theoretical response is calculated for the assumed horizontally layered profile using three-dimensional computer models of surface wave propagation (Roësset et al., 1991). The response is analyzed to obtain a theoretical dispersion curve. The theoretical dispersion curve is compared with the experimental dispersion curve. Adjustments are made to the assumed elastic properties and layer thicknesses in the profile until satisfactory agreement between the theoretical and experimental dispersion curves is obtained. The final theoretical dispersion curve for the sample experimental curve is also shown in Fig. 2.5. It is assumed that the elastic properties, densities, and layer thicknesses for the final theoretical dispersion curve represent the actual profile of the site. Presented in Table 2.1 is the layered model used to determine the final theoretical dispersion shown in Fig. 2.5.

Recent work by Nazarian et al. (1994) and Joh (1996) has shown that the forward modeling process can be automated, at least for simple sites. Nazarian et al. report that the time for testing and determining a V_S profile at a site like the one shown in Fig. 2.4b can be accomplished in about 30 minutes.

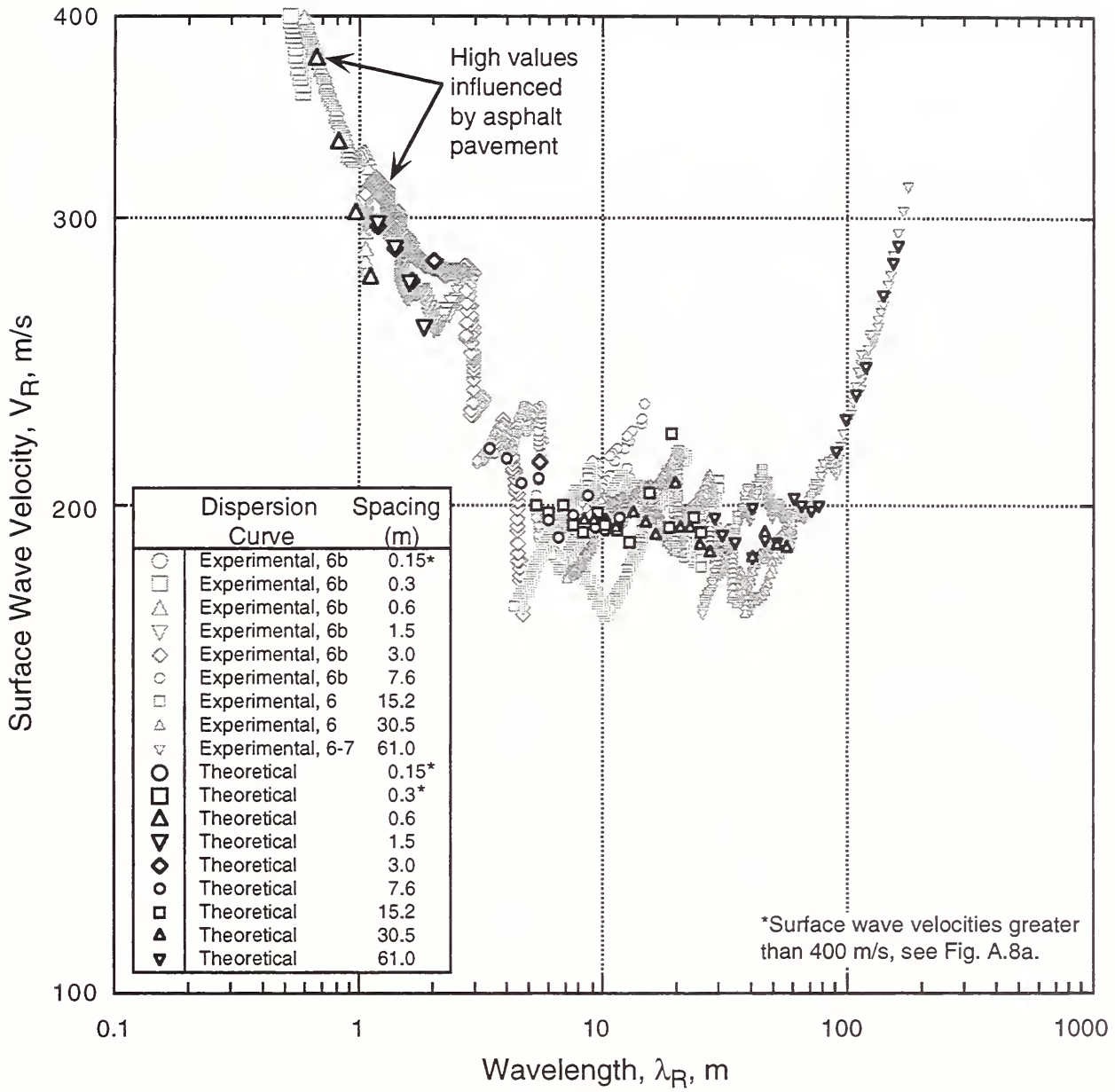

Fig. 2.5 - Comparison of Experimental and Theorectical Dispersion Curves from SASW Testing at the Treasure Island Approach to Pier Site, Array SA-6. (Note that Array SA-6 Lies Within the Improved Area.)

Table 2.1 - Layered Model Used to Determine the Final Theoretical Dispersion Curve for SASW Array SA-6 (see Fig. 2.5) at the Treasure Island Approach to Pier Site.

Layer No.	Layer Thickness (m)	Layer Depth (m)	Assumed Values				Estimated Shear Wave Velocity (m/s)
			Compression Wave Velocity (m/s)	Poisson's Ratio	Density (Mg/m^3)	Damping	
1	0.05	0.00 to 0.05	-----	0.20	1.92	0.02	1439
2	0.04	0.05 to 0.09	-----	0.20	1.92	0.02	945
3	0.06	0.09 to 0.15	-----	0.20	1.92	0.02	512
4	0.3	0.15 to 0.5	-----	0.33	1.76	0.02	244
5	0.6	0.5 to 1.1	-----	0.33	1.76	0.02	222
6	0.9	1.1 to 2.0	-----	0.33	1.76	0.02	183
7	1.1	2.0 to 3.0	1524	-----	1.92	0.02	168
8	1.2	3.0 to 4.3	1523	-----	1.92	0.02	186
9	1.5	4.3 to 5.8	1524	-----	1.92	0.02	177
10	2.4	5.8 to 8.2	1524	-----	1.92	0.02	195
11	4.6	8.2 to 12.8	1524	-----	1.92	0.02	207
12	3.0	12.8 to 15.8	1524	-----	1.92	0.02	192
13	11.6	15.8 to 27.4	1524	-----	1.92	0.02	180
14	15.2	27.4 to 42.7	1524	-----	1.92	0.02	177
15	42.7	42.7 to 85.3	1524	-----	1.92	0.02	286
16	-----	Half-space	-----	0.33	1.92	0.02	1829

2.5 SASW PROCEDURE FOR THIS STUDY

Field tests were performed at the Treasure Island Approach to Pier site following the general procedure outlined in the preceding paragraphs using a truck-mounted seismic vibrator (or vibroseis) weighing 18,000 kg (40,000 lbs) as the principal source and velocity transducers (or geophones) having a natural frequency of 1 Hz (Mark Products[1] Model L-4) as the receivers. The vibroseis (Mertz Model 12), shown in Fig. 2.6, was owned and operated by Subsurface Exploration Company of Pasadena, California. During testing the weight of the vibroseis rested on a metal plate that was 1.2 m wide and 2.3 m long. Conventional vibroseis control electronics modified at The University of Texas at Austin were used in conjunction with a waveform analyzer (Hewlett-Packard Model 3562A Dynamic Signal Analyzer) to control the vibroseis output. The vibroseis output consisted of a sine function that was varied over a range of frequencies. At higher frequencies the sine sweep progressed rapidly. At low frequencies (less than about 5 Hz) the sine sweep progressed rather slowly. Receiver spacings used were as long as 76 m and as short as 1.5 m. Profiling was performed by marching the source-receiver array along an alignment using one or two spacings (typically 15 m and 30 m). To increase productivity, however, hand-held hammers and dropped weights weighing about 10 kg (25 lbs) were generally used at receiver spacings less than 7.6 m. Signals from each receiver were recorded and processed using the analyzer. A total of eight, 30-m-long sections were tested using various receiver spacings at the site.

Fig. 2.6 - Photograph of SASW Testing at the Treasure Island Approach to Pier Site, Array SA-2, Using a Vibroseis as the Source and 1 Hz Geophones as the Receivers.

[1] Trade or manufacture's names appear herein because they are essential to the objectives of this document. The United States Government does not endorse products or manufacturers.

One complicating factor at the site was the asphalt pavement cover. To characterize this stiff layer, additional testing was performed at two locations (Arrays SA-4b and SA-6b) using accelerometers having natural frequency of 23 kHz (Wilcoxon Research Model 728T) and small hand-held hammers. The common midpoint geometry was used for these tests. Typical distances between accelerometers were 0.15 m, 0.3 m, 0.8 m and 1.5 m. Results of these additional tests were used to establish the experimental dispersion curves at short wavelengths (see Fig. 2.5).

To obtain shear wave velocity profiles, data reduction and forward modeling programs developed at The University of Texas at Austin (Roësset et al., 1991; Joh, 1996) were used. Experimental dispersion curves were created from the field data and compacted (or averaged) using the computer programs called WinSASW and Avg.Data7. Theoretical dispersion curves were created and matched with the experimental curve for each receiver spacing using a program called Fit7. Fit7 allows the user to select two- or three-dimensional wave propagation modeling. The three-dimensional model (Roësset et al., 1991) was select throughout the forward modeling process. The assumed properties (primarily V_S) were adjusted until satisfactory agreement between the theoretical and experimental dispersion curves was obtained. Layer thicknesses were based on available borehole and cone sounding information. Where no layer information was available, such as the asphalt pavement thickness and the top of bedrock, layer thicknesses were adjusted to obtain the best comparison. Agreement between the two dispersion curves was assessed visually and by a maximum likelihood method formulation. Both assessment methods were used throughout the forward modeling process. However, the maximum likelihood method was used to finalize the layered model. As part of the maximum likelihood method formulation (Joh, 1996), a root mean square (rms) error was calculated for the difference between the compacted experimental dispersion curve and theoretical dispersion curve. The search for the minimum rms error involved increasing or decreasing the shear wave velocity for each layer in the assumed profile by as little as 3 m/s. Presented in Appendix A are the properties and layer thicknesses for the final theoretical dispersion curves. Experimental and final theoretical dispersion curves for each SASW test array are presented in Appendix B.

2.6 LIMITATIONS

As explained by Stokoe and Rix (1987), the results obtained by the SASW test are considered a more averaged measurement than are results from other *in situ* seismic tests, such as the crosshole and downhole tests. The "averaging" occurs because relatively wide receiver spacings and long wavelengths are required by the SASW method to sense material properties at depth, compared with the small volume of material sampled in the crosshole test. A conceptual view of this difference is shown in Fig. 2.7. The two tests will yield similar results if the material properties do not vary laterally at the site.

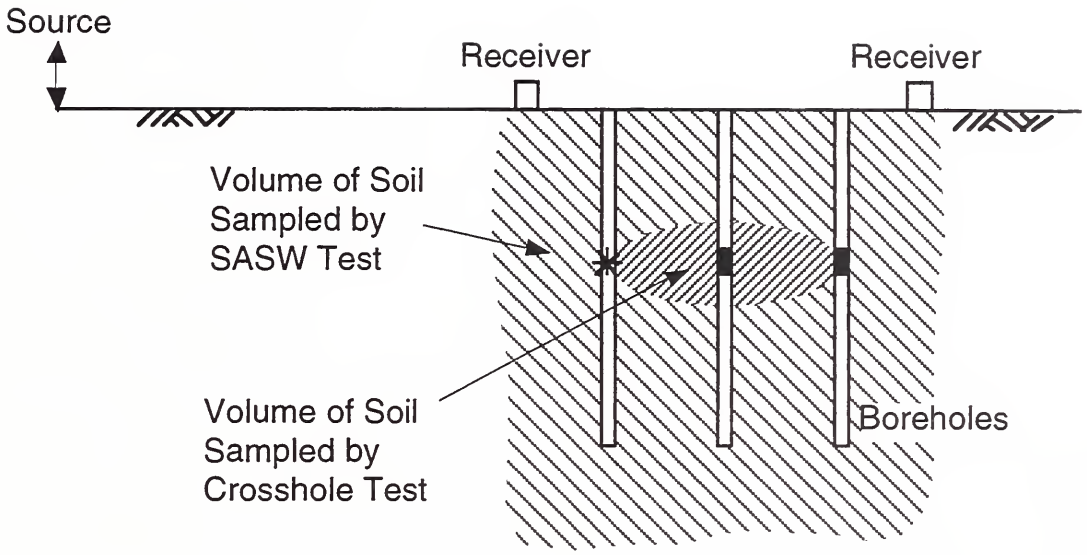

Fig. 2.7 - Conceptual Comparison of Material Sampled During SASW and Crosshole Testing.

The depth of resolution is limited by the receiver spacing and the ability of source to generate long wavelengths. Rix and Leipski (1991) suggest that the maximum wavelength be at least 1 to 2 times the desired depth of resolution. Results obtained during this study indicate that the maximum wavelength obtained is about 2 to 3 times the receiver spacing. Thus, the maximum depth of resolution is roughly equal to 1 to 1.5 times the receiver spacing. This estimate of maximum depth of resolution is reasonable where there is not a large velocity contrast between layers, which is the case at many liquefaction sites.

Where there is a large velocity contrast between layers, such as soil over rock, the maximum wavelengths should be 3 to 10 times the depth to accurately characterize both layers (Sohiel Nazarian, The University of Texas at El Paso, personal communication to Ronald D. Andrus, 1998). Thus, receiver spacings may need to be as much as 5 times the depth. This limitation can be overcome if either the depth to rock or the shear wave velocity of the rock is known. One approach sometimes used to estimate the shear wave velocity of rock at depth is to determine the compression wave velocity of the rock from refraction measurements and assume a Poisson's ratio. While not necessary for liquefaction evaluations in this study, reported field shear wave velocity measurements made at other locations within the bedrock formation were assumed in order to establish the depth to bedrock and accurately characterize the overlying stiff soil layer.

The accuracy of the SASW inversion process depends on the assumed layering. Rix and Leipski (1991) found that if the assumed layering coincides with the actual layering at the site, the forward modeling process will generate an accurate profile. However, if an assumed layer spans across the actual layer boundary, a velocity closer to the average for the two layers will be determined. This limitation can be avoided by using layering defined by other field methods or by using layers thin enough to reproduce the variations in the true profile.

The uncertainty in the value of shear wave velocity determined for a given layer is not easy to quantify, and current analytical procedures are dependent upon the variables of the starting model. Rix and Leipski (1991) suggest using ratios of the final variances to the initial variances for each layer as an indicator of uncertainty. The variances are a product of the inversion process, equal to the square of the standard deviation. They found that at a particular depth the ratios (or uncertainties) are greater for relatively thin layers than for layers that are thick. Joh (1996) suggests evaluating layer sensitivity by examining various matrix terms (the row component of the model parameter spread function and the diagonal term of the resolution matrix), and adjusting layer thicknesses to obtain layers of moderate sensitivity. The root mean square error between the experimental and theoretical dispersion data is then used in the procedure by Joh as an indicator of over all goodness of fit. These procedures depend on the number and spacing of averaged experimental dispersion curve points.

Two limitations of using V_S measurements to evaluate liquefaction are (Youd et al., 1997; Andrus and Stokoe, 1997): (1) Measurements are made at small strains, whereas liquefaction is a large strain phenomenon. This limitation can be significant for cemented soils, since small-strain measurements are highly sensitive to weak interparticle bonding which is eliminated at large strains. It can also be significant in silty soils above the water table where negative pore water pressures can increase V_S. (2) No samples are obtained for classification of soils and identification of non-liquefiable soft clayey soils. Non-liquefiable soils by the so-called Chinese criteria have clay contents (particles smaller than 5 μm) greater than 15%, liquid limits greater than 35%, and moisture contents less than 90% of the liquid limit (Seed and Idriss, 1982). To compensate for these limitations, a limited number of borings should be drilled and samples taken to identify weakly cemented soils that might be liquefiable but classed as non-liquefiable by V_S-criteria, to identify unsaturated silty soils that might have lower values of V_S should the water table rise, and to identify non-liquefiable clay-rich soils that otherwise might be classed as liquefiable.

Finally, large ground vibrations generated by the vibroseis will restrict its use near structures. In this study, whenever the vibroseis was located close to a structure, ground vibrations were monitored with the geophones used in the SASW test. The vibration level was kept below about 2.5 mm/s (0.1 in/s), a factor of 10 below the level damaging to structures (Richart et al., 1970). For structures with sensitive equipment, the vibration level may need to be kept even lower. In addition, noise produced by the compressor on the vibroseis will also restrict its use in residential areas.

CHAPTER 3

INVESTIGATION AND LIQUEFACTION ANALYSIS AT THE APPROACH TO PIER SITE

3.1 INTRODUCTION

The Approach to Pier site is located on the south-eastern corner of Treasure Island near Pier 1. A photograph of the area is shown in Fig. 3.1. Lying about 3 m above mean low low water (M.L.L.W.), the area is essentially level and capped by a 127 mm thick layer of asphalt pavement. At the water front, the island surface slopes into the water at an angle from the horizontal of about 24 degrees. This sloping surface is covered with rock riprap.

Because of concern for the seismic instability of the water front slope, the fill beneath the approach to Pier 1 was densified to a depth of about 12 m by a vibrating probe technique in 1985. As shown in Fig. 3.2, the area penetrated by the vibrating probe was 23 m wide and 97 m long. Following the 1989 Loma Prieta earthquake (moment magnitude, $M_w = 7.0$), no signs of ground disturbance were observed in the improved area, while sinkholes, sand boils and cracks were seen in the adjacent unimproved areas (Geomatrix Consultants, 1990; Mitchell and Wentz, 1991). In March 1996, Spectral-Analysis-of-Surface-Wave (SASW) tests were performed along the alignments shown in Fig. 3.2. General subsurface conditions of the improved and unimproved areas are described in Section 3.2. Liquefaction effects are discussed in Section 3.3. In Section 3.4, results of SASW testing are presented. Simplified liquefaction assessment procedures are applied in Section 3.5.

3.2 SUBSURFACE CONDITIONS

A generalized two-dimensional soil profile of the SASW test alignment is shown in Fig. 3.3. This profile was developed from borings and cone soundings performed by other investigators (Baker, 1985; Geomatrix Consultants, 1990; Harding Lawson Associates, 1996). The upper 12 m of soil is sand fill initially deposited in a loose to medium dense state during hydraulic filling. Grain-size distribution curves for three samples taken from the unimproved fill are shown in Fig. 3.4. Samples above a depth of 6 m contain as much as 17% fines (silt and clay). Below 6 m, samples contain 1% to 4% fines. The fill is underlain by 3 m of native silty clayey sand (Shoal Sands) followed by 27 m of soft to stiff clay with interbedded sand layers which thin away from Yerba Buena Island (see Fig. 1.1). The clay (Young Bay Mud) is underlain by alternating layers of very stiff sandy clay (Old Bay Clay) and dense sand. At the time of SASW testing, the water surface in the bay was about 2 m below the ground surface.

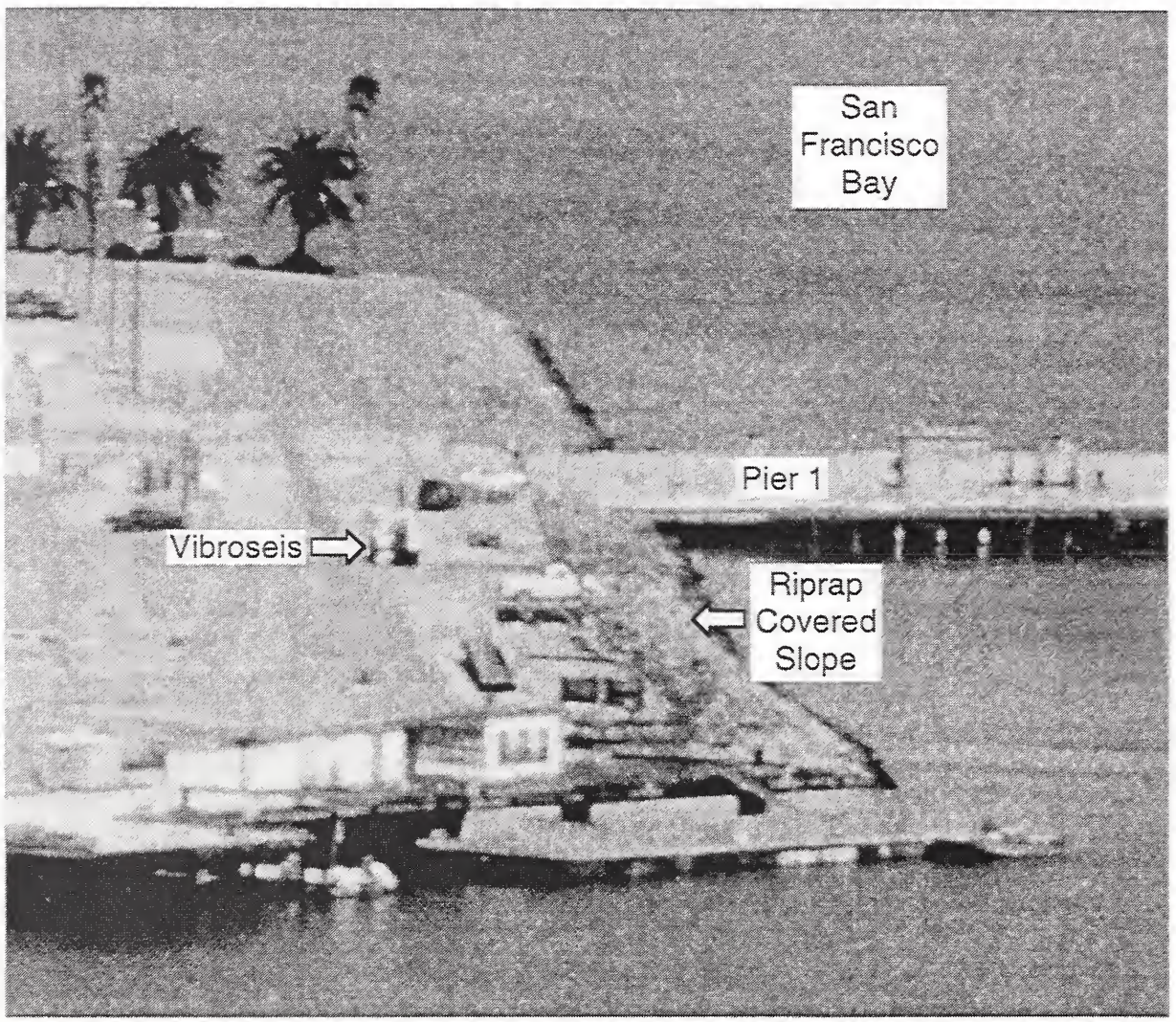

Fig. 3.1 - Photograph of the South-Eastern Corner of Treasure Island Showing the Approach to Pier Site. (Location of the Vibroseis is Near SASW Test Array 4b, see Fig. 3.2.)

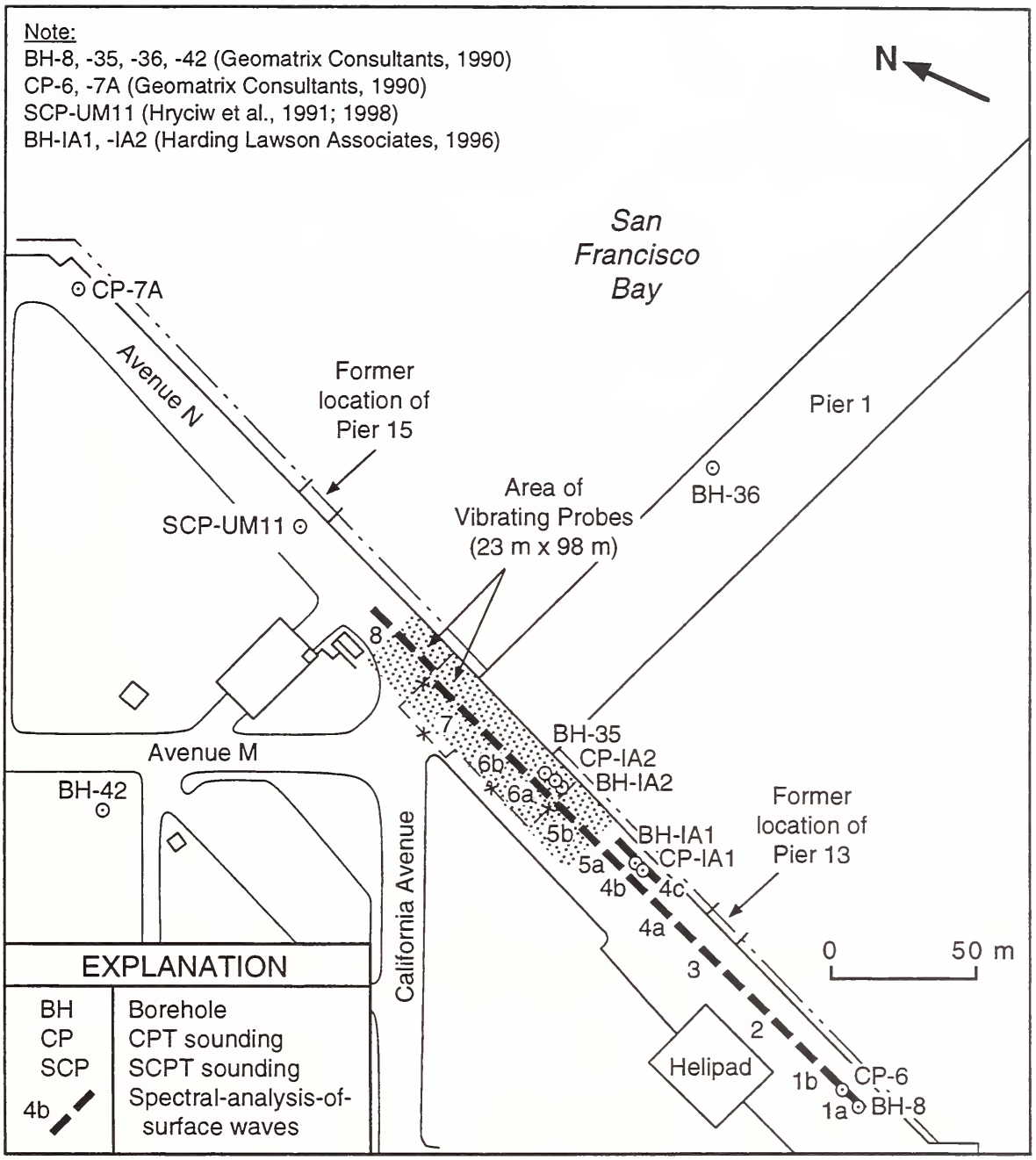

Fig. 3.2 - Map of the Approach to Pier Site Showing Locations of Structures (de Alba and Faris 1996a) and Tests.

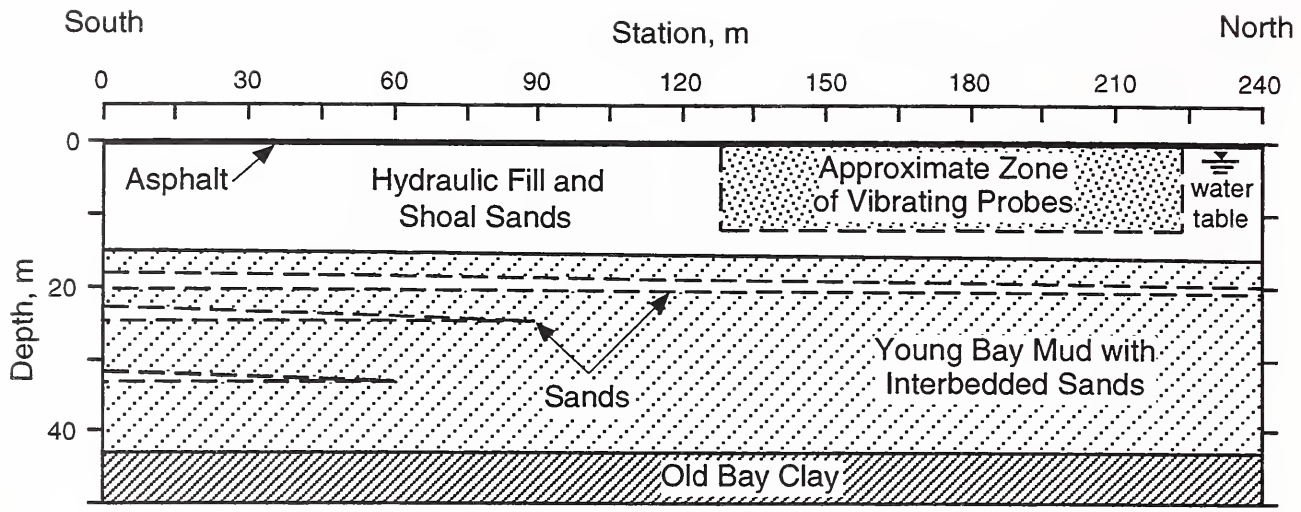

Fig. 3.3 - Generalized Soil Profile of the SASW Test Alignment.

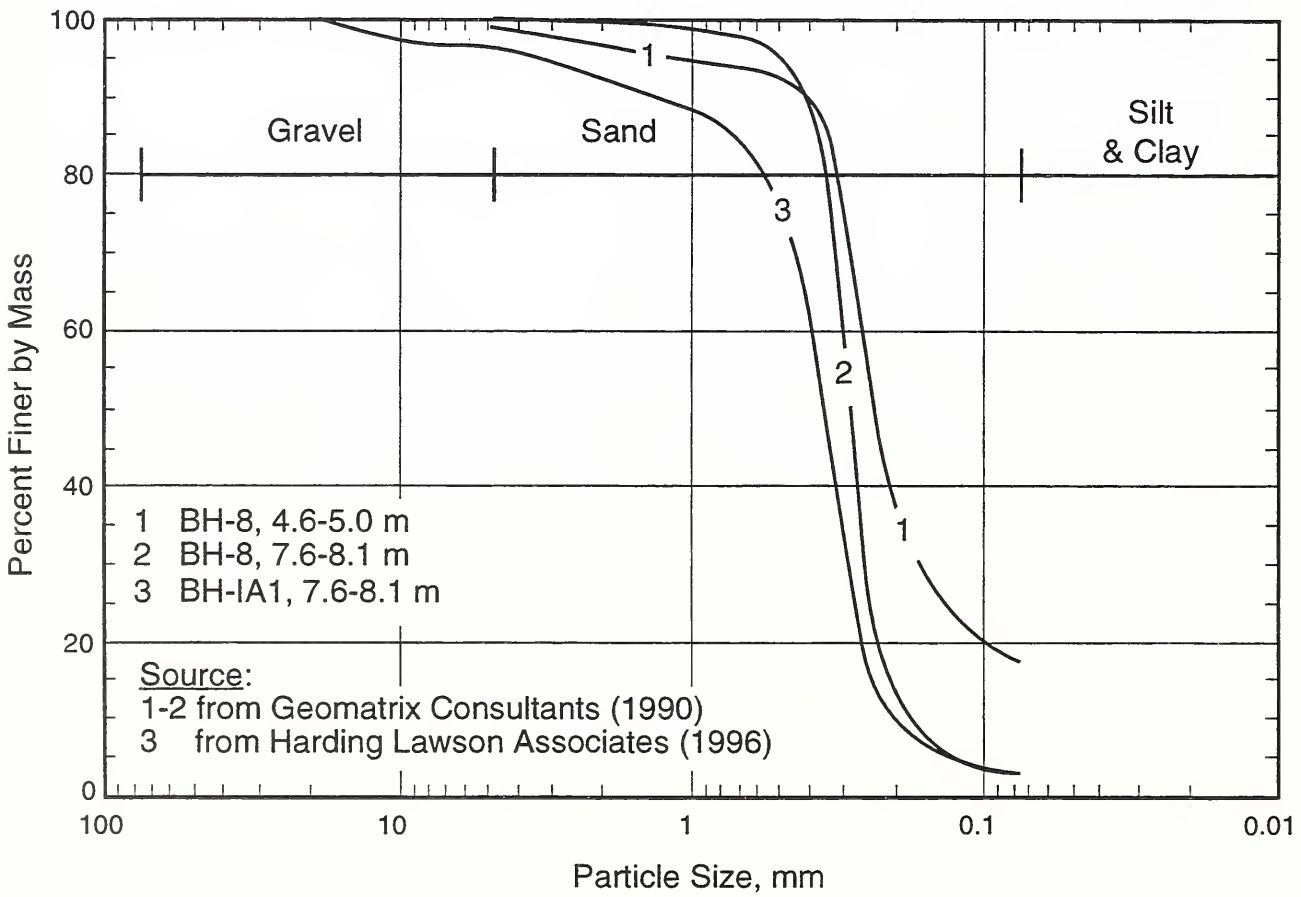

Fig. 3.4 - Grain-size Distribution Curves of Three Split-barrel Samples Taken from the Unimproved Hydraulic Fill Sand.

Sandstone and shale bedrock occurs at a depth of 87 m at the fire station (de Alba and Faris, 1996a). It is assumed that the bedrock surface slopes upward from the fire station to the sandstone rock forming Yerba Buena Island.

3.2.1 Vibrating Probe Technique

From construction drawings by Foundation Contractor, Inc., initial vibrating probes and penetration tests were conducted at the northwest corner of the improved area to determine the optimal probe spacing. Subsequent production probes were performed to produce a final 1.90-m or 2.24-m probe spacing in a triangular grid pattern, as illustrated in Fig. 3.5.

Mr. Gerald Manning of Foundation Constructors, Inc. (personal communication to Ronald D. Andrus, March 1998; SI conversions are shown in brackets) described the vibrating probe technique as follows:

> "The tool we used was a KM6-6000E Tomen (Kencho) Vibrator which had a vibratory force of 81 metric tons.
>
> A circular probe was clamped to the Tomen vibrator measuring [15 m] fifty feet in length. The diameter and wall thickness was [710 mm] 28" x [16 mm] 5/8" wall. Elliptical shaped windows measuring about [150 mm] six inches wide by [200 mm] eight inches high were cut in the probe and spaced about [510 mm] twenty inches center to center.
>
> The specified material was spread over the area to be improved to a depth of [0.9 m] three feet. The material was pushed up against the probe as the tube was vibrated into the ground. The natural soil offered almost no resistance to the penetration of the probe. To allow the material to enter the 'windows', the rate of advance of the probe was slowed to about [2.5 m] eight feet per minute. After the area was probed, the ground was back at it's original elevation.
>
> The specified material was a subgrade (road base) mixture. It contained about three to five percent fines. It is the writer's [Mr. Manning] opinion that we should have achieved better ground improvement had the material been free of all fines."

Mr. Manning adds that the metal-tube probe was opened at the bottom to permit vibration of the specified material into the surrounding sand fill.

Grain-size distribution curves 4, 5 and 6 shown in Fig. 3.6 are for three split-barrel samples taken from the improved soil. Also shown are the curves (1, 2 and 3) for three samples taken from unimproved soil. These curves suggest that the specified material used contained about 20% to 40% coarse sand, and as much as 15% gravel.

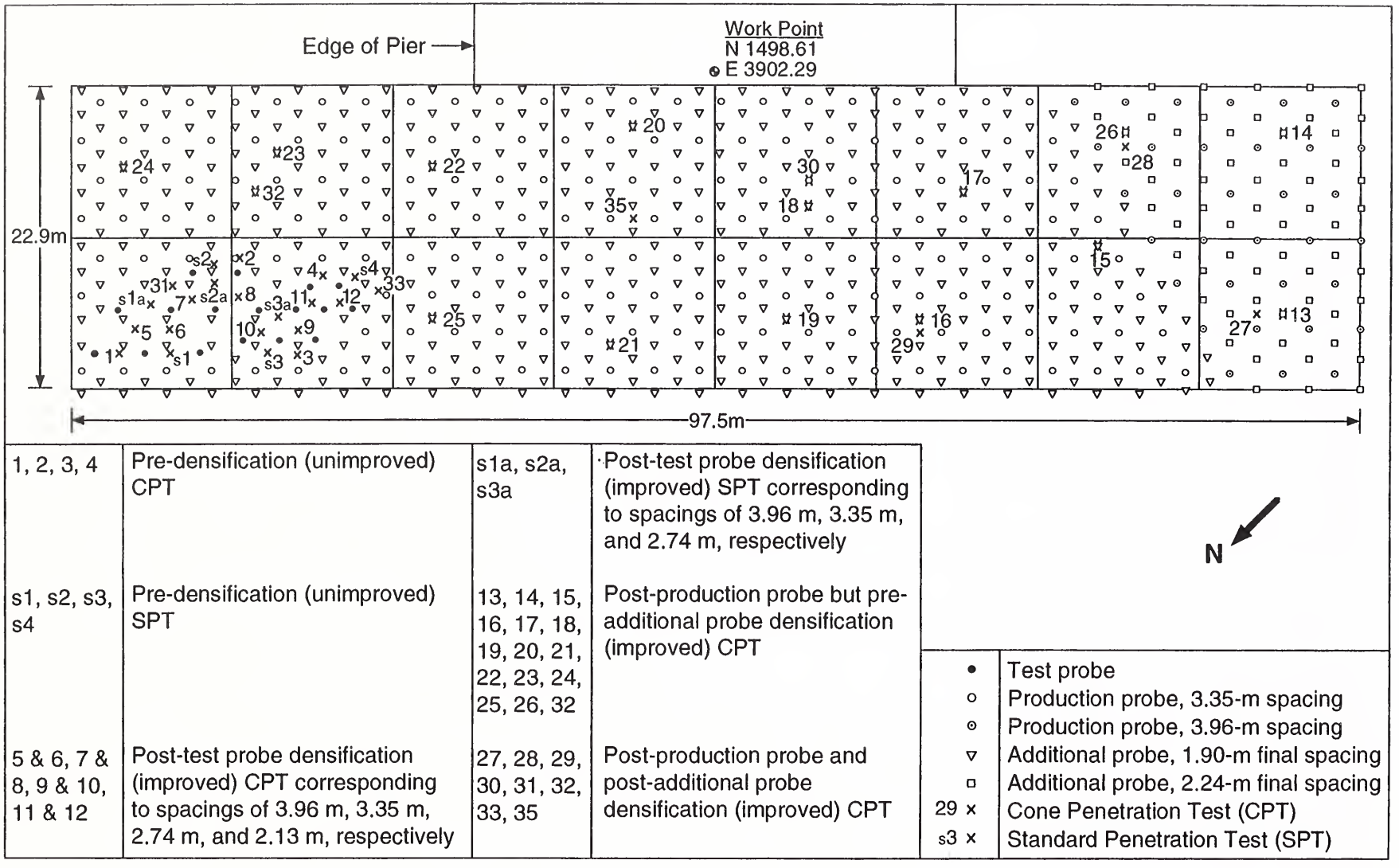

Fig. 3.5 - Construction Drawing of Improved Soil Area Showing Locations of Vibrating Probes and Penetration Tests Performed in April and May of 1985 (redrawn from construction drawing prepared by Foundation Constructors, Inc., 1985; information provided by Richard Faris, Naval Facilities Engineering Command, 1996).

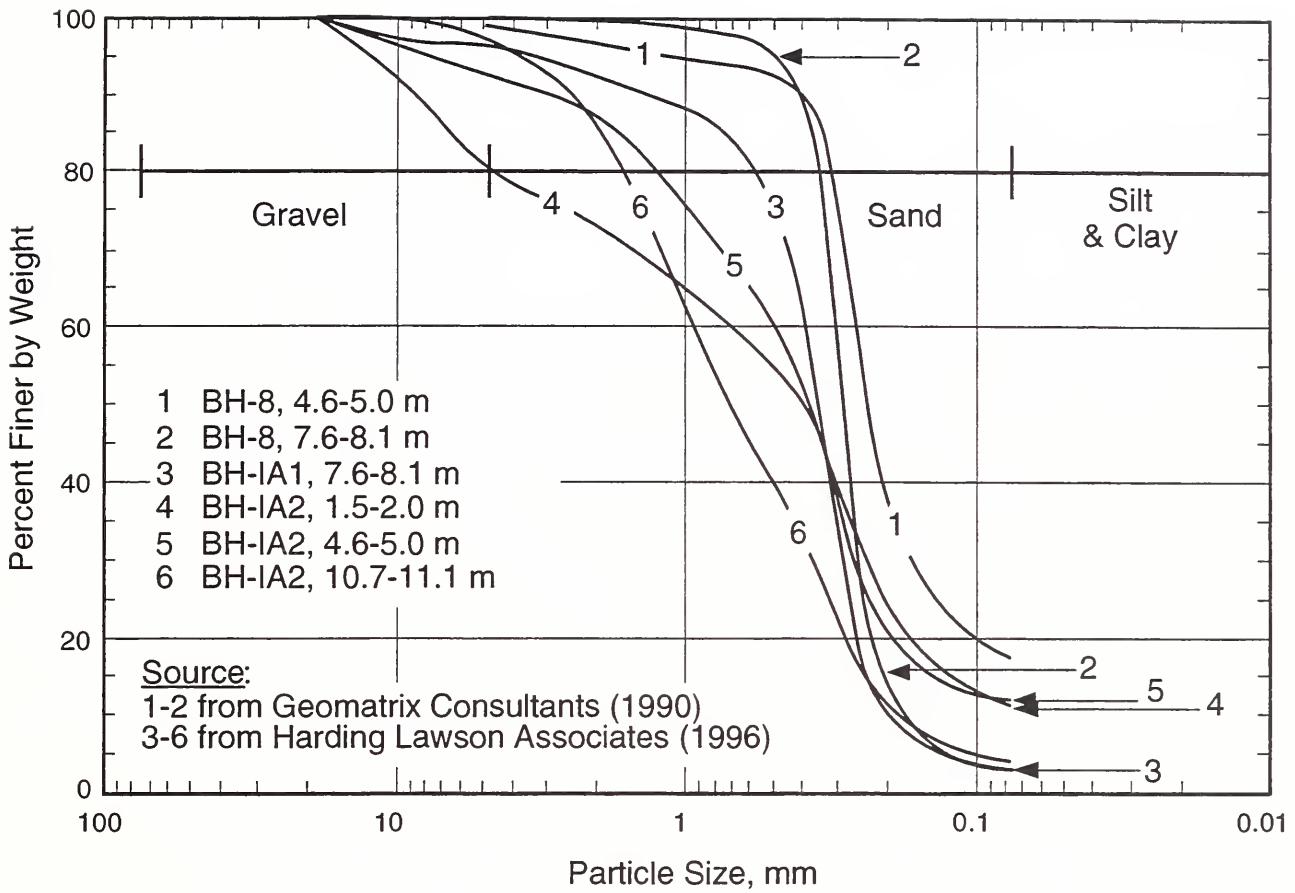

Fig. 3.6 - Comparison of Grain-size Distribution Curves of Split-barrel Samples Taken from the Unimproved and Improved Sand Fill.

The criteria for improvement was based on the Standard Penetration Test (SPT) and Cone Penetration Test (CPT), as given in Table 3.1. A multiplier of 4.0 was used to convert the SPT blow count, N, to equivalent CPT tip resistance, q_c. According to Mitchell and Wentz (1991; 1998), the SPTs were performed at points equidistant from vibration probe locations and depth intervals of 0.75 m. The average of three consecutive N values was to be no less than the values listed in Table 3.1. The CPTs were also to be performed at points equidistant from vibration probe locations. The values of q_c were to be no less than the values listed in Table 3.1, except where the friction ratio was greater than 2.0%. Locations of boreholes and cone soundings performed during construction are shown in Fig. 3.5.

Table 3.1 - Criteria for Soil Improvement (after Mitchell and Wentz, 1998).

Depth below ground surface, m (ft)	SPT N value, blows / 0.3 m	CPT $q_c = 4N$, MPa (tons/ft^2)
1.5 (5)	11	4.2 (44)
3.0 (10)	15	5.7 (60)
4.6 (15)	19	7.3 (76)
6.1 (20)	22	8.6 (90)
7.6 (25)	25	9.6 (100)
9.1 (30)	27	10.2 (105)
10.7 (35)	28	10.9 (114)
12.2 (40)	30	11.5 (120)

Presented in Figs. 3.7 and 3.8 are profiles of cone tip resistance measurements performed before and after soil improvement. CPT profiles shown in Fig. 3.7 are for measurements performed in 1985 at the time of soil improvement. CPT profiles shown in Fig. 3.8 are for measurements performed in 1996. Also shown in these figures is the minimum q_c requirement for materials with friction ratio greater than 2.0%. Based on these comparison, the densification criteria appear to have been generally met, except between depths of 3 m and 6 m where the sand fill contains as much as 17% plastic fines.

3.3 LIQUEFACTION EFFECTS

Geologists from Geomatrix Consultants and the United States Geological Survey mapped the liquefaction effects which formed within about 60 m of the slope crest during the 1989 Loma Prieta earthquake (Geomatrix Consultants, 1990; Egan and Wang, 1991; Power et al., 1998). The liquefaction features near Pier 1 are shown in Fig. 3.9. It is interesting to note that most of the sinkholes and sand boils that formed lie along the perimeter of the improved area, suggesting that maybe the ground was disturbed and loosened by the vibrating probes.

Photographs of the sinkhole and sand boils near the improved area are presented in Figs. 3.10 and 3.11. Based on grain-size analysis by Bennett (1998), the sand boil shown in Fig. 3.10b contains 2% gravel, 97% sand, and 1% silt and clay. The median grain size, D_{50}, and coefficient of uniformity, C_u, for this material are 0.289 mm and 1.9, respectively. These characteristics are very similar to characteristics exhibited by borehole samples 2 and 3 take from depths of 6.8 m and 8.8 m shown in Fig. 3.6, evidence that liquefaction occurred at these depths.

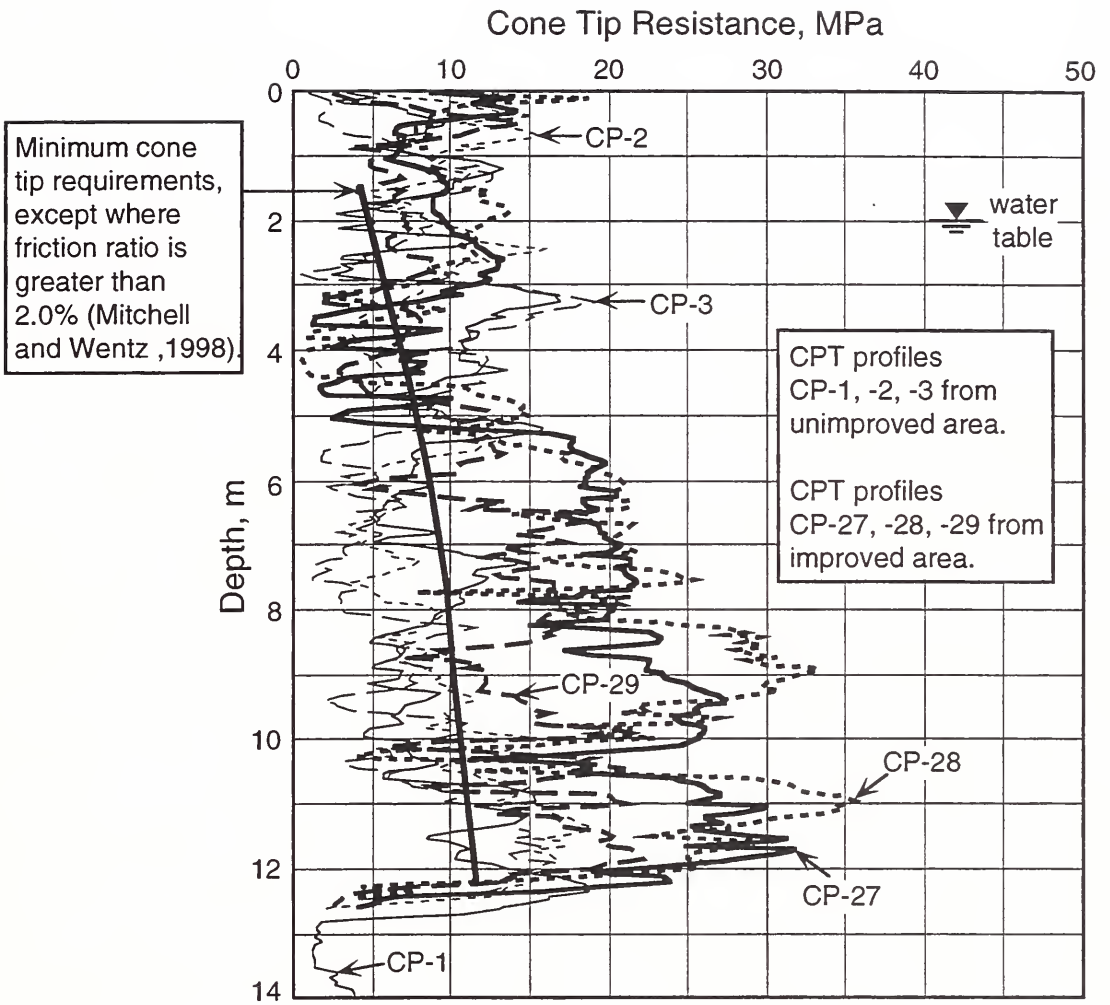

Fig. 3.7 - Comparison of Criteria for Soil Improvement with Cone Tip Resistance Measurements Performed Before Improvement (3 April 1985) and Shortly After Improvement (3 May 1985). (information provided by Richard Faris, Naval Facilities Engineering Command, 1996; unpublished cone penetration test data by V. A. Baker, 1985).

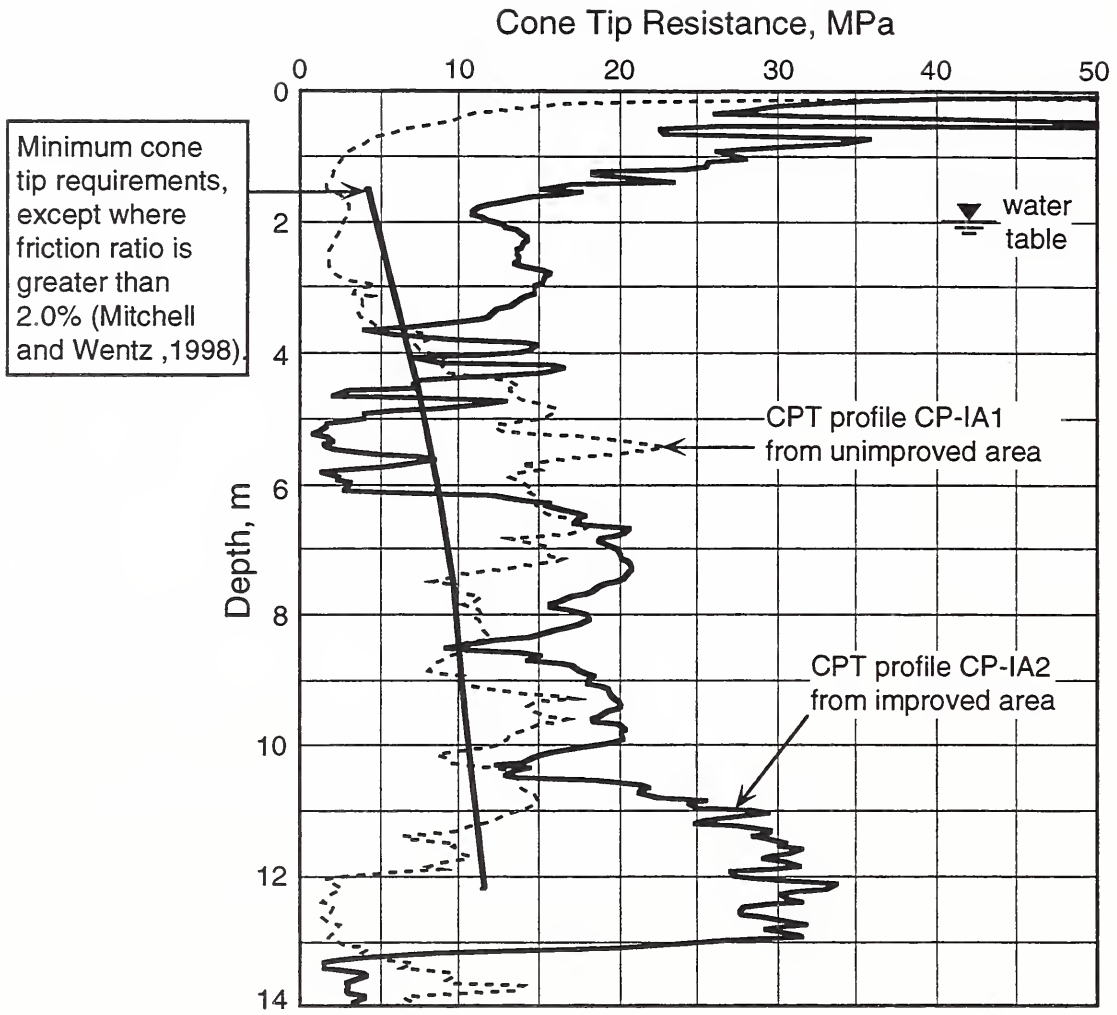

Fig. 3.8 - Comparison of Criteria for Soil Improvement with Cone Tip Resistance Measurements Performed After the 1989 Loma Prieta Earthquake (15 May 1996) in the Improved and Unimproved Areas (Harding Lawson Associates, 1996).

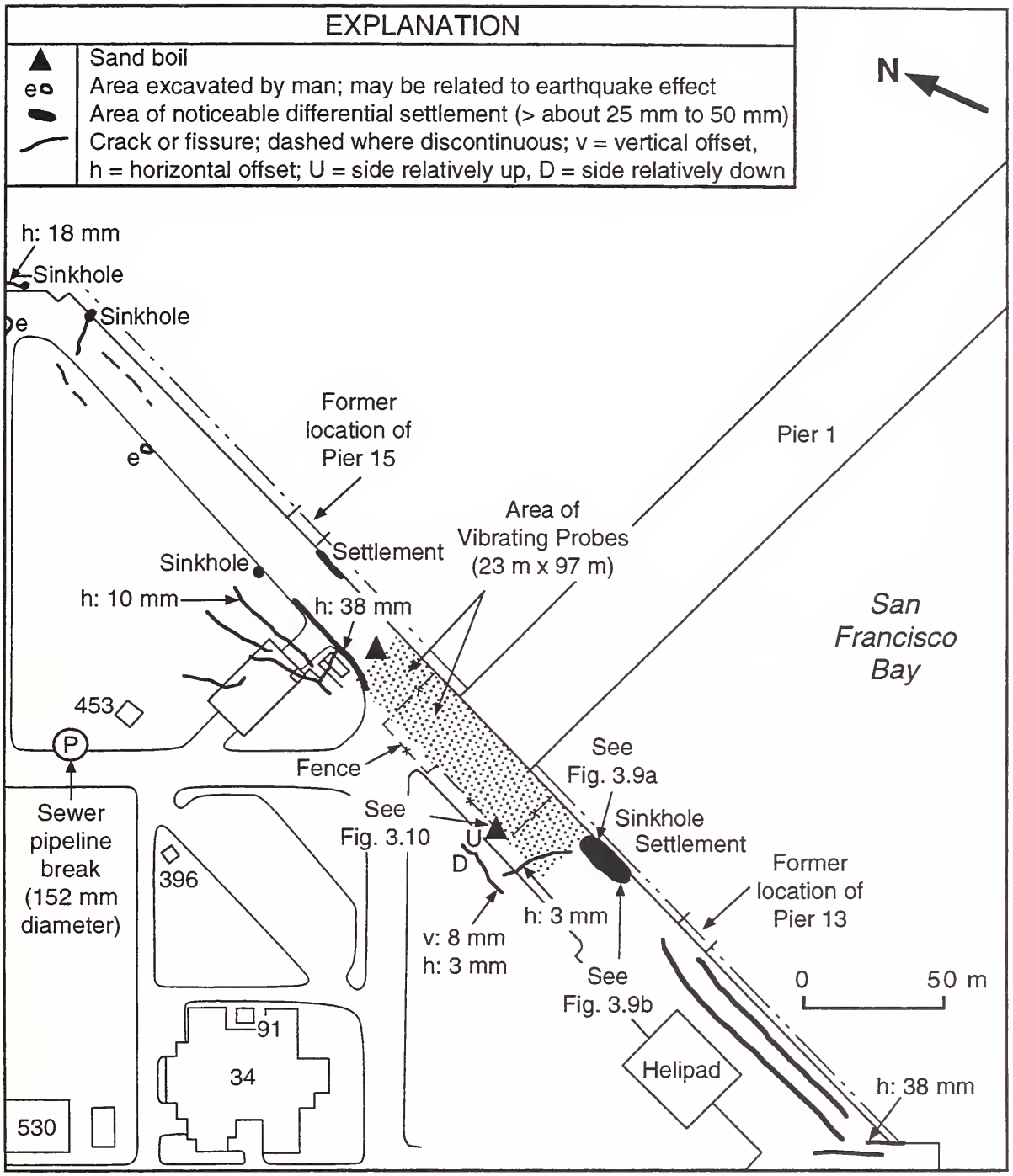

Fig. 3.9 - Map of the Approach to Pier Site Showing Locations of Structures (de Alba and Faris, 1996a) and Liquefaction Effects Generated by the 1989 Loma Prieta Earthquake (modified from Geomatrix Consultants, 1990; Power et al., 1998).

(a) North End of Sinkhole

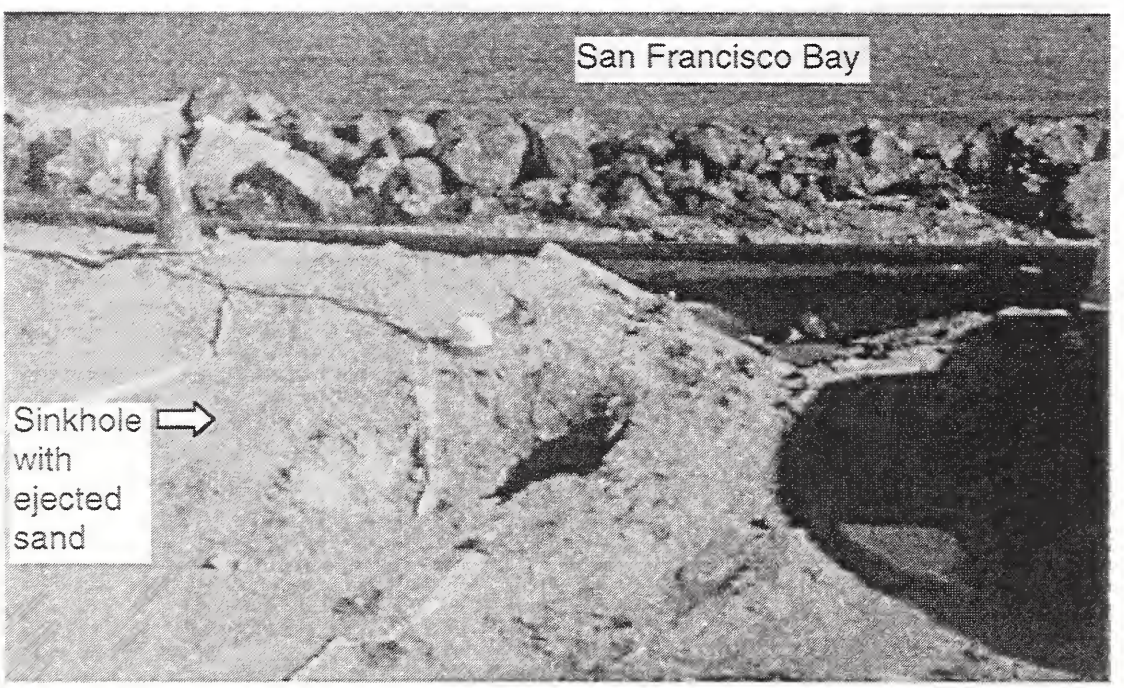

(b) South End of Sinkhole

Fig. 3.10 - Photographs of Sinkhole Near Southern Boundary of the Area of Vibrating Probes, as Noted in Fig. 3.9. (Photographs by Michael J. Bennett, U.S. Geological Survey)

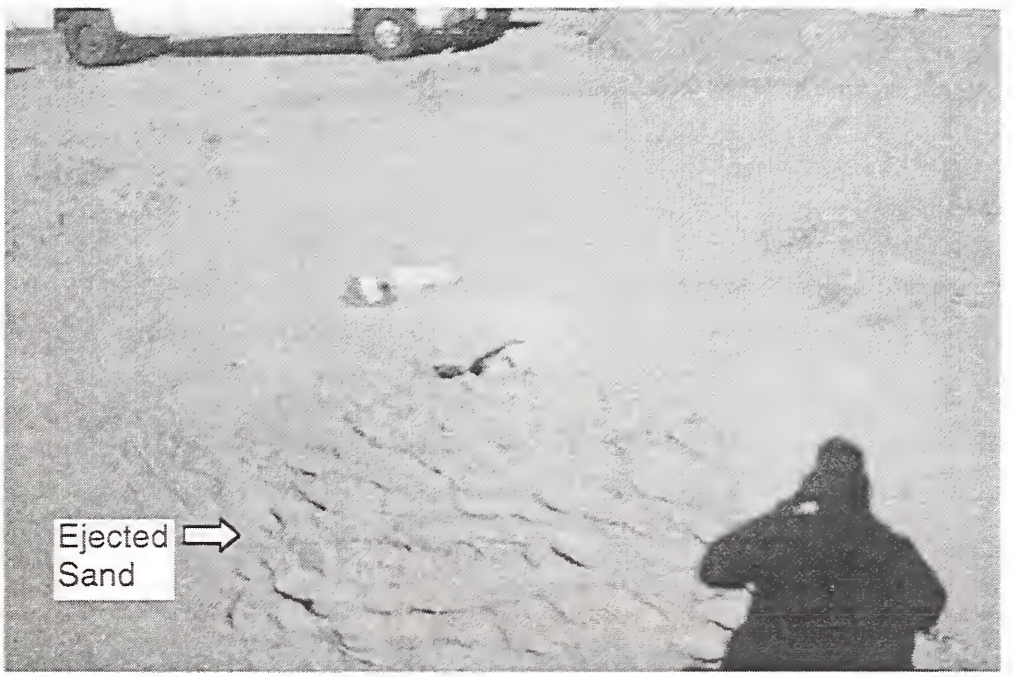

Fig. 3.11 - Photograph of Sand Boil Near the Area of Vibrating Probes, as Noted in Fig. 3.9. (Photograph by Michael J. Bennett, U.S. Geological Survey)

Nearly all the cracks which formed in the asphalt pavement covering the unimproved areas ran parallel to the water front, and are less than about 40 mm wide (see Fig. 3.9). Summation of crack widths indicates bayward movement of the perimeter of the island on the order of 80 mm at this location. This amount of movement is relatively small compared with the several meters of movement that can occur during liquefaction. Located close to the perimeter of island, sloping ground may have contributed to the amount of lateral movement. Based on these findings, liquefaction in the unimproved area is considered marginal.

3.4 SASW TEST RESULTS

SASW tests were conducted in the areas of improved and unimproved soil along the 240-m-long test alignment shown in Fig. 3.2. The relative locations of receiver spacings of 7.6 m, 15.2 m, and 30.5 m with respect to the area of vibrating probes are shown in Fig. 3.12. Experimental dispersion data obtained for these 29 test setups are plotted in Figs. 3.13, 3.14 and 3.15. The dispersion data for test arrays in the improved area (solid symbols) are distinctly separated from the dispersion data for test arrays in the unimproved area (open symbols). The dispersion data for two arrays located 40% to 50% within the improved area (+ symbols) lie between the open and solid symbols, as shown in Figs. 3.14 and 3.15. Values of V_R for the improved area are as much as 90 m/s higher than values of V_R for the unimproved area at a wavelength of 3 m. This difference in V_R-values decreases to about 15 m/s at a wavelength of 30 m. Between wavelengths of 5 m and 24 m, the average difference in V_R-values is 31 m/s.

SASW test array 4c is located next to a sinkhole formed by liquefaction during the 1989 Loma Prieta earthquake, as shown in Fig. 3.2. Values of V_R for test array 4c are among the lowest measured, as shown in Figs. 3.13 and 3.14. This observation was expected, since array 4c lies closest to the waterfront slope where overburden pressures in underlying soils are lower.

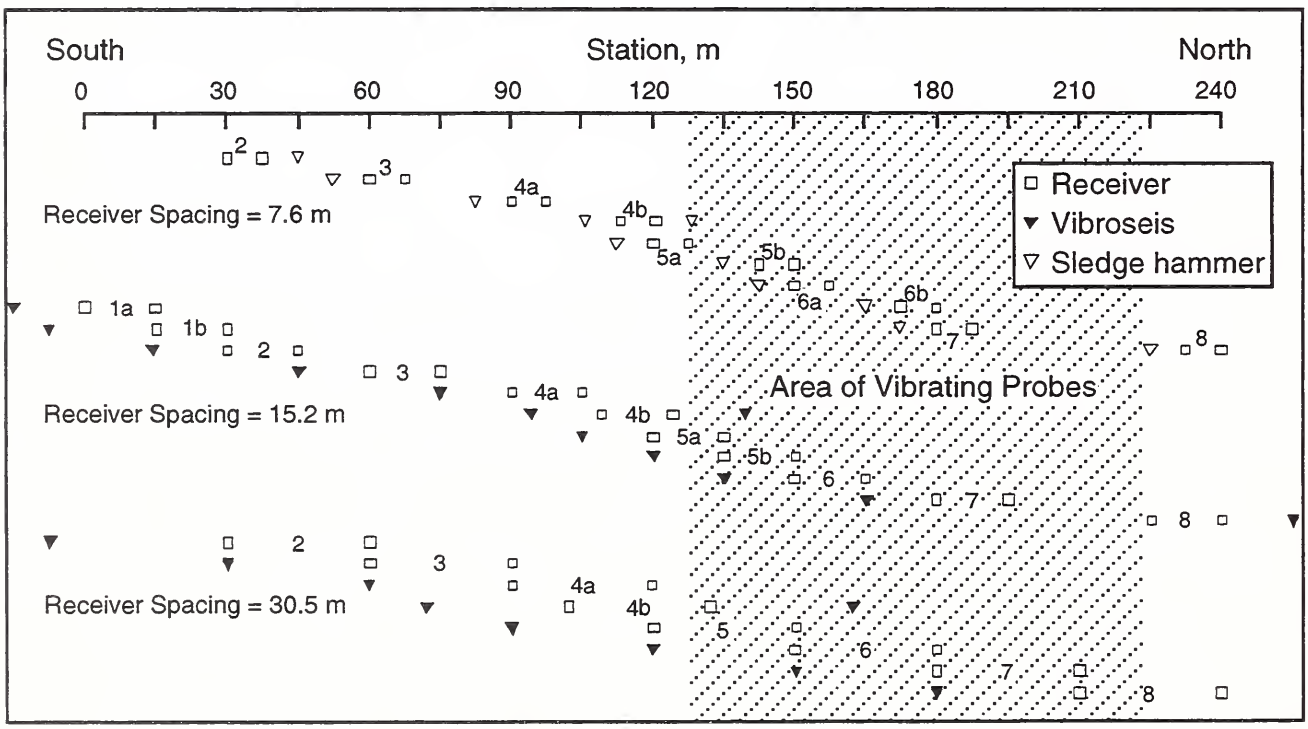

Fig. 3.12 - Relative Locations of SASW Source and Receivers With Respect to the Area of Vibrating Probes for Receiver Spacings of 7.6 m, 15.2 m, and 30.5 m. (Actual Location of the Test Alignment is Shown in Fig. 3.2.)

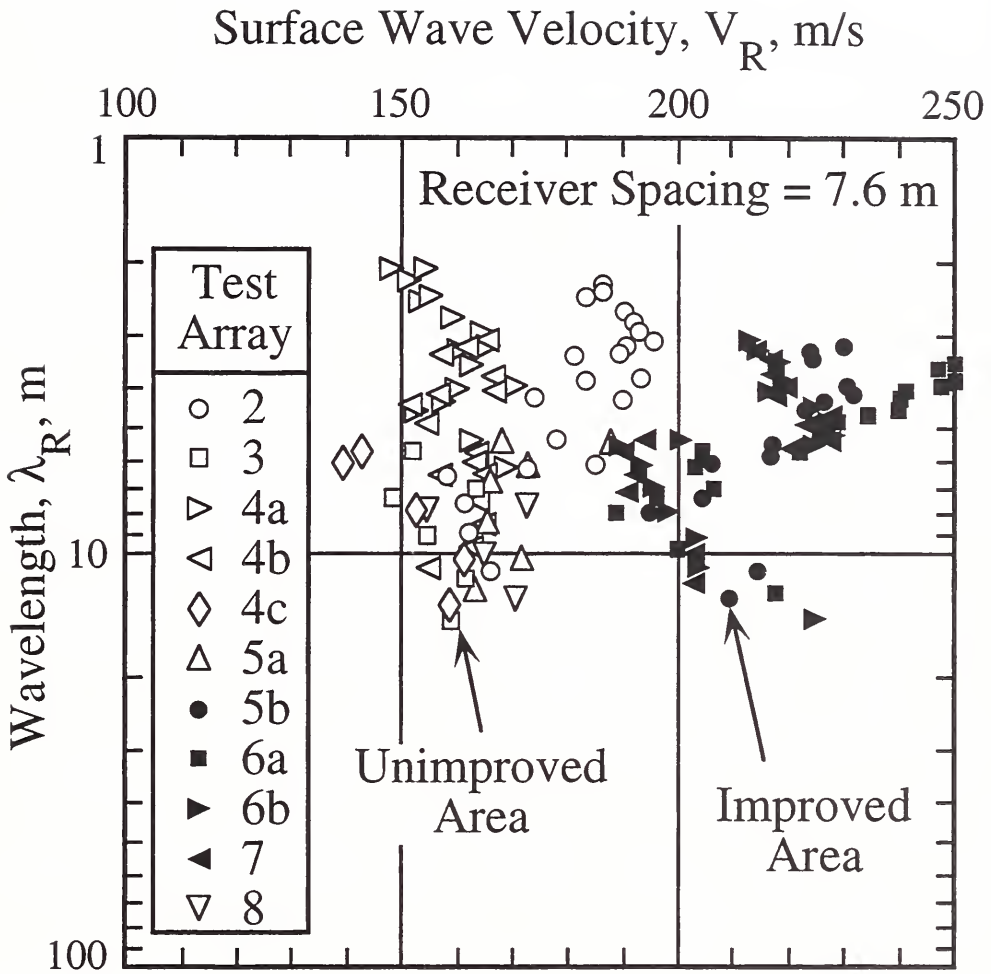

Fig. 3.13 - Experimental Dispersion Data for SASW Tests Conducted at the Approach to Pier Site with Receiver Spacing of 7.6 m.

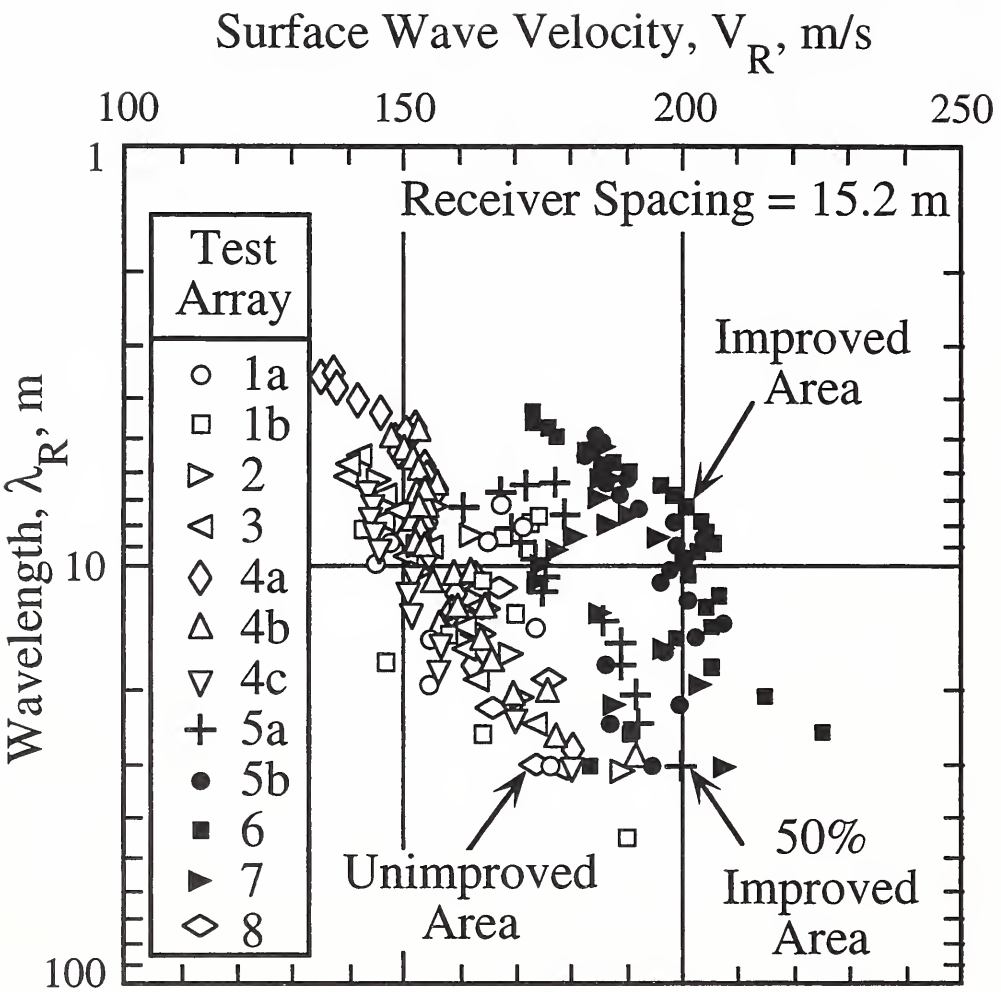

Fig. 3.14 - Experimental Dispersion Data for SASW Tests Conducted at the Approach to Pier Site with Receiver Spacing of 15.2 m. Dispersion Data for Receiver Setup Located 50% with the Improved Area Indicated by + Symbol.

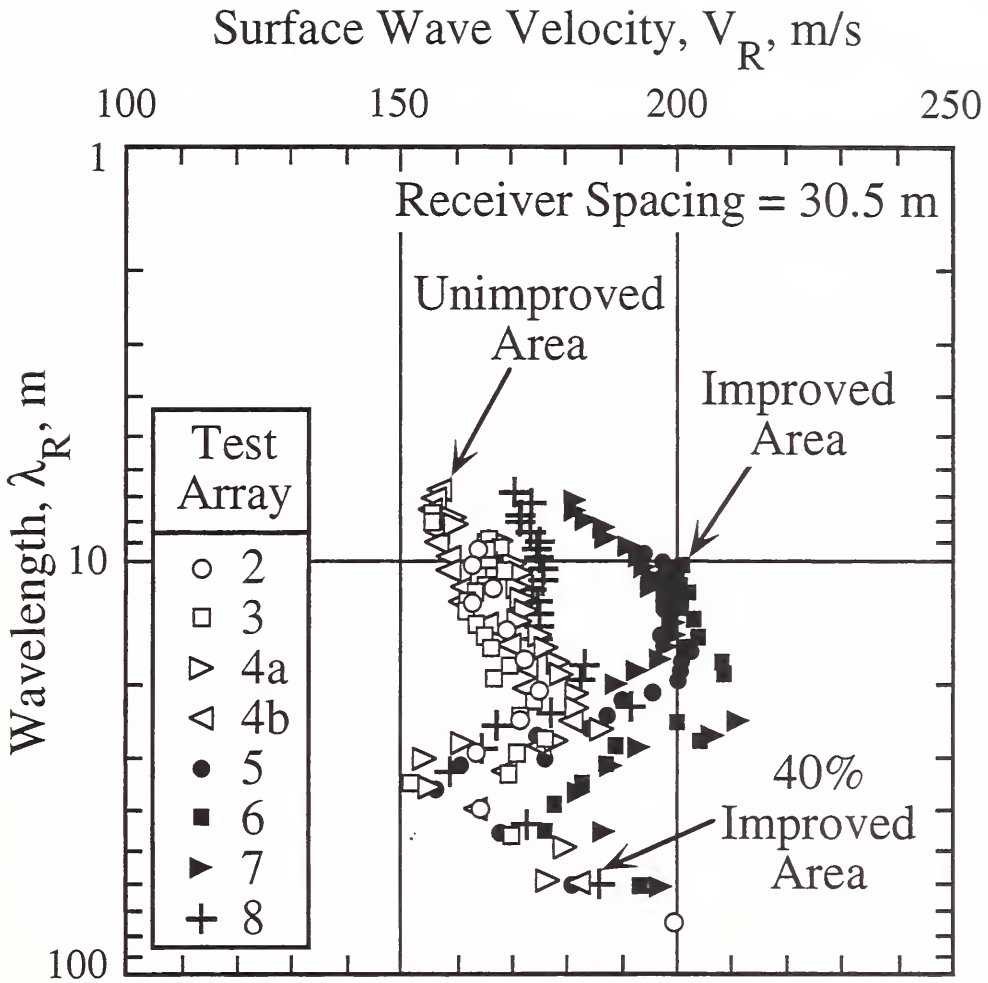

Fig. 3.15 - Experimental Dispersion Data for SASW Tests Conducted at the Approach to Pier Site with Receiver Spacing of 30.5 m. Dispersion Data for Receiver Setup Located 40% with the Improved Area Indicated by + Symbol.

Shear wave velocity profiles for SASW tests conducted in the improved and unimproved areas are shown in Figs, 3.16 and 3.17, respectively. These V_S-profiles are determined from forward modeling using experimental dispersion curves composed of the dispersion data for receiver spacing of 0.15 m to 61 m, as given in Appendix B. The variability in site stiffness indicated by the V_S-profiles is similar to variability in site stiffness suggested by the dispersion data (see Figs. 3.13, 3.14 and 3.15).

Presented in Fig. 3.18 are average shear wave velocity profiles for the improved and unimproved areas. Values of V_S for the improved area are about 94 m/s higher than values of V_S for the unimproved area at a depth of 1 m (226 m/s versus 132 m/s). Between depths of 2 m and 13 m, average values of V_S for the undensified and densified fill are 167 m/s and 192 m/s, respectively. In other words, values of V_S measured in saturated soils of the improved area are about 15% higher than values of V_S measured in the saturated soils of the unimproved area. This increase in V_S clearly shows the improvement to the site. At a depth of 13 m, the difference between V_S-values is about 7 m/s (193 m/s versus 186 m/s), clearly showing little, if any, improvement. The trend is similar to the measurements of V_R (see Figs. 3.13, 3.14 and 3.15). Also, the trend is similar to the values of N given in Figs. 3.16 and 3.17, and values of cone tip resistance given in Fig. 3.8. A depth of 13 m for no improvement agrees well with the reported depth of densification of 12 m.

Assembling the dispersion curves and V_S-profiles presented in Figs. 3.13 through 3.17 leads to the two-dimensional velocity profiles shown in Fig. 3.19. Fig. 3.19a was constructed by plotting the dispersion curves at the location midway between receivers. No corrections were made to the dispersion data to account for effects of receiver spacing or to make the spatial distribution of the data even. Fig. 3.19b was constructed by plotting the V_S-profiles at the center location of the test section shown in Fig. 3.12 and given in Appendix A. The lateral limits of the zone of vibrating probes shown in Fig. 3.19 are from construction drawings (see Fig. 3.5). The depth limit of the zone of vibrating probes is 12 m, and depth is roughly 1/3 to 1/2 times wavelength based on an empirical rule of thumb. Several test setups near the southern end of the improved area permit good resolution of the boundary separating densified and undensified sands. At the northern end of the improved area, however, the number of test setups are limited and the agreement between the velocity profiles and the lateral limit of vibrating probes is rather poor. Nevertheless, the zone of densified sand is clearly identified in both velocity profiles.

Since the process for obtaining dispersion curves is not computationally intensive, two-dimensional profiles, such as the one shown in Fig. 3.19a, could be completed during field testing. For the measurements presented in this report, field testing was completed within a 7 hour period. This time could be reduced once a routine is established. Thus, similar two-dimensional profiles with lengths of 500 m to 1000 m could be generated in a day.

The process used in this study for obtaining a single V_S-profile was computationally intensive, often requiring more than 8 hours of computer time to complete.

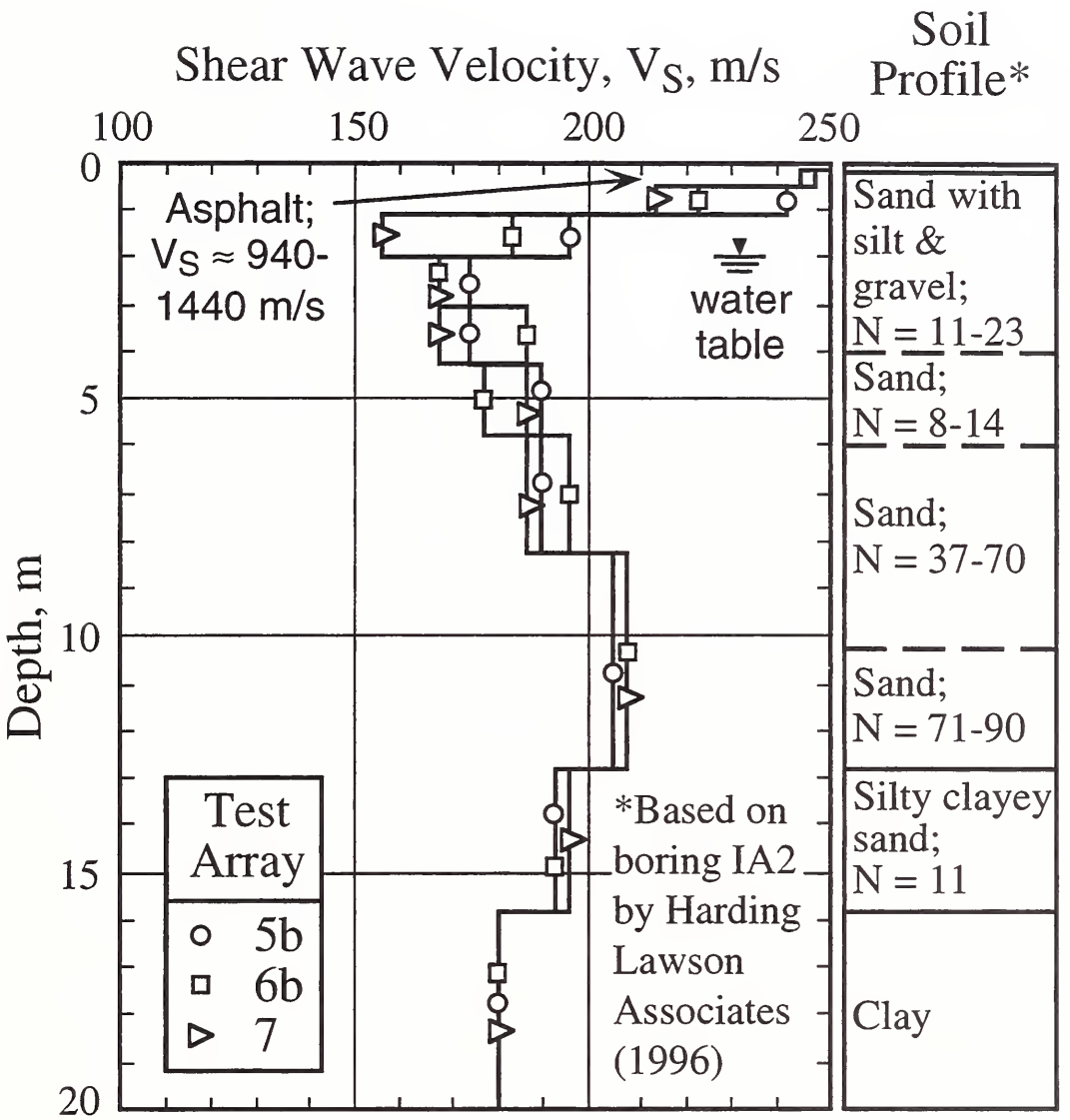

Fig. 3.16 - Three Shear Wave Velocity Profiles for SASW Tests Conducted in the Improved Area.

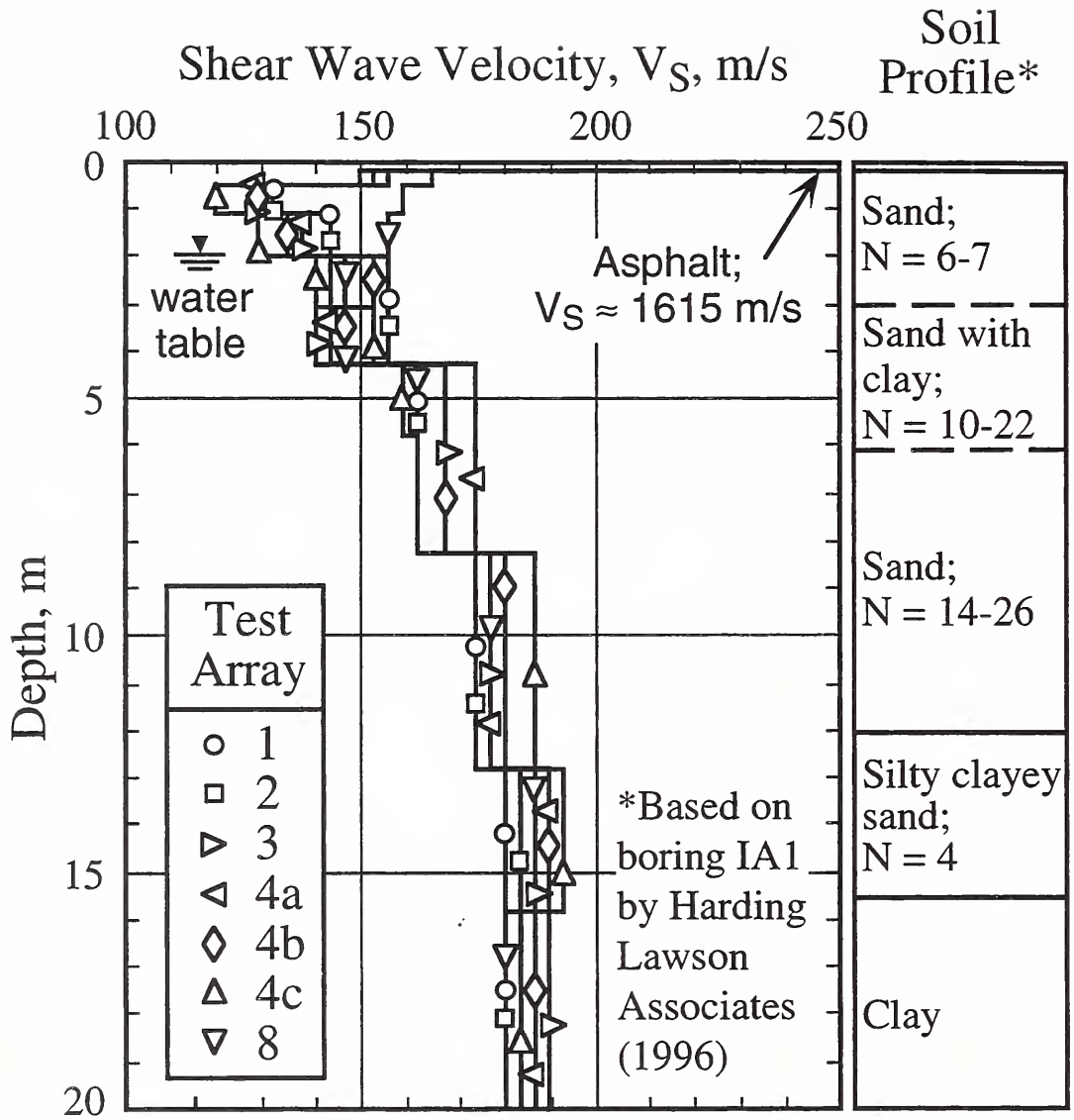

Fig. 3.17 - Seven Shear Wave Velocity Profiles for SASW Tests Conducted in the Unimproved Area.

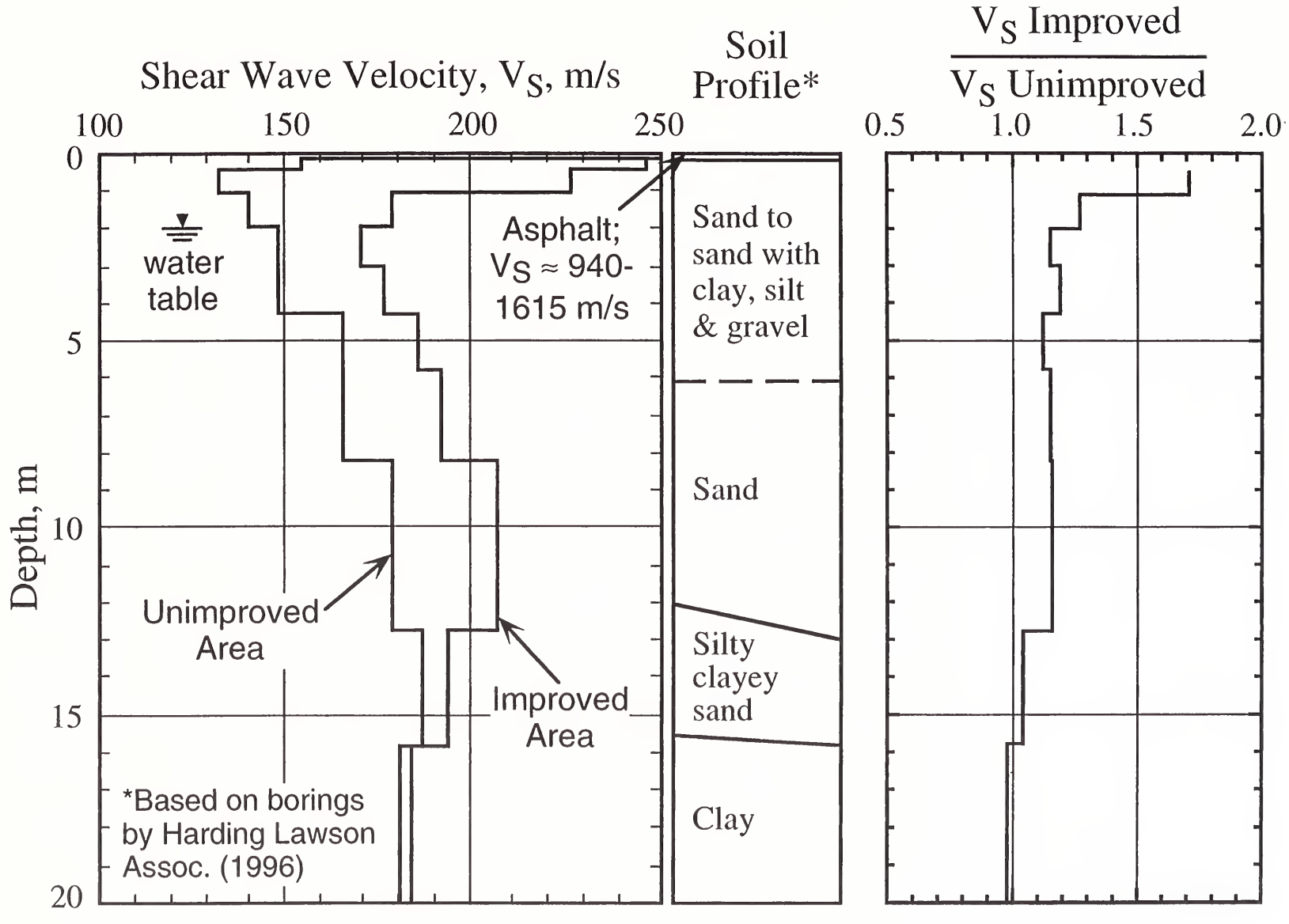

Fig. 3.18 - Comparison of Average Shear Wave Velocities Profiles Determined by SASW Testing for the Improved and Unimproved Areas.

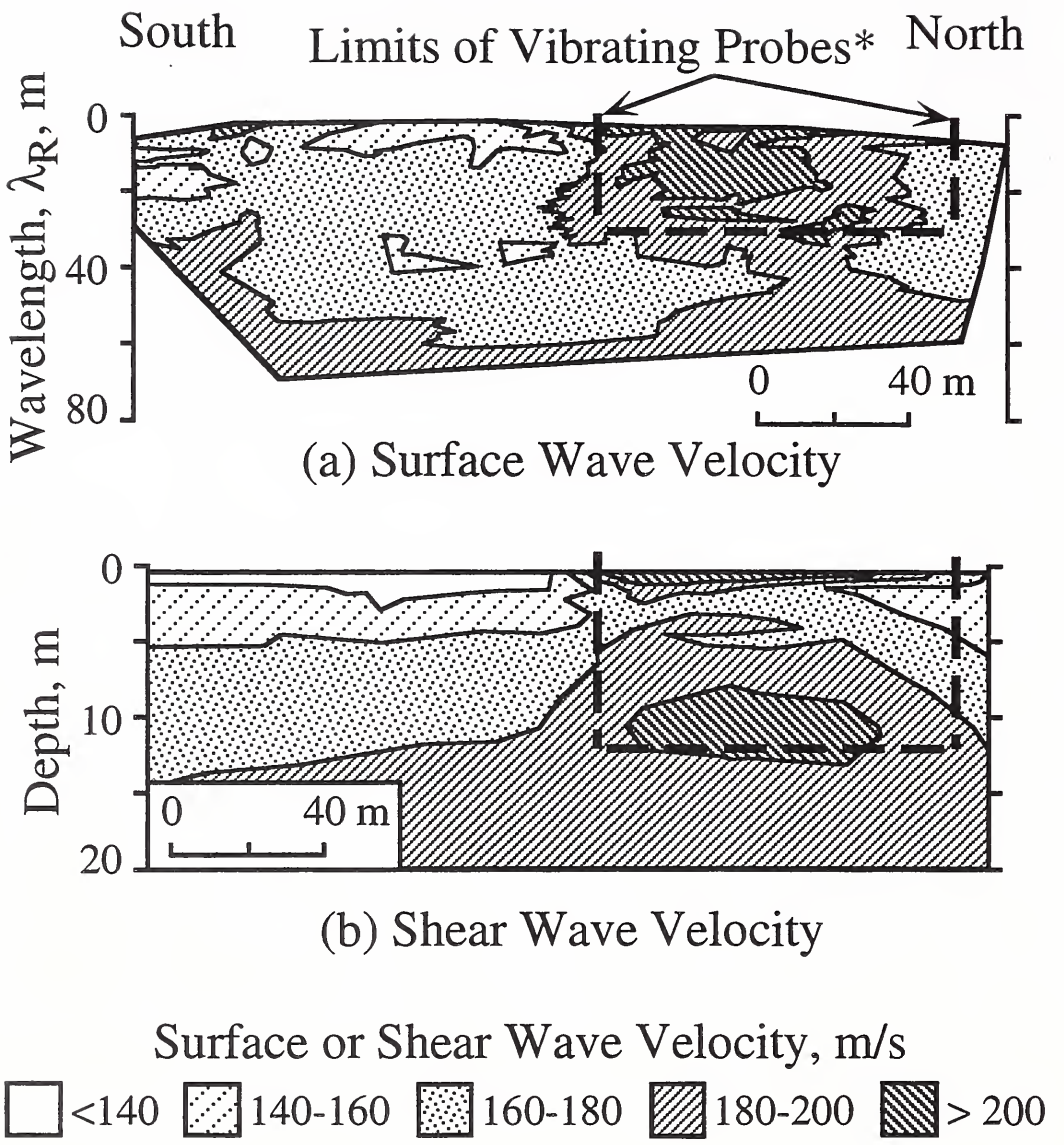

Fig. 3.19 - Two-dimensional Velocity Profiles Showing Zone of Improved Soil. (Note that the Amount of Data Used to Construct Profile Shown in Fig. 3.19a Decreases with Depth, see Figs. 3.13-3.15; and the Uncertainty of Profile Shown in Fig. 3.19b Increases with Depth, see Figs. 3.16-3.17.)

3.5 LIQUEFACTION ANALYSIS USING SIMPLIFIED PROCEDURES

As reviewed in a recent National Center for Earthquake Engineering Research (NCEER) workshop paper by Andrus and Stokoe (1997), several liquefaction assessment procedures based on V_S have been proposed during the past decade. Shown in Fig. 3.20 are five curves separating liquefaction and no liquefaction proposed by various researchers. These curves are based on correlations between shear wave velocity corrected to a reference overburden stress, V_{S1}, and a cyclic loading parameter called cyclic stress, or resistance, ratio. A discussion of these parameters will be given following this introduction. The curve by Tokimatsu et al. (1991) was developed from laboratory cyclic triaxial test results. The curves by Robertson et al. (1992), Kayen et al. (1992), and Lodge (1994) were developed from limited field performance data. The curve by the NCEER workshop was developed using liquefaction and non-liquefaction case histories from 20 earthquakes and over 50 sites in soils ranging from sandy gravel with cobbles to profiles including silty clay layers. This curve is considered to be a conservative bound for uncemented, Holocene-age soils with fines content (particles less than 75 μm) of 5% or less, since average values of V_{S1} for the critical layer were used in its development.

Shear wave velocity and penetration measurements from the Approach to Pier site provide an important opportunity for comparison between velocity- and penetration-based simplified liquefaction assessment procedures.

3.5.1 Liquefaction Assessment Based on V_{S1} and CSR

The procedure recommended by the NCEER workshop (Youd et al., 1997; Andrus and Stokoe, 1997) follows the general format of the penetration-based procedures, where penetration or V_S is correlated with a parameter called cyclic stress ratio. The cyclic stress ratio, CSR, at a particular depth in a level soil deposit can be expressed as (Seed and Idriss, 1971):

$$CSR = \tau_{av}/\sigma'_v = 0.65\ (a_{max}/g)\ (\sigma_v/\sigma'_v)\ r_d \qquad (3.1)$$

in which τ_{av} is average cyclic shear stress generated by the earthquake, a_{max} is maximum horizontal ground surface acceleration, σ'_v is initial effective vertical (overburden) stress, σ_v is total overburden stress, g is acceleration of gravity, and r_d is a shear stress reduction factor with a value less than 1. Based on a_{max} of 0.16 g and 0.11 g recorded in the x and y directions at the fire station during the Loma Prieta earthquake (Brady and Shakal, 1994), an average value of 0.14 g is assumed for the analyses. Overburden stresses are calculated using density measurements of fill materials from other locations on Treasure Island with similar depth and values of penetration and V_S. The density of the unimproved fill is about 1.76 Mg/m^3 above the water table, and 1.98 Mg/m^3 below the water table. For the improved fill, the density is about 1.92 Mg/m^3 above the water table, and 2.0-2.16 Mg/m^3 below the water table.

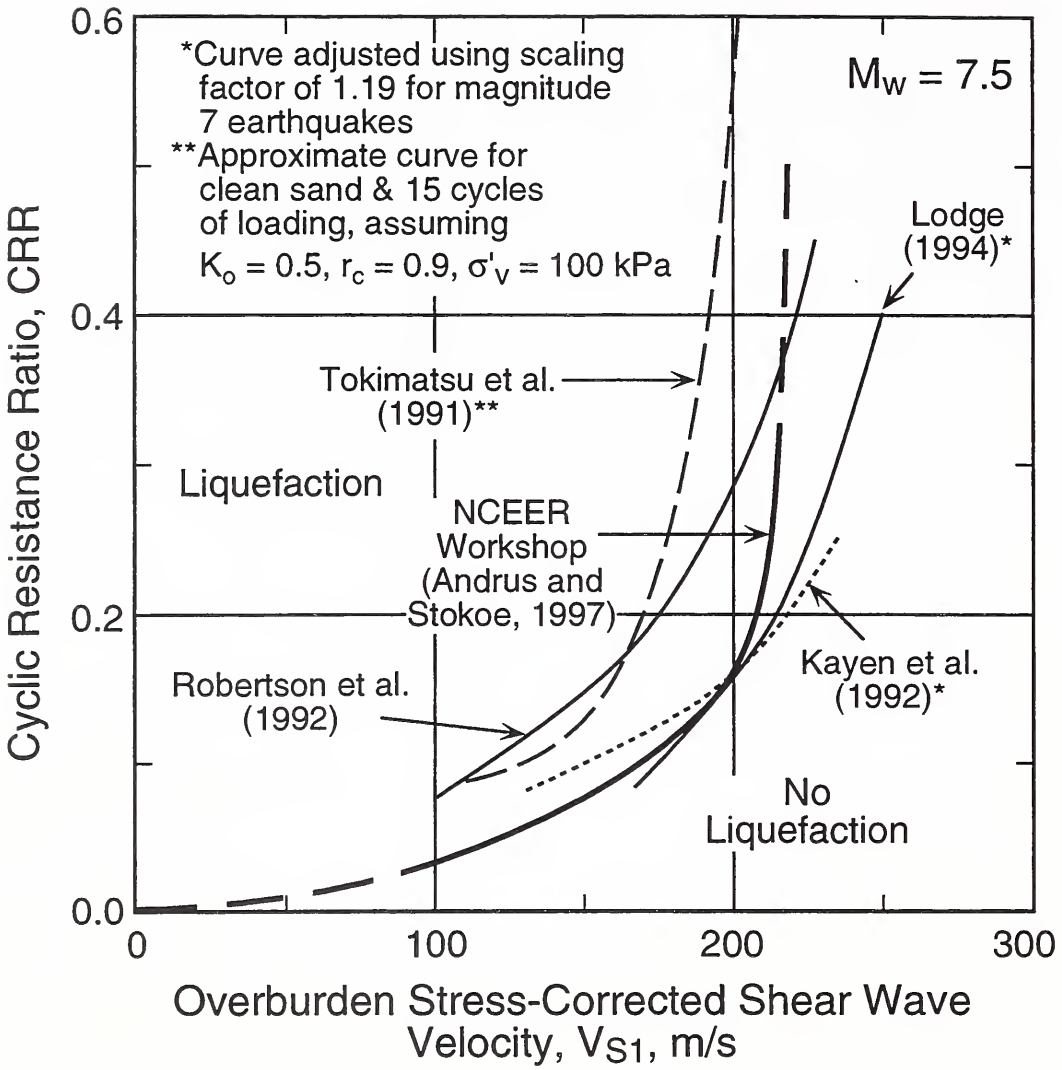

Fig. 3.20 - Comparison of Five Liquefaction Resistance Curves Based on Overburden Stress-Corrected Shear Wave Velocity. The Curve by the NCEER Workshop (Youd et al., 1997; Andrus and Stokoe, 1997) is for Uncemented Soils of Holocene Age with Fines Content Less than or Equal to 5%.

The shear wave velocity is corrected with respect to a reference overburden stress, P_a, by (Robertson et al., 1992):

$$V_{S1} = V_S (P_a/\sigma'_v)^{0.25} \quad (3.2)$$

where P_a is typically 100 kPa or approximately atmospheric pressure, and σ'_v is the effective overburden stress in kPa. Equation 3.2 ignores the effects of horizontal stress on V_S.

At Treasure Island, liquefaction in the unimproved soils most likely occurred where values of V_{S1} are least, and where values of cyclic stress ratio are greatest. These conditions occur between the depths of 6 m and 12 m.

Resistance to liquefaction can be approximated by (Andrus and Stokoe, 1997; modified from Dobry, 1996):

$$CRR = a(V_{S1}/100)^2 + b[1/(V_{S1c} - V_{S1}) - 1/V_{S1c}] \quad (3.3)$$

where CRR is the cyclic resistance ratio, V_{S1c} is the limiting value of V_{S1} which separates contractive and dilative behavior, and "a" and "b" are curve fitting parameters. The assumption of a limiting value of V_{S1} is equivalent to the assumption commonly made in the SPT-based procedure where liquefaction is considered not possible above a N-value of 30 (see Fig. 3.23). The relationship developed as part of the NCEER workshop for magnitude 7.5 earthquakes and clean sands is defined by V_{S1c} = 220 m/s, a = 0.03, and b = 0.9. For magnitude 7 earthquakes, Eq. 3.3 is multiplied by a scaling factor of about 1.25.

Using Eq. 3.3 with the above mentioned best-fit values, the curve separating liquefaction and no liquefaction for magnitude 7 earthquakes is shown in Fig. 3.21. Also plotted in Fig. 3.21 are values of V_{S1} and cyclic stress ratio for the critical layer. The data point for the improved area correctly lies in the region of no liquefaction defined by the curve. For the unimproved area, the data point lies on the curve. Thus, marginal liquefaction is correctly predicted for the unimproved area.

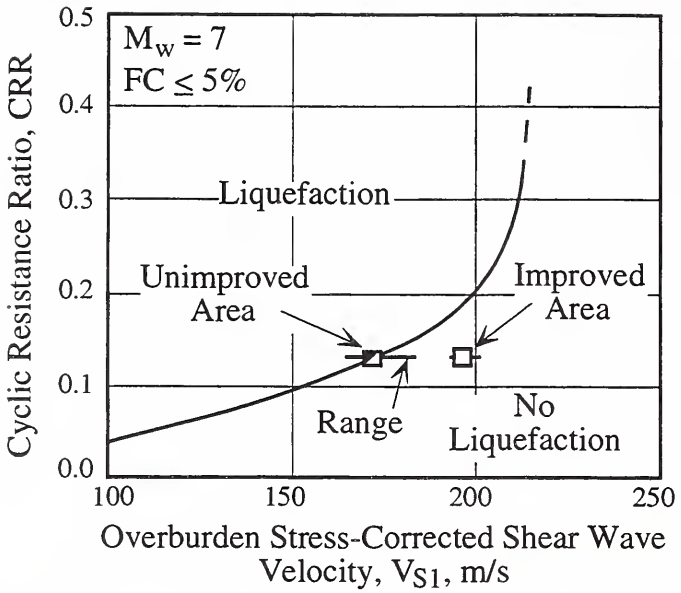

Fig. 3.21 - Comparison of the Liquefaction Assessment Chart Based on V_{S1} and CRR Recommended by NCEER Workshop (Youd et al., 1997; Andrus and Stokoe, 1997) for Clean Soils with Results from the Approach to Pier Site Between Depths of 6 m and 12 m.

3.5.2 Liquefaction Assessment Based on V_S and a_{max}

Another method relating liquefaction potential and V_S has evolved from the strain approach by Dobry et al. (1982) and analytical studies by Stokoe et al. (1988b). In this method liquefaction resistance is related to V_S and a_{max} directly. By combining Eqs. 3.1, 3.2 and 3.3, a relationship for magnitude 7.5 earthquakes based on V_S and a_{max} can be obtained in the form of (Andrus and Stokoe, 1997):

$$a_{max}/g = f_1\{a(f_2 V_S/100)^2 + b[1/(V_{S1c} - f_2 V_S) - 1/V_{S1c}]\} \quad (3.4)$$

where $f_1 = \sigma'_v/(0.65\ \sigma_v\ r_d)$ and $f_2 = (P_a/\sigma'_v)^{0.25}$. Assuming (1) the water table is located midway between the ground surface and the center of the most vulnerable layer and (2) the density of soil is 1.76 Mg/m^3 above the water table and 1.92 Mg/m^3 below the water table, then f_1 and f_2 can be approximated by:

$$f_1 \approx 1.1/r_d \quad (3.5)$$

and

$$f_2 \approx (7.3/z)^{0.25} \quad (3.6)$$

where z is the depth to the center of the most vulnerable layer in meters. Eqs. 3.4, 3.5, and 3.6 provide a simple relationship between V_S and a_{max} that depends on depth.

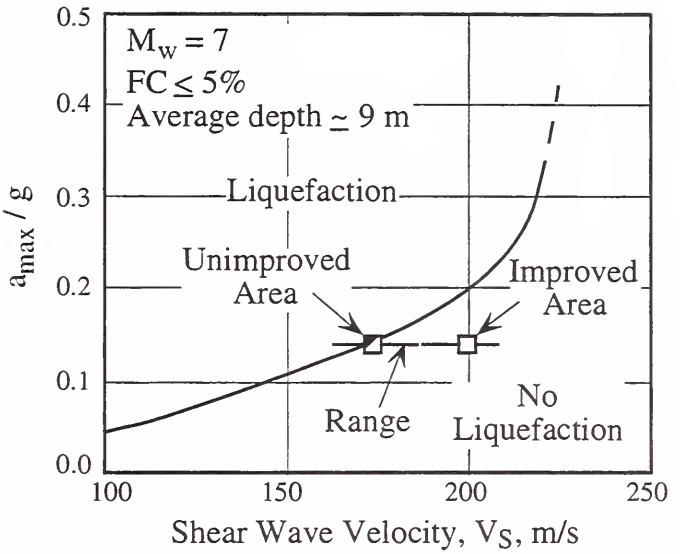

Fig. 3.22 - Comparison of Liquefaction Assessment Chart Based on V_S and a_{max} (Andrus and Stokoe, 1997) for Clean Soils with Results from the Approach to Pier Site Between Depths of 6 m and 12 m.

The curve for magnitude 7 earthquakes and depth of 9 m is shown in Fig. 3.22. Liquefaction behavior predicted by this method is similar to the method based on V_{S1} and CSR (see Fig. 3.21).

3.5.3 Liquefaction Assessment Based on $(N_1)_{60}$ and CSR

The most widely used simplified procedure for assessing liquefaction resistance is the procedure developed by the late Prof. H.B. Seed and his colleagues (1971, 1982, 1983, and 1985) based on modified SPT blow count. The NCEER sponsored workshop (Youd et al., 1997) reviewed the procedure and recommended some revisions. This updated procedure is applied here using the measured standard penetration resistances given in Figs. 3.16 and 3.17.

The measured standard penetration resistance, N_m, is modified to an equivalent clean-sand standard penetration resistance, $(N_1)_{60}$, by the following equation:

$$(N_1)_{60} = N_m C_N C_E C_B C_R C_S \qquad (3.7)$$

where C_N is a correction factor for overburden pressure, C_E is a correction factor for hammer energy ratio, C_B is a correction factor for borehole diameter, C_R is a correction factor for rod length, and C_S is a correction factor for samplers with or without liners. The overburden correction factor is commonly calculated by (Liao and Whitman, 1986):

$$C_N = (P_a/\sigma'_v)^{0.5} \tag{3.8}$$

where P_a is atmospheric pressure (about 100 kPa), and σ'_v is the effective overburden stress in kPa. The N_m-values given in Figs. 3.16 and 3.17 were measured by Harding Lawson Associates (1996) in a 150-mm borehole using a standard sampler with a 35 mm inside diameter not needing liners and a safety hammer. Typical correction factors for this equipment are: C_E = 1.0, C_B = 1.05, and C_S = 1.0. For the rod length correction, NCEER workshop recommended values of C_R are 0.95 for lengths of 6 m to 10 m, and 1.0 for lengths of 10 m to 20 m (Youd et al., 1997).

Plotted in Fig. 3.23 are $(N_1)_{60}$-values and cyclic stress ratios for the critical layer between depths of 6 m and 12 m. Also plotted is the boundary separating liquefaction and no liquefaction recommended for magnitude 7 earthquakes by the NCEER workshop (Youd et al., 1997), assuming a magnitude scaling factor of 1.25. The data for the improved area correctly lie in the region of no liquefaction. At an average modified blow count of 54 and a minimum modified blow count of 41, these data points lie well above the critical value of 30 suggested by Seed et al. (1985), as shown in Fig. 3.23.

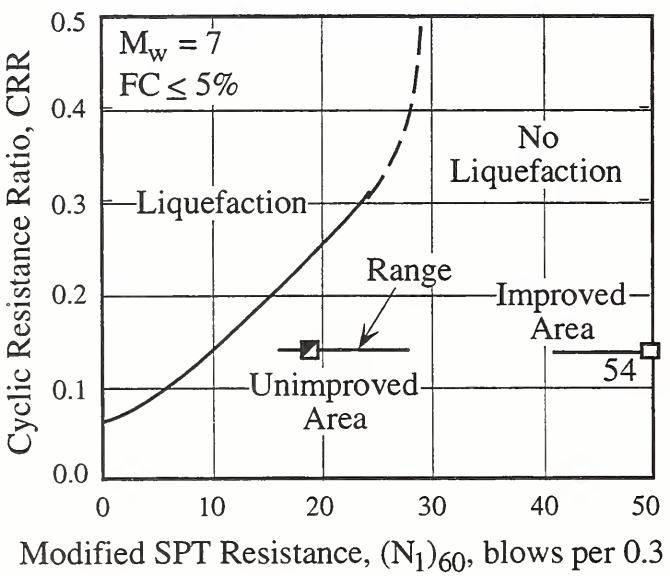

Fig. 3.23 - Comparison of Liquefaction Assessment Chart Based on $(N_1)_{60}$ and CSR Recommended by the NCEER Workshop (Youd et al., 1997; modified from Seed et al., 1985) for Clean Sands with Results from the Approach to Pier Site, Borings IA1 and IA2 Between Depths of 6 m and 12 m.

For the unimproved area, the average and minimum values of $(N_1)_{60}$ also lie in the region of predicted no liquefaction. With boring BH-IA1 located close to a sinkhole (see Figs. 3.2 and 3.9), a prediction of no liquefaction appears to be inconsistent with field behavior. One possible explanation for this inconsistency is that liquefaction was localized or marginal at this site. In the original chart by Seed et al. (1985) and in a later chart by Youd and Noble (1997), there are a few reported liquefaction and marginal liquefaction case histories that plot in the region of no liquefaction. Another explanation is that the ground shaking caused the soil to settle and densify, resulting in higher post-earthquake penetration and velocity measurements.

3.5.4 Liquefaction Assessment Based on q_{c1N} and CSR

In recent years, the Cone Penetration Test (CPT) has become popular due to its greater repeatability and nearly continuous profile. The abundance of field performance data has lead to the development of various liquefaction assessment procedures. These procedures were reviewed during a recent NCEER workshop (Youd et al., 1997; Robertson and Wride, 1997; Olsen, 1997). The procedure recommended by the workshop is applied here using the CPT profiles listed in Figs. 3.7 and 3.8.

The measured cone penetration tip resistance, q_c, is corrected and normalized by the following equation:

$$q_{c1N} = C_Q (q_c/P_a) \tag{3.9}$$

where

$$C_Q = (P_a/\sigma'_v)^n \tag{3.10}$$

C_Q is a correction factor for overburden pressure, P_a is atmospheric pressure (about 100 kPa), and n is an exponent dependent on grain size characteristics of the soil. A typical value of n is 0.5 for clean sands.

Plotted in Fig. 3.24 are average q_{c1N}-values and cyclic stress ratios for the critical layer between depths of 6 m and 12 m. Also plotted is the boundary separating liquefaction and no liquefaction recommended by the NCEER workshop (Youd et al., 1997) for magnitude 7 earthquakes, assuming a magnitude scaling factor of 1.25. The data for the improved area correctly lie in the region of no liquefaction.

For the unimproved area, the average values of q_{c1N} also lie in the region of predicted no liquefaction, with the exception of one lying on the curve. Thus, marginal to no liquefaction is predicted. A prediction of marginal to no liquefaction is in between the predictions obtained by the SPT- and V_S-based procedures (see Figs. 3.21, 3.22 and 3.23).

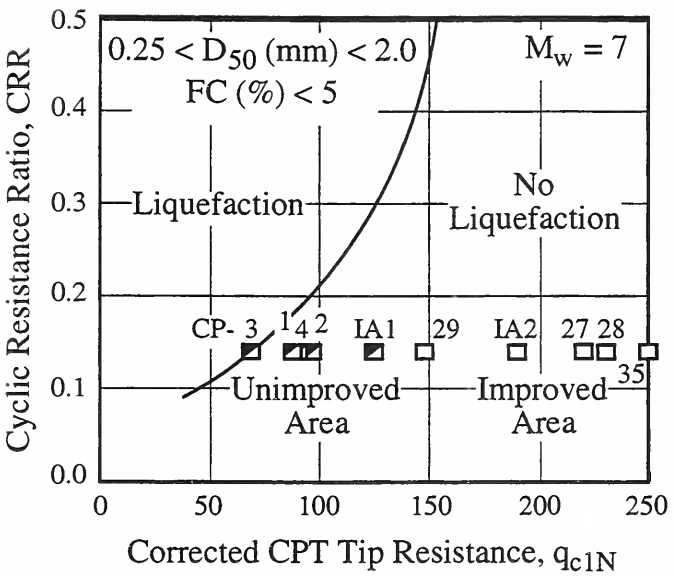

Fig. 3.24 - Comparison of Liquefaction Assessment Chart Based on q_{c1N} and CSR Recommended by the NCEER Workshop (Youd et al., 1997; after Robertson and Wride, 1997) with Results from the Approach to Pier Site Between Depths of 6 m and 12 m.

CHAPTER 4

SUMMARY AND RECOMMENDATIONS

4.1 SUMMARY

SASW tests were conducted along a 240 m-long alignment at the Treasure Island Approach to Pier site using a seismic vibrator as principal source with receiver spacings ranging from 7.6 m to 76 m. Additional tests were conducted at smaller spacings to characterize near-surface layers using hand-held hammers and dropped weights as the sources. Shear wave velocity profiles were determined from the SASW field data by forward modeling using a computer model with three-dimensional wave propagation.

The zone of densified sand adjacent to Pier 1 at Treasure Island was correctly identified in V_R-curves and V_S-profiles obtained from SASW tests. Shear wave velocities determined for the improved soil zone averaged about 25 m/s greater than shear wave velocities determined for the unimproved zones. This represents a 15% increase in shear wave velocity due to soil improvement. Two liquefaction assessment procedures based on V_S correctly predicted no liquefaction for the improved area, and marginal liquefaction for the unimproved area. Although less conservative, liquefaction assessment procedures based on the SPT and CPT provide similar predictions.

This study further supports the usefulness of in situ V_S for predicting liquefaction potential, and demonstrates the potential of the SASW test method for rapid delineation of weak soil layers. For large study areas, a cost-effective investigation program might be to first develop curves, or profiles, of V_R in the field (assuming an approximate sampling depth equal to $\lambda_R/3$ to $\lambda_R/2$). The V_R-profiles would then be used to select locations for determining V_S-profiles, which require a large computational effort, and sites for borehole sampling and penetration testing.

4.2 RECOMMENDATIONS FOR FUTURE STUDY

The following recommendations are provided to identify areas that need further study.

1. Develop a better measure of goodness of fit between the experimental and theoretical dispersion curves. The maximum likelihood method formulation used in this study calculated the root mean square error between dispersion curves. However, this parameter depends on the number and spacing of averaged experimental dispersion curve points. A change in the spacing of averaged experimental dispersion curve points in the asphalt layer can significantly change the value of the root mean square error.

2. Develop/improve procedures for quantifying uncertainty in SASW measurements. Current analytical procedures used to estimate uncertainty are dependent upon the variables of the starting model. It would be useful to know what the absolute standard deviation, or variance, is for the V_S-profiles.

3. Determine the minimal layer thickness that can be accurately resolved at depth. This study showed that thick layers with different stiffnesses can be delineated by the SASW test. However, it would be useful to know what the minimal layer thickness that can be accurately resolved with an uncertainty in V_S of $\pm 5\%$ at a depth of say 10 m.

4. Compare inversion and forward modeling computer models developed by various researchers for determining V_S-profiles from surface wave measurements. These V_S-profiles should then be compared with profiles measured by other seismic methods.

5. Conduct crosshole and other seismic tests at the Approach to Pier site to compare with shear wave velocity profiles determined from SASW testing.

6. Develop general guidelines for estimating uncertainty in SASW V_S-profiles.

7. Compile additional liquefaction and no liquefaction case histories where SASW tests have been performed.

APPENDIX A

SHEAR WAVE VELOCITY PROFILES BASED ON SASW TESTS

AT APPROACH TO PIER SITE

ON TREASURE ISLAND, CALIFORNIA

March 23-24, 1996

Table A.1 - Shear Wave Velocity Profile Data from SASW Tests at Approach to Pier Site.

Layer No.	Layer Thickness (m)	Layer Depth (m)	Assumed Values: P-Wave Velocity (m/s)	Assumed Values: Poisson's Ratio	Assumed Values: Density (Mg/m^3)	Assumed Values: Damping	Estimated S-Wave Velocity[a] (m/s)
(a) Test Array SA-1 (unimproved area; STA 0+00 m to STA 0+30 m)							
1	0.16	0.00 to 0.16	----	0.20	1.92	0.02	1615
2	0.3	0.16 to 0.5	----	0.33	1.76	0.02	152
3	0.6	0.5 to 1.1	----	0.33	1.76	0.02	131
4	0.9	1.1 to 2.0	----	0.33	1.76	0.02	143
5	2.3	2.0 to 4.3	1524	----	1.92	0.02	155
6	3.9	4.3 to 8.2	1524	----	1.92	0.02	162
7	4.6	8.2 to 12.8	1524	----	1.92	0.02	174
8	3.0	12.8 to 15.8	1523	----	1.92	0.02	180
9	11.6	15.8 to 27.4	1524	----	1.92	0.02	180
10	15.2	27.4 to 42.7	1524	----	1.92	0.02	168
11	42.7	42.7 to 85.3	1524	----	1.92	0.02	274
12	----	Half-space	----	0.33	1.92	0.02	1829[b]
(b) Test Array SA-2 (unimproved area; STA 0+30 m to STA 0+60 m)							
1	0.16	0.00 to 0.16	----	0.20	1.92	0.02	1615
2	0.3	0.16 to 0.5	----	0.33	1.76	0.02	152
3	0.6	0.5 to 1.1	----	0.33	1.76	0.02	131
4	0.9	1.1 to 2.0	----	0.33	1.76	0.02	143
5	2.3	2.0 to 4.3	1524	----	1.92	0.02	155
6	3.9	4.3 to 8.2	1524	----	1.92	0.02	162
7	4.6	8.2 to 12.8	1524	----	1.92	0.02	174
8	3.0	12.8 to 15.8	1523	----	1.92	0.02	183
9	11.6	15.8 to 27.4	1524	----	1.92	0.02	180
10	15.2	27.4 to 42.7	1524	----	1.92	0.02	168
11	42.7	42.7 to 85.3	1524	----	1.92	0.02	274
12	----	Half-space	----	0.33	1.92	0.02	1829[b]
(c) Test Array SA-3 (unimproved area; STA 0+60 m to STA 0+90 m)							
1	0.16	0.00 to 0.16	----	0.20	1.92	0.02	1615
2	0.3	0.16 to 0.5	----	0.33	1.76	0.02	155
3	0.6	0.5 to 1.1	----	0.33	1.76	0.02	128
4	0.9	1.1 to 2.0	----	0.33	1.76	0.02	137
5	2.3	2.0 to 4.3	1524	----	1.92	0.02	140
6	3.9	4.3 to 8.2	1524	----	1.92	0.02	168
7	4.6	8.2 to 12.8	1524	----	1.92	0.02	177
8	3.0	12.8 to 15.8	1523	----	1.92	0.02	186
9	11.6	15.8 to 27.4	1524	----	1.92	0.02	189
10	15.2	27.4 to 42.7	1524	----	1.92	0.02	162
11	42.7	42.7 to 85.3	1524	----	1.92	0.02	271
12	----	Half-space	----	0.33	1.92	0.02	1829[b]

[a]Based on 3-D computer model described by Röesset et al. (1991) and maximum likelihood method formulation by Joh (1996).

[b]Assumed value, based on shear wave velocities measured in the Franciscan bedrock at the fire station and on Yerba Buena Island (de Alba and Faris, 1996b).

Table A.1 (cont.) - Shear Wave Velocity Profile Data from SASW Tests at Approach to Pier Site.

Layer No.	Layer Thickness (m)	Layer Depth (m)	Assumed Values: P-Wave Velocity (m/s)	Assumed Values: Poisson's Ratio	Assumed Values: Density (Mg/m^3)	Assumed Values: Damping	Estimated S-Wave Velocity[a] (m/s)
(d) Test Array SA-4a (unimproved area; STA 0+90 m to STA 1+20 m)							
1	0.16	0.00 to 0.16	----	0.20	1.92	0.02	1615
2	0.3	0.16 to 0.5	----	0.33	1.76	0.02	149
3	0.6	0.5 to 1.1	----	0.33	1.76	0.02	128
4	0.9	1.1 to 2.0	----	0.33	1.76	0.02	137
5	2.3	2.0 to 4.3	1524	----	1.92	0.02	143
6	3.9	4.3 to 8.2	1524	----	1.92	0.02	174
7	4.6	8.2 to 12.8	1524	----	1.92	0.02	177
8	3.0	12.8 to 15.8	1523	----	1.92	0.02	189
9	11.6	15.8 to 27.4	1524	----	1.92	0.02	186
10	15.2	27.4 to 42.7	1524	----	1.92	0.02	165
11	42.7	42.7 to 85.3	1524	----	1.92	0.02	271
12	----	Half-space	----	0.33	1.92	0.02	1829[b]
(e) Test Array SA-4b (unimproved area; STA 1+03 m to STA 1+33 m)							
1	0.16	0.00 to 0.16	----	0.20	1.92	0.02	1615
2	0.3	0.16 to 0.5	----	0.33	1.76	0.02	155
3	0.6	0.5 to 1.1	----	0.33	1.76	0.02	128
4	0.9	1.1 to 2.0	----	0.33	1.76	0.02	134
5	1.1	2.0 to 3.0	1524	----	1.92	0.02	152
6	1.2	3.0 to 4.3	1524	----	1.92	0.02	146
7	1.5	4.3 to 5.8	1524	----	1.92	0.02	168
8	2.4	5.8 to 8.2	1523	----	1.92	0.02	168
9	4.6	8.2 to 12.8	1524	----	1.92	0.02	180
10	3.0	12.8 to 15.8	1524	----	1.92	0.02	189
11	11.6	15.8 to 27.4	1524	----	1.92	0.02	186
12	15.2	27.4 to 42.7	1524	----	1.92	0.02	165
13	42.7	42.7 to 85.3	1524	----	1.92	0.02	271
14	----	Half-space	----	0.33	1.92	0.02	1829[b]

[a]Based on 3-D computer model described by Röesset et al. (1991) and maximum likelihood method formulation by Joh (1996).

[b]Assumed value, based on shear wave velocities measured in the Franciscan bedrock at the fire station and on Yerba Buena Island (de Alba and Faris, 1996b).

Table A.1 (cont.) - Shear Wave Velocity Profile Data from SASW Tests at Approach to Pier Site.

Layer No.	Layer Thickness (m)	Layer Depth (m)	Assumed Values: P-Wave Velocity (m/s)	Assumed Values: Poisson's Ratio	Assumed Values: Density (Mg/m^3)	Assumed Values: Damping	Estimated S-Wave Velocity[a] (m/s)
(f) Test Array SA-4c (unimproved area; STA 1+03 m to STA 1+33 m; offset 6.1 m towards bay, see Figure 3.2)							
1	0.16	0.00 to 0.16	—	0.20	1.92	0.02	1615
2	0.3	0.16 to 0.5	—	0.33	1.76	0.02	149
3	0.6	0.5 to 1.1	—	0.33	1.76	0.02	119
4	0.9	1.1 to 2.0	—	0.33	1.76	0.02	128
5	1.1	2.0 to 3.0	1524	—	1.92	0.02	140
6	1.2	3.0 to 4.3	1524	—	1.92	0.02	153
7	1.5	4.3 to 5.8	1524	—	1.92	0.02	158
8	2.4	5.8 to 8.2	1523	—	1.92	0.02	162
9	4.6	8.2 to 12.8	1524	—	1.92	0.02	186
10	3.0	12.8 to 15.8	1524	—	1.92	0.02	192
11	11.6	15.8 to 27.4	1524	—	1.92	0.02	183
12	15.2	27.4 to 42.7	1524	—	1.92	0.02	165
13	42.7	42.7 to 85.3	1524	—	1.92	0.02	274
14	—	Half-space	—	0.33	1.92	0.02	1829[b]
(g) Test Array SA-5b (improved area; STA 1+20 m to STA 1+50 m)							
1	0.05	0.00 to 0.05	—	0.20	1.92	0.02	1439
2	0.04	0.05 to 0.09	—	0.20	1.92	0.02	945
3	0.06	0.09 to 0.15	—	0.20	1.92	0.02	512
4	0.3	0.15 to 0.5	—	0.33	1.76	0.02	244
5	0.6	0.5 to 1.1	—	0.33	1.76	0.02	241
6	0.9	1.1 to 2.0	—	0.33	1.76	0.02	195
7	2.3	2.0 to 4.3	1524	—	1.92	0.02	174
8	3.9	4.3 to 8.2	1523	—	1.92	0.02	189
9	4.6	8.2 to 12.8	1524	—	1.92	0.02	204
10	3.0	12.8 to 15.8	1524	—	1.92	0.02	192
11	11.6	15.8 to 27.4	1524	—	1.92	0.02	180
12	15.2	27.4 to 42.7	1524	—	1.92	0.02	177
13	42.7	42.7 to 85.3	1524	—	1.92	0.02	286
14	—	Half-space	—	0.33	1.92	0.02	1829[b]

[a]Based on 3-D computer model described by Röesset et al. (1991) and maximum likelihood method formulation by Joh (1996).

[b]Assumed value, based on shear wave velocities measured in the Franciscan bedrock at the fire station and on Yerba Buena Island (de Alba and Faris, 1996b).

Table A.1 (cont.) - Shear Wave Velocity Profile Data from SASW Tests at Approach to Pier Site.

Layer No.	Layer Thickness (m)	Layer Depth (m)	Assumed Values: P-Wave Velocity (m/s)	Assumed Values: Poisson's Ratio	Assumed Values: Density (Mg/m^3)	Assumed Values: Damping	Estimated S-Wave Velocity[a] (m/s)
(h) Test Array SA-6 (improved area; STA 1+50 m to STA 1+80 m)							
1	0.05	0.00 to 0.05	—	0.20	1.92	0.02	1439
2	0.04	0.05 to 0.09	—	0.20	1.92	0.02	945
3	0.06	0.09 to 0.15	—	0.20	1.92	0.02	512
4	0.3	0.15 to 0.5	—	0.33	1.76	0.02	244
5	0.6	0.5 to 1.1	—	0.33	1.76	0.02	222
6	0.9	1.1 to 2.0	—	0.33	1.76	0.02	183
7	1.1	2.0 to 3.0	1524	—	1.92	0.02	168
8	1.2	3.0 to 4.3	1523	—	1.92	0.02	186
9	1.5	4.3 to 5.8	1524	—	1.92	0.02	177
10	2.4	5.8 to 8.2	1524	—	1.92	0.02	195
11	4.6	8.2 to 12.8	1524	—	1.92	0.02	207
12	3.0	12.8 to 15.8	1524	—	1.92	0.02	192
13	11.6	15.8 to 27.4	1524	—	1.92	0.02	180
14	15.2	27.4 to 42.7	1524	—	1.92	0.02	177
15	42.7	42.7 to 85.3	1524	—	1.92	0.02	286
16	—	Half-space	—	0.33	1.92	0.02	1829[b]
(i) Test Array SA-7 (improved area; STA 1+80 m to STA 2+10 m)							
1	0.05	0.00 to 0.05	—	0.20	1.92	0.02	1439
2	0.04	0.05 to 0.09	—	0.20	1.92	0.02	945
3	0.06	0.09 to 0.15	—	0.20	1.92	0.02	512
4	0.3	0.15 to 0.5	—	0.33	1.76	0.02	247
5	0.6	0.5 to 1.1	—	0.33	1.76	0.02	213
6	0.9	1.1 to 2.0	—	0.33	1.76	0.02	155
7	2.3	2.0 to 4.3	1524	—	1.92	0.02	168
8	3.9	4.3 to 8.2	1523	—	1.92	0.02	186
9	4.6	8.2 to 12.8	1524	—	1.92	0.02	207
10	3.0	12.8 to 15.8	1524	—	1.92	0.02	195
11	11.6	15.8 to 27.4	1524	—	1.92	0.02	180
12	15.2	27.4 to 42.7	1524	—	1.92	0.02	180
13	42.7	42.7 to 85.3	1524	—	1.92	0.02	283
14	—	Half-space	—	0.33	1.92	0.02	1829[b]

[a]Based on 3-D computer model described by Röesset et al. (1991) and maximum likelihood method formulation by Joh (1996).

[b]Assumed value, based on shear wave velocities measured in the Franciscan bedrock at the fire station and on Yerba Buena Island (de Alba and Faris, 1996b).

Table A.1 (cont.) - Shear Wave Velocity Profile Data from SASW Tests at Approach to Pier Site.

Layer No.	Layer Thickness (m)	Layer Depth (m)	Assumed Values: P-Wave Velocity (m/s)	Assumed Values: Poisson's Ratio	Assumed Values: Density (Mg/m^3)	Assumed Values: Damping	Estimated S-Wave Velocity[a] (m/s)
(j) Test Array SA-8 (unimproved area; STA 2+10 m to STA 2+40 m)							
1	0.16	0.00 to 0.16	-----	0.20	1.92	0.02	1615
2	0.3	0.16 to 0.5	-----	0.33	1.76	0.02	165
3	0.6	0.5 to 1.1	-----	0.33	1.76	0.02	158
4	0.9	1.1 to 2.0	-----	0.33	1.76	0.02	155
5	2.3	2.0 to 4.3	1524	-----	1.92	0.02	146
6	3.9	4.3 to 8.2	1524	-----	1.92	0.02	162
7	4.6	8.2 to 12.8	1524	-----	1.92	0.02	177
8	3.0	12.8 to 15.8	1523	-----	1.92	0.02	186
9	11.6	15.8 to 27.4	1524	-----	1.92	0.02	180
10	15.2	27.4 to 42.7	1524	-----	1.92	0.02	177
11	42.7	42.7 to 85.3	1524	-----	1.92	0.02	290
12	-----	Half-space	-----	0.33	1.92	0.02	1829[b]

[a]Based on 3-D computer model described by Röesset et al. (1991) and maximum likelihood method formulation by Joh (1996).

[b]Assumed value, based on shear wave velocities measured in the Franciscan bedrock at the fire station and on Yerba Buena Island (de Alba and Faris, 1996b).

APPENDIX B

DISPERSION CURVES FOR SASW TESTS

AT APPROACH TO PIER SITE

ON TREASURE ISLAND, CALIFORNIA

March 23-24, 1996

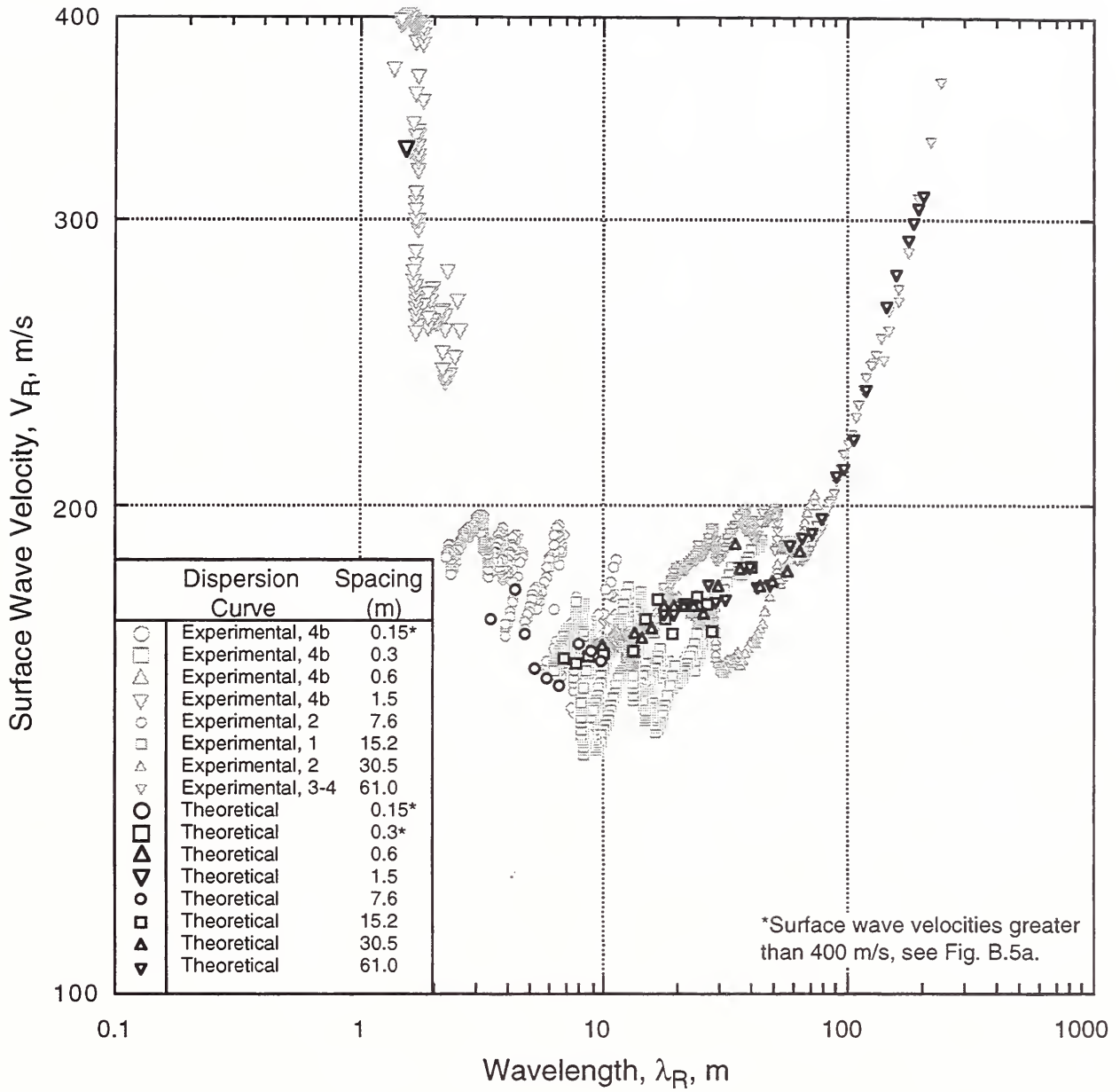

Fig. B.1 - Comparison of Experimental and Theoretical SASW Dispersion Curves for the Treasure Island Approach to Pier Site, Test Array SA-1. (Note that Test Array SA-1 Lies Outside the Improved Area.)

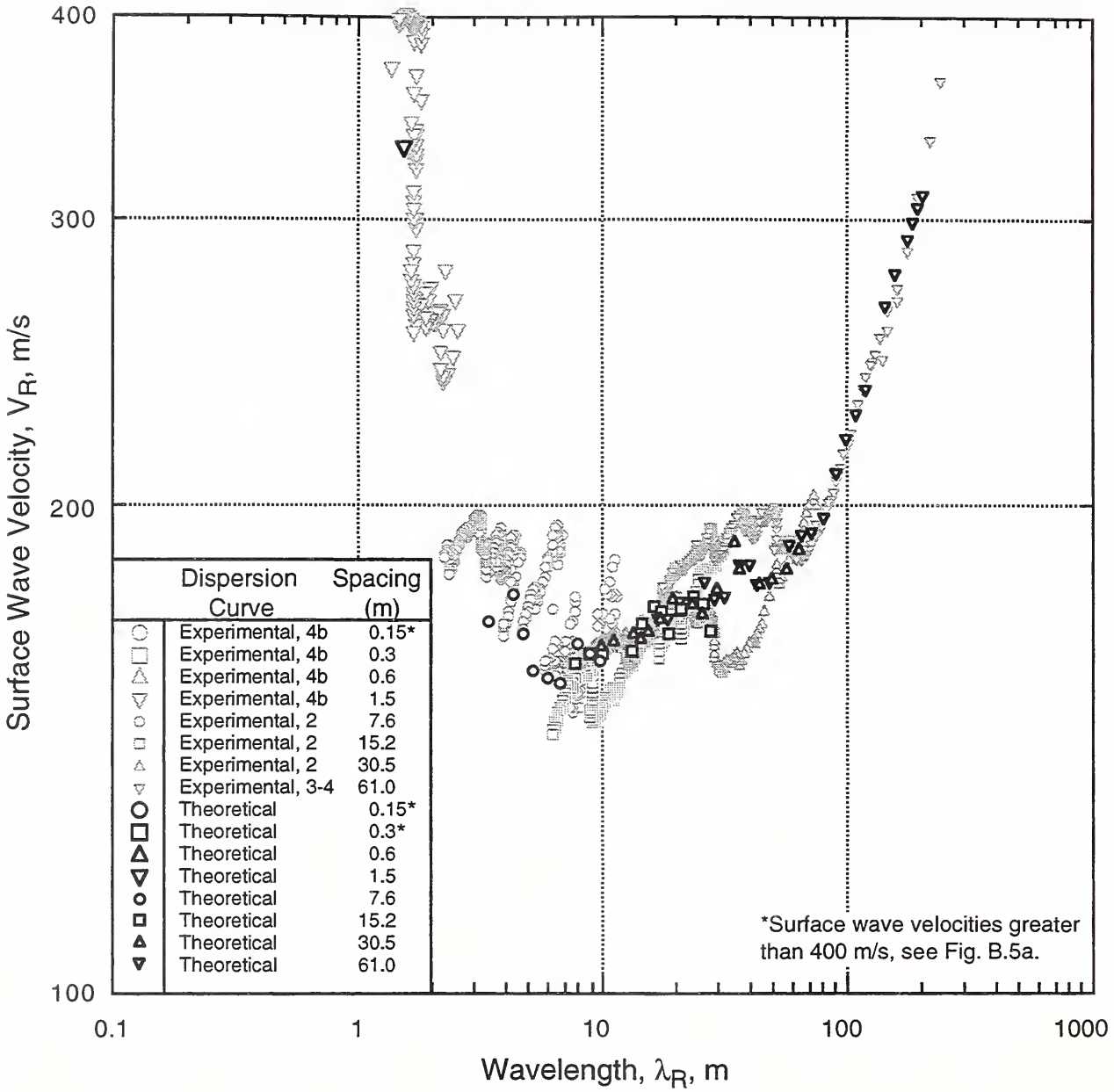

Fig. B.2 - Comparison of Experimental and Theoretical SASW Dispersion Curves for the Treasure Island Approach to Pier Site, Test Array SA-2. (Note that Test Array SA-2 Lies Outside the Improved Area.)

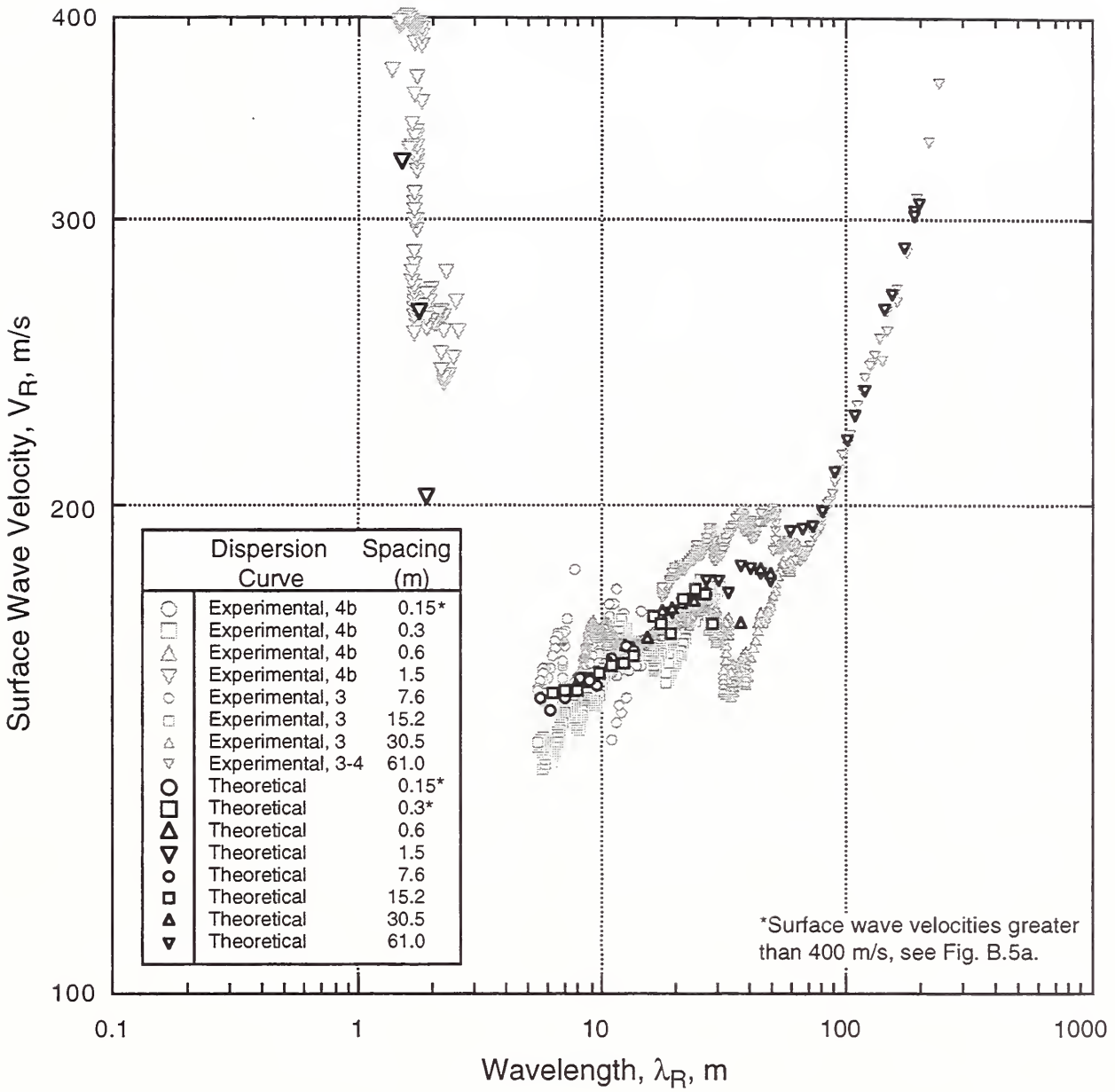

Fig. B.3 - Comparison of Experimental and Theoretical SASW Dispersion Curves for the Treasure Island Approach to Pier Site, Test Array SA-3. (Note that Test Array SA-3 Lies Outside the Improved Area.)

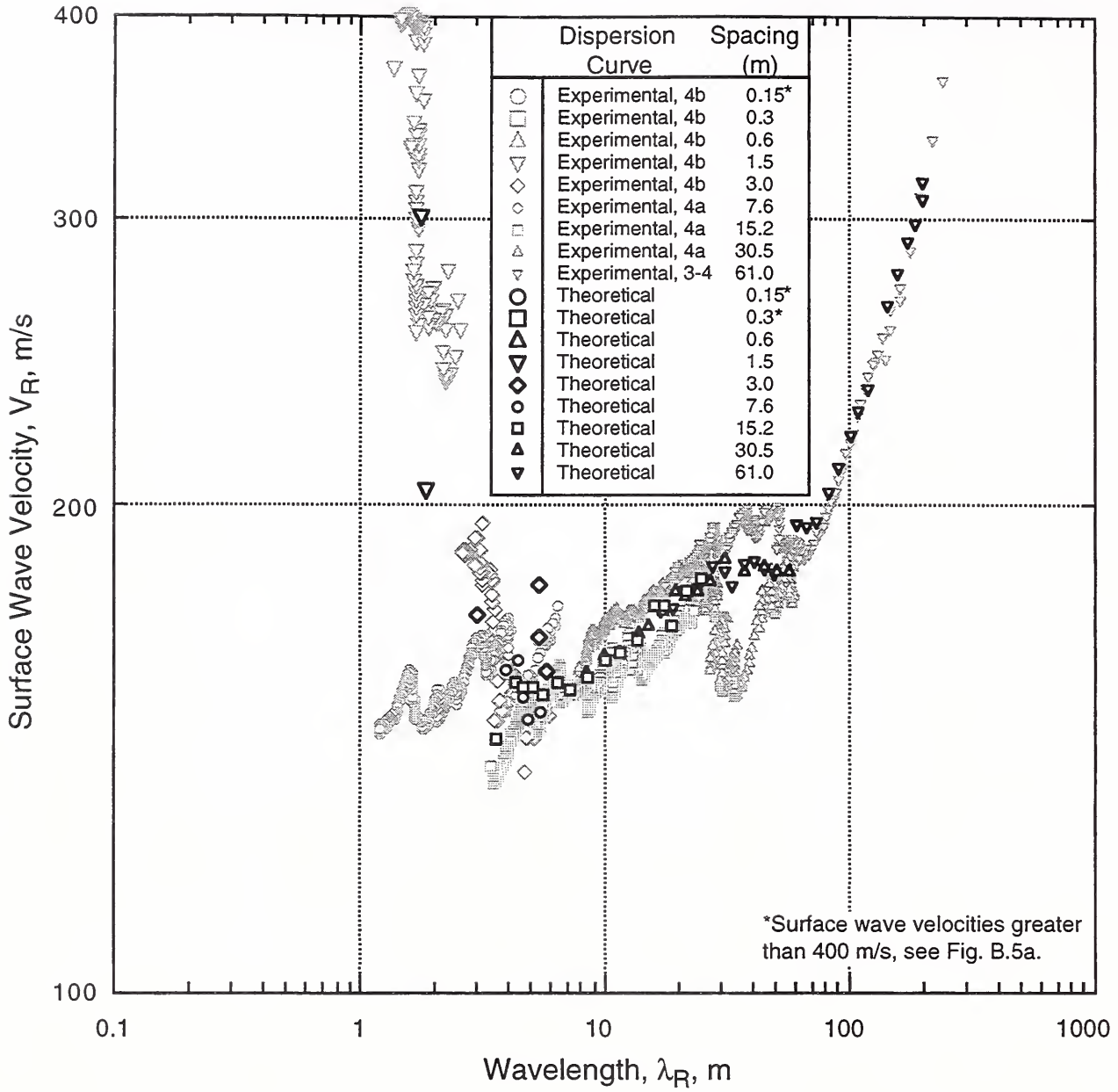

Fig. B.4 - Comparison of Experimental and Theoretical SASW Dispersion Curves for the Treasure Island Approach to Pier Site, Test Array SA-4a. (Note that Test Array SA-4a Lies Outside the Improved Area.)

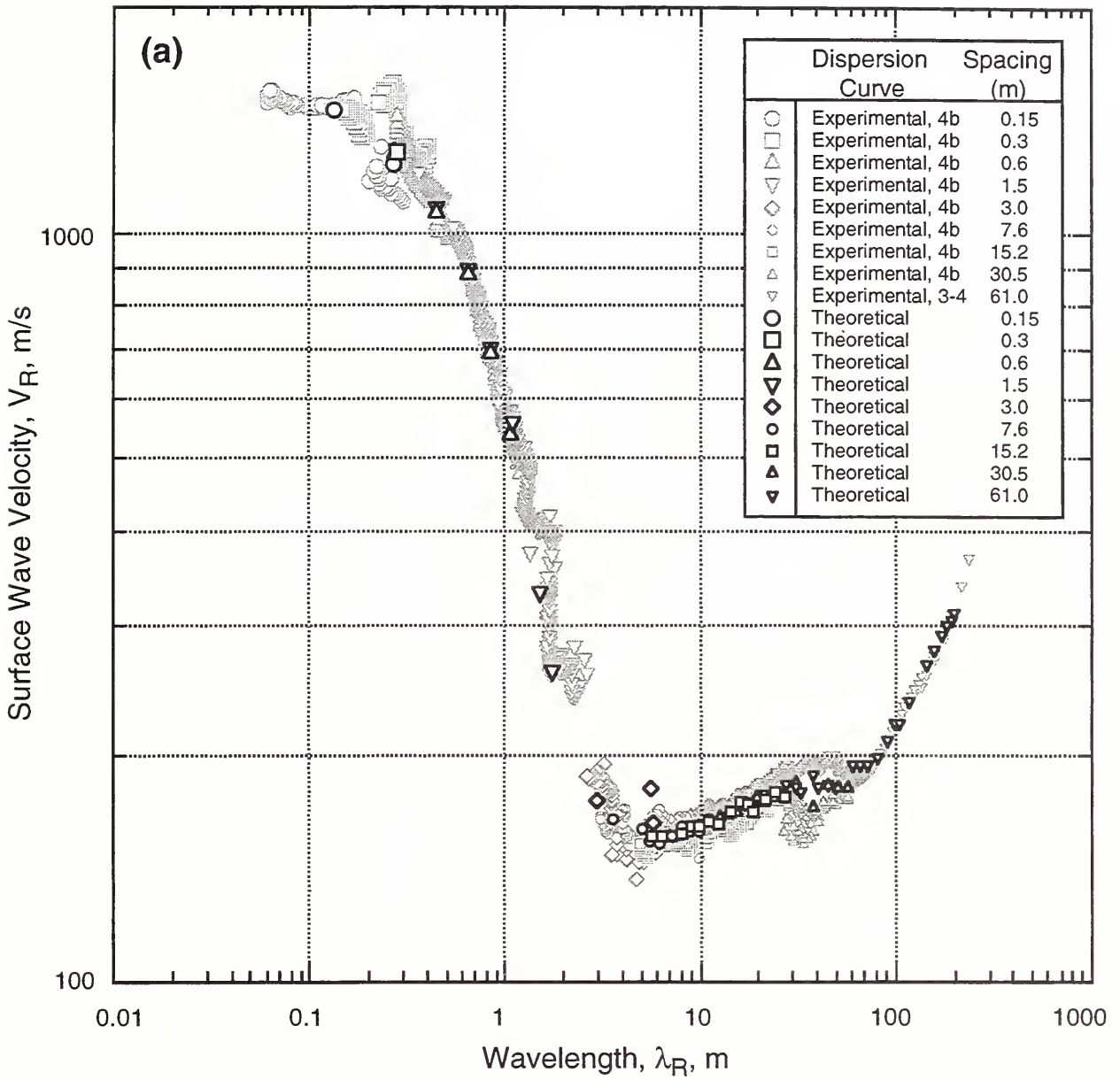

Fig. B.5 - Comparison of Experimental and Theoretical SASW Dispersion Curves for the Treasure Island Approach to Pier Site, Test Array SA-4b. (Note that Test Array SA-4b Lies Outside the Improved Area.)

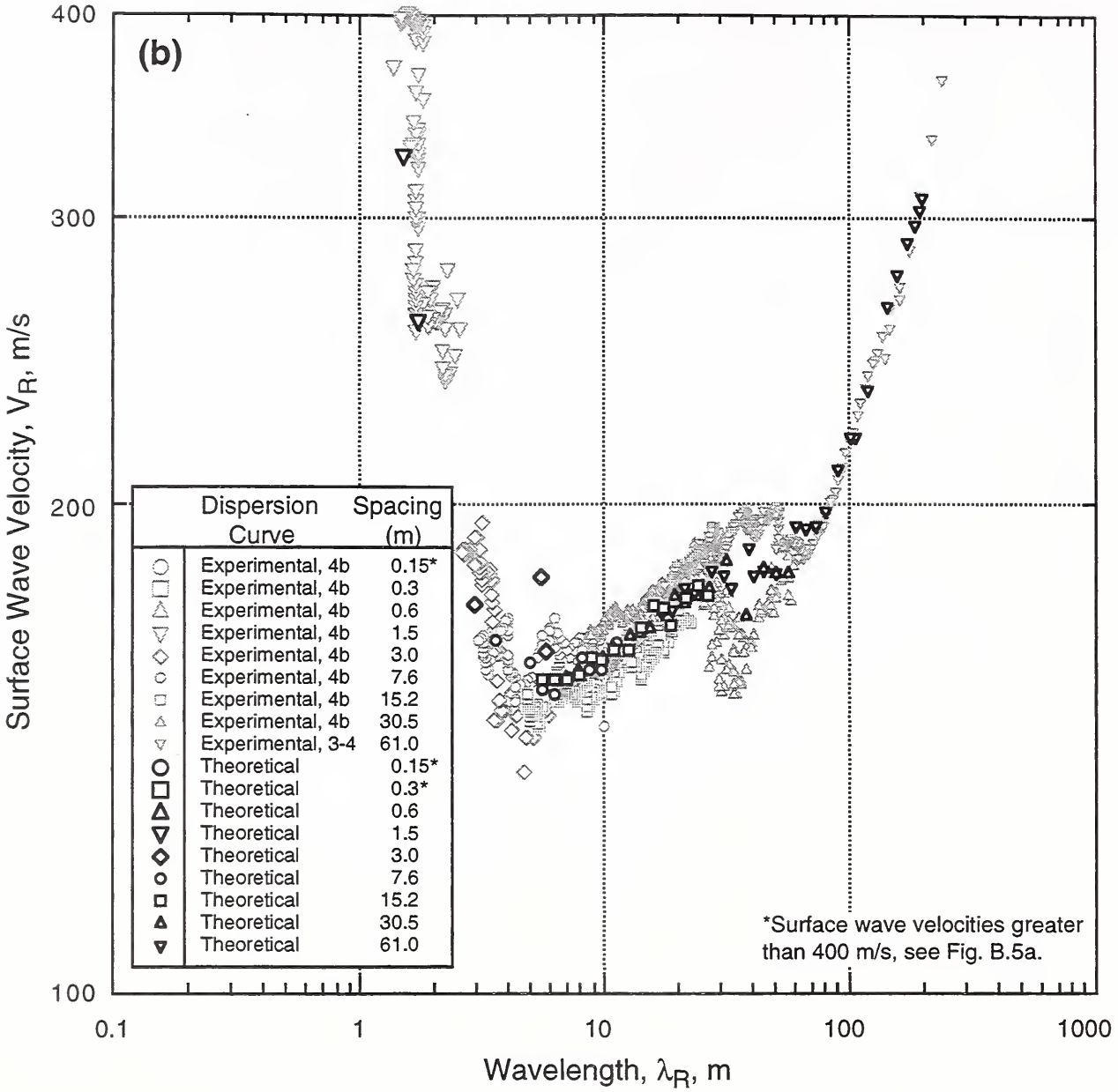

Fig. B.5 (cont.) - Comparison of Experimental and Theoretical SASW Dispersion Curves for the Treasure Island Approach to Pier Site, Test Array SA-4b. (Note that Test Array SA-4b Lies Outside the Improved Area.)

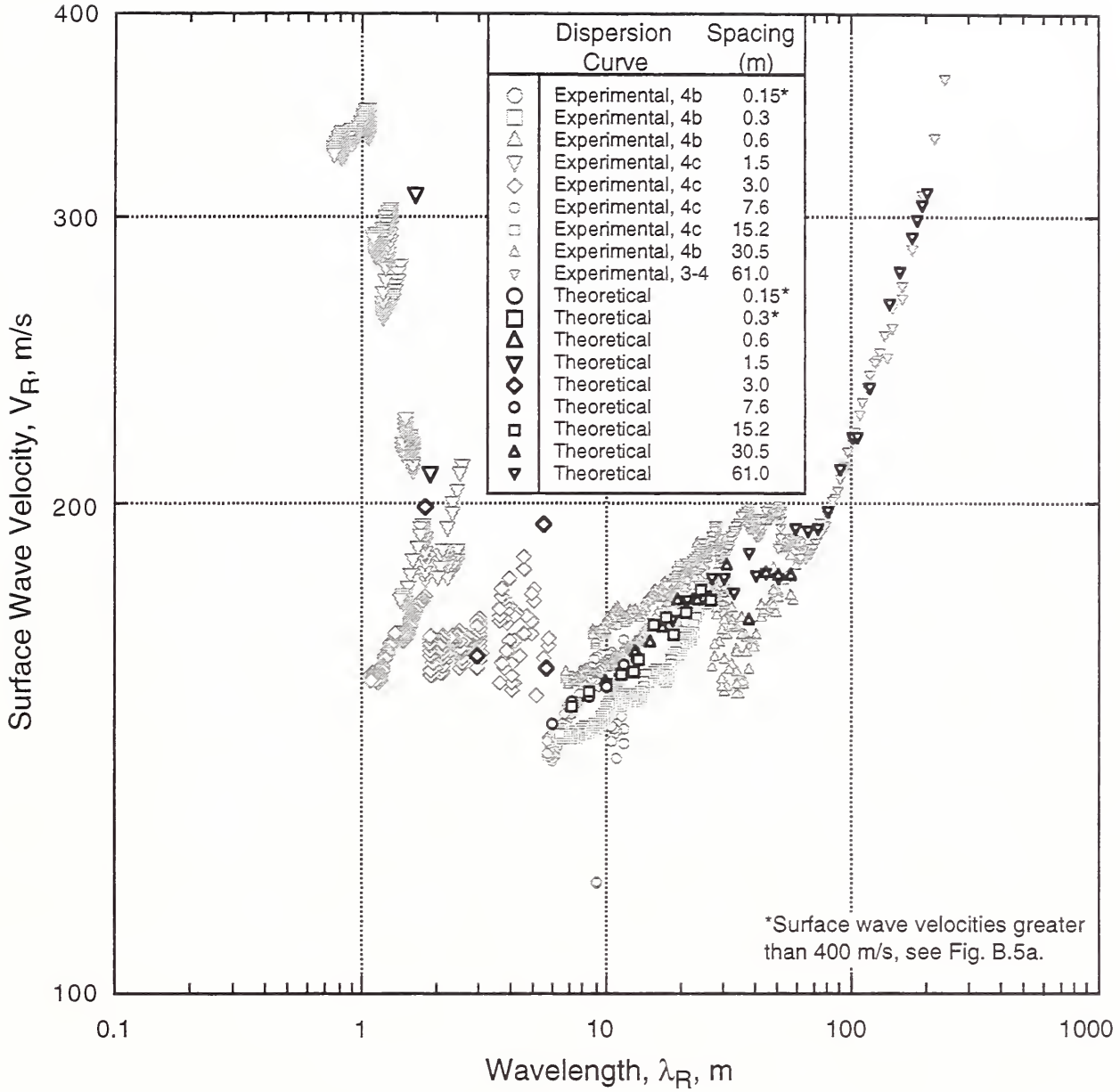

Fig. B.6 - Comparison of Experimental and Theoretical SASW Dispersion Curves for the Treasure Island Approach to Pier Site, Test Array SA-4c. (Note that Test Array SA-4c Lies Outside the Improved Area.)

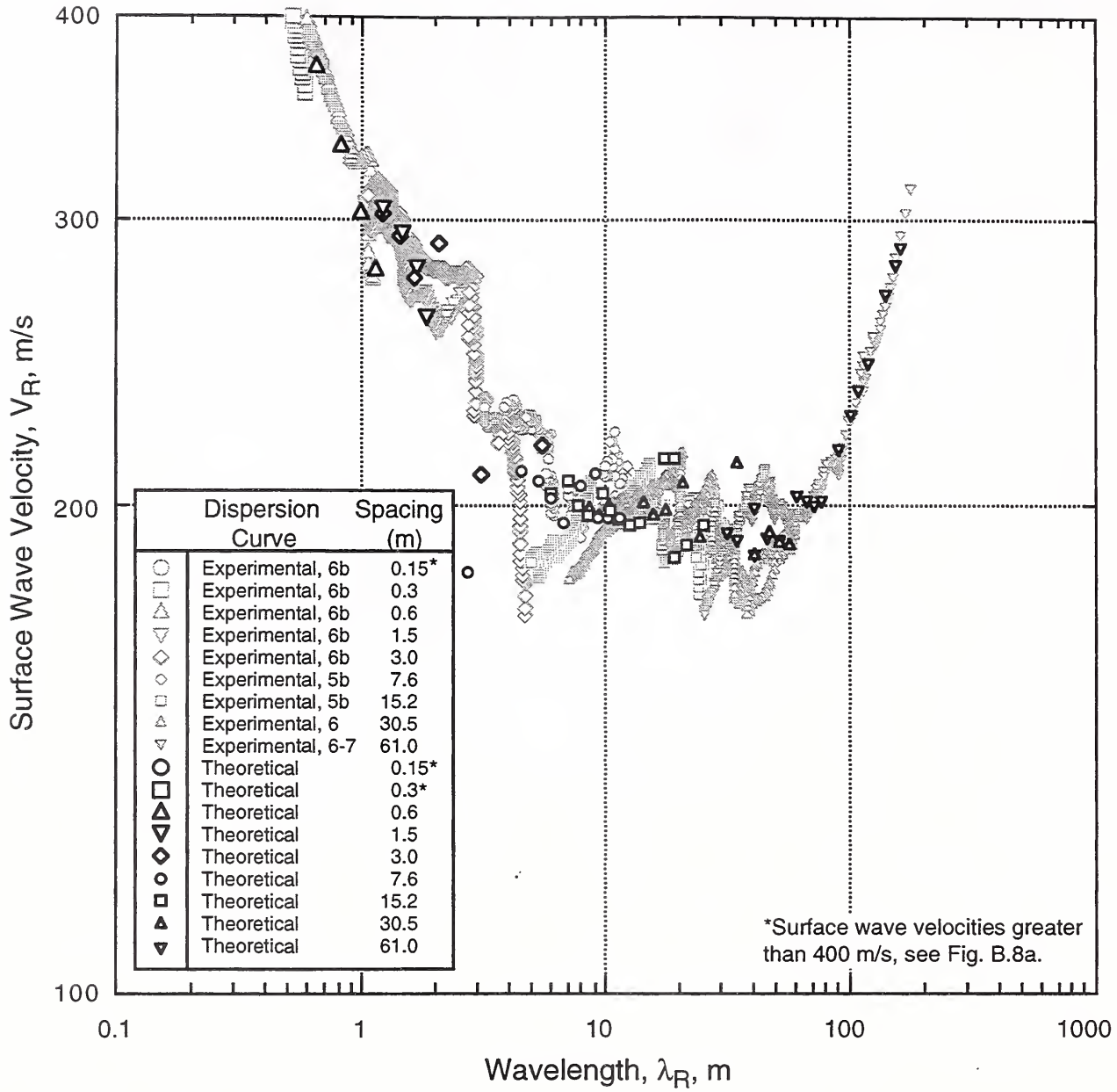

Fig. B.7 - Comparison of Experimental and Theoretical SASW Dispersion Curves for the Treasure Island Approach to Pier Site, Test Array SA-5b. (Note that Test Array SA-5b Lies Within the Improved Area.)

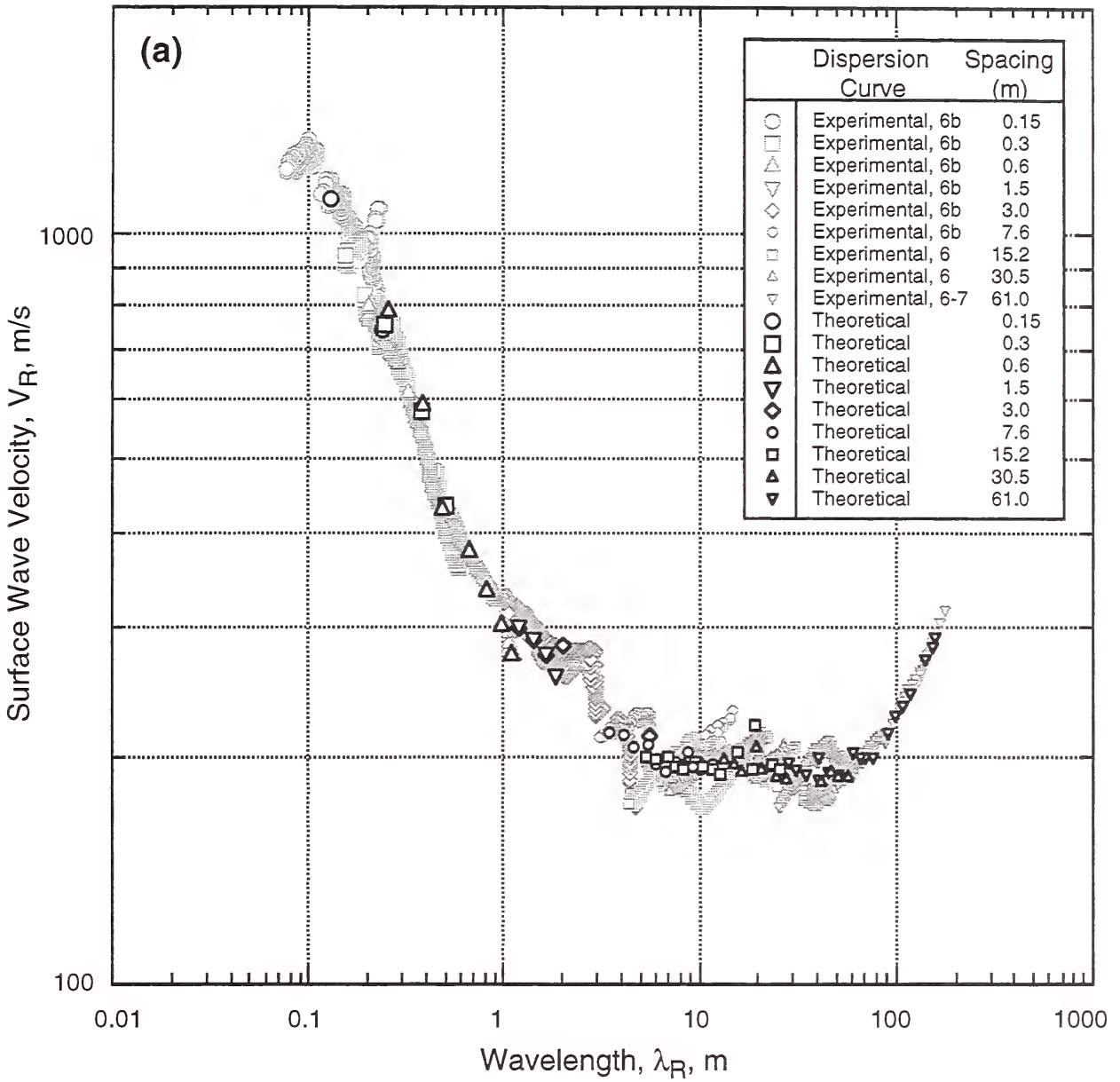

Fig. B.8 - Comparison of Experimental and Theoretical SASW Dispersion Curves for the Treasure Island Approach to Pier Site, Test Array SA-6. (Note that Test Array SA-6 Lies Within the Improved Area.)

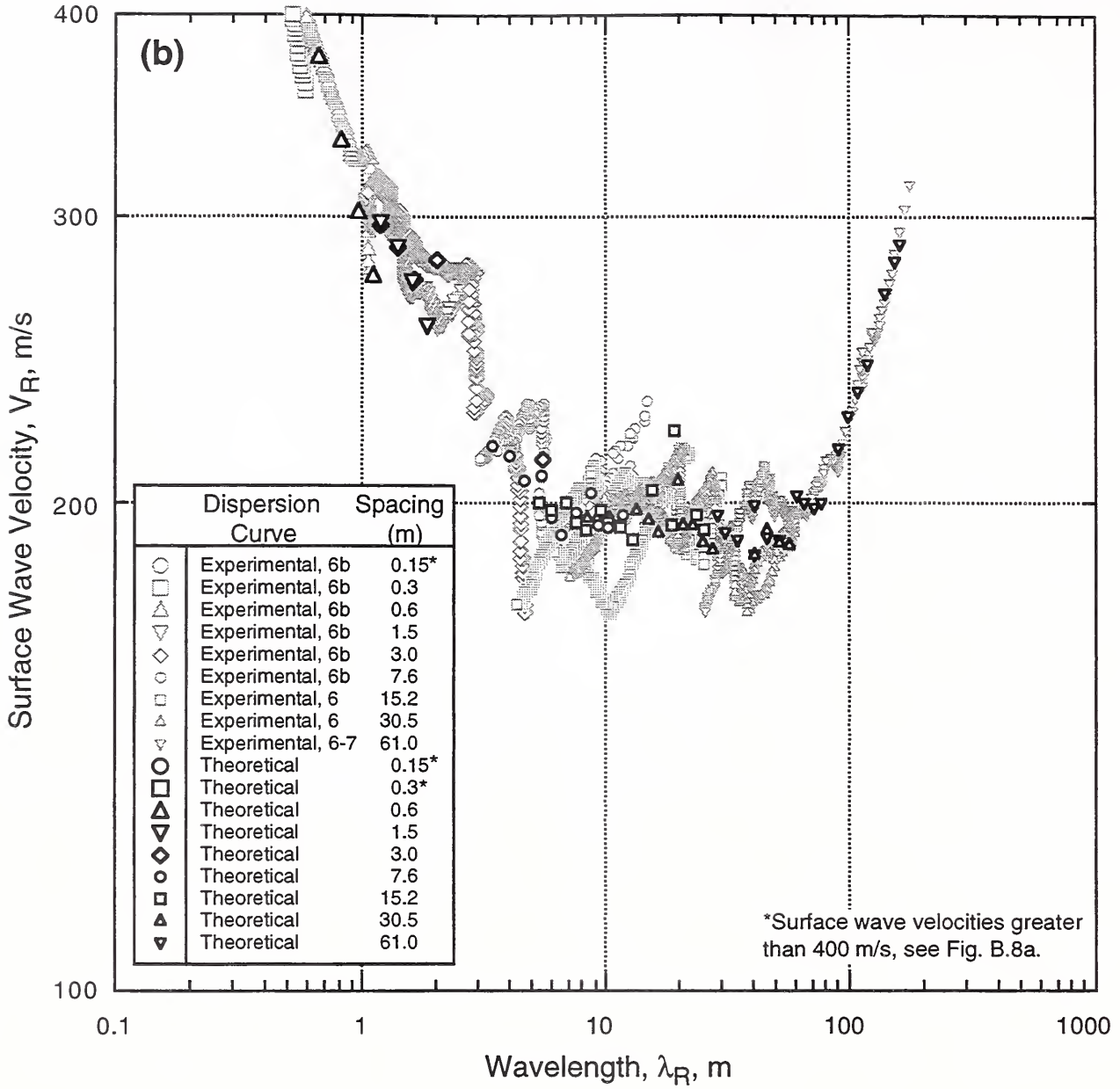

Fig. B.8 (cont.) - Comparison of Experimental and Theoretical SASW Dispersion Curves for the Treasure Island Approach to Pier Site, Test Array SA-6. (Note that Test Array SA-6 Lies Within the Improved Area.)

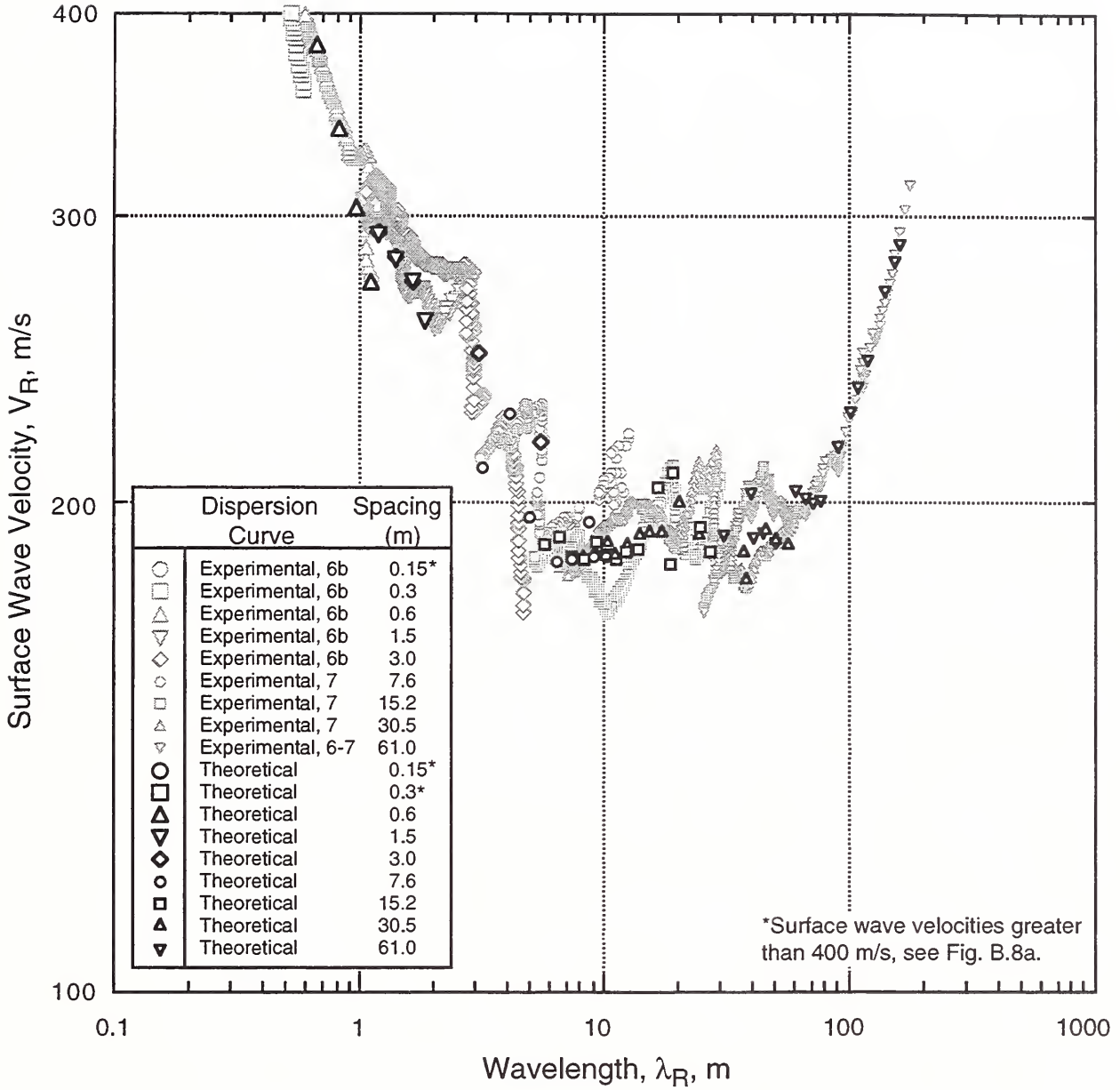

Fig. B.9 - Comparison of Experimental and Theoretical SASW Dispersion Curves for the Treasure Island Approach to Pier Site, Test Array SA-7. (Note that Test Array SA-7 Lies Within the Improved Area.)

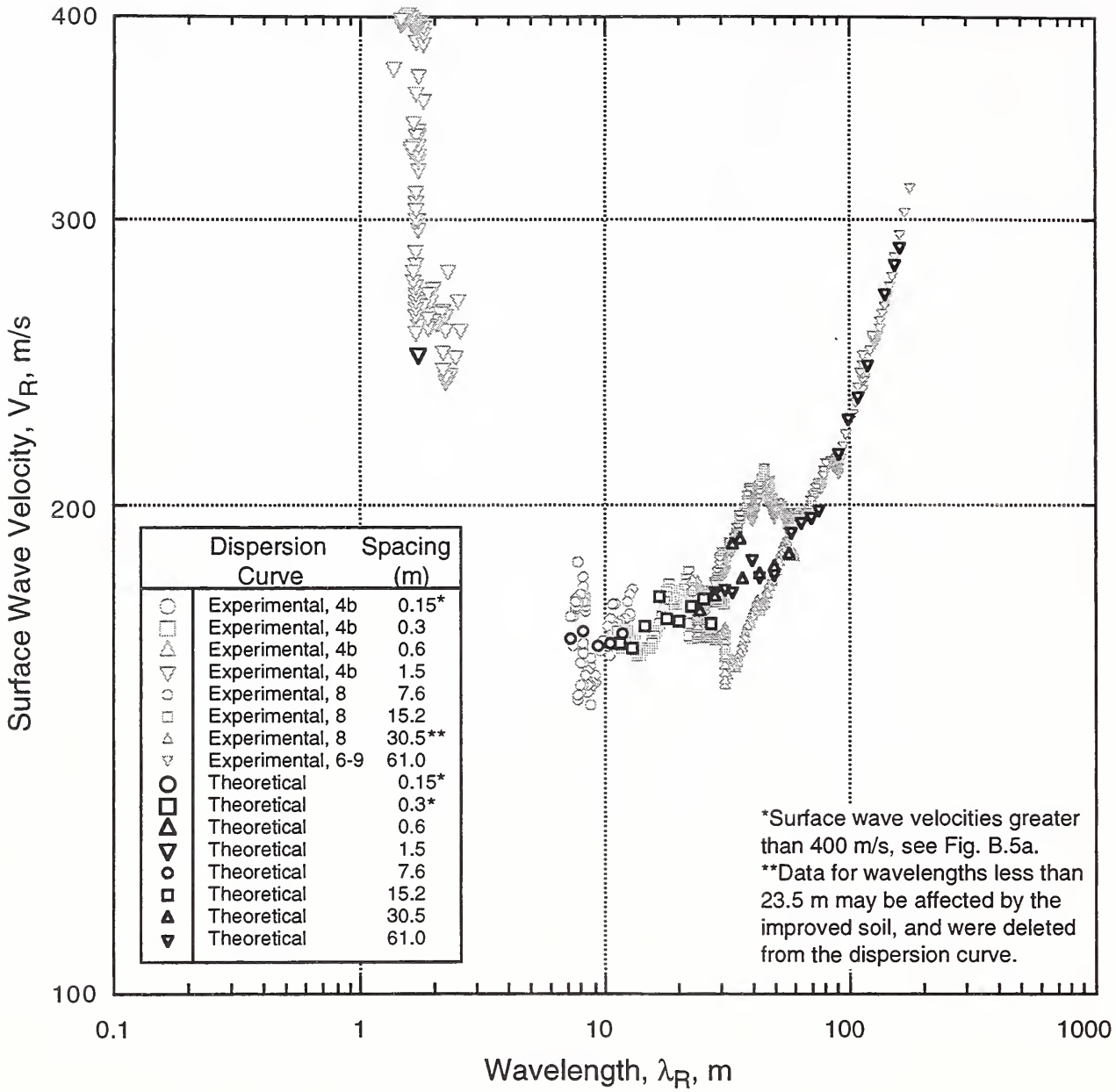

Fig. B.10 - Comparison of Experimental and Theoretical SASW Dispersion Curves for the Treasure Island Approach to Pier Site, Test Array SA-8. (Note that Test Array SA-8 Lies Outside the Improved Area.)

REFERENCES

Andrus, R. D., and Stokoe, K. H., II (1997). "Liquefaction Resistance Based on Shear Wave Velocity," NCEER Workshop on Evaluation of Liquefaction Resistance of Soils, Technical Report NCEER-97-0022, T. L. Youd and I. M. Idriss, Eds., National Center for Earthquake Engineering Research, Buffalo, N.Y., pp. 89-128.

Andrus, R. D., Stokoe, K. H., II, Bay, J. A., and Chung, R. M. (1998). "Delineation of Densified Sand at Treasure Island by SASW Testing," Geotechnical Site Characterization, P. K. Robertson and P. W. Mayne, Eds., A. A. Balkeman, Rotterdam, Netherlands, pp. 459-464.

Baker, V. A. (1985). Unpublished cone penetration test data by Virgil Baker Inc. of Oakland, California.

Brady, A. G. and Shakal, A. F. (1994). "Strong-Motion Recordings," The Loma Prieta, California, Earthquake of October 17, 1989--Strong Ground Motion, U.S. Geological Survey Professional Paper 1551-A, R. D. Borcherdt, Ed., U.S. Gov. Printing Office, Washington, D.C., pp. A9-A38.

Bennett, M. J. (1998). "Sand Boils and Settlement of Treasure Island after the Earthquake," The Loma Prieta, California Earthquake of October 17, 1989--Liquefaction, U.S. Geological Survey Professional Paper 1551-B, T. L. Holzer, Ed., U.S. Gov. Printing Office, Washington, D.C., pp. B121-B128.

Benoît, J. and de Alba, P., Eds. (1991). Proceedings of Workshop on Selection and Management of National Geotechnical Experimentation Sites, Report to the National Science Foundation and the Federal Highway Administration, University of New Hampshire.

de Alba, P., Benoît, J., Pass, D. G., Carter, J. J., Youd, T. L. and Shakal, A. F. (1994). "Deep Instrumentation Array at the Treasure Island Naval Station," The Loma Prieta, California, Earthquake of October 17, 1989--Strong Ground Motion, U.S. Geological Survey Professional Paper 1551-A, R.D. Borcherdt, Ed., U.S. Gov. Printing Office, Washington, D.C., pp. A155-A168.

de Alba, P. and Faris, J. R. (1996a). "Workshop on Future Research Deep Instrumentation Array, Treasure Island NGES, July 27, 1996: Report to the Workshop Current State of Site Characterization and Instrumentation," Univ. of New Hampshire, 45 p.

de Alba, P. and Faris, J. R. (1996b). "Workshop on Future Research Deep Instrumentation Array, Treasure Island NGES, July 27, 1996: Final Report," Univ. of New Hampshire, 17 p.

Dobry, R. (1996). Personal communication to R. D. Andrus.

Dobry, R., Ladd, R. S., Yokel, F. Y., Chung, R. M. and Powell, D. (1982). "Prediction of Pore Water Pressure Buildup and Liquefaction of Sands During Earthquakes by the Cyclic Strain Method," NBS Building Science Series 138, U.S. Department of Commerce, National Bureau of Standards, Gaithersburg, Md., 152 p.

Egan, J. A. and Wang, Z.-L. (1991). "Liquefaction-Related Ground Deformation and Effects on Facilities at Treasure Island, San Francisco, During the 17 October 1989 Loma Prieta Earthquake," Proceedings, Third Japan-U.S. Workshop on Earthquake Resistant Design of Lifeline Facilities and Countermeasures for Soil Liquefaction, Technical Report NCEER-91-0001, T. D. O'Rourke and M. Hamada, Eds., National Center for Earthquake Engineering Research, Buffalo, N.Y., pp. 57-76.

Geomatrix Consultants (1990). Evaluation of Interior Area Performance, Naval Station Treasure Island, San Francisco, California, report prepared for U.S. Navy, Naval Facilities Engineering Command, Western Division, San Bruno, Calif., Vols. 3 and 5.

Gucunski, N., and Woods, R. D. (1991), "Instrumentation for SASW Testing," Recent Advances in Instrumentation, Data Acquisition and Testing in Soil Dynamics, Geotechnical Special Publication No. 29, ASCE, New York, N.Y., pp. 1-16.

Harding Lawson Associates (1996). "Geotechnical Engineering Services National Geotechnical Experimentation Site Soil Boring and Sampling Phase II, NS Treasure Island, California," report prepared for U.S. Navy, Naval Facilities Engineering Command, Western Division, San Bruno, Calif., December.

Heisey, J. S. (1981). "Determination of In Situ Shear Wave Velocity from Spectral Analysis of Surface Waves," M.S. Thesis, Univ. of Texas at Austin.

Hiltunen, D. R., and Woods, R. D. (1990). "Influence of Source and Receiver Geometry on the Testing of Pavements by the Surface Waves Method," a paper prepared for presentation at the 69th Annual Meeting of the Transportation Research Board, Washington, D.C., January.

Hryciw, R. D., Rollins, K. M., Homolka, M., Shewbridge, S. E. and McHood, M. (1991). "Soil Amplification at Treasure Island During the Loma Prieta Earthquake," Proceedings, 2nd International Conf. on Recent Advances in Geotechnical Earthquake Eng. and Soil Dynamics, S. Prakash, Ed., Univ. of Missouri-Rolla, Vol. 2, pp. 1679-1685.

Hryciw, R. D., Shewbridge, S. E., Kropp, A., and Homolka, M. (1998). "Postearthquake Investigation at Liquefaction Sites in Santa Cruz and on Treasure Island," The Loma Prieta, California Earthquake of October 17, 1989--Liquefaction, U.S. Geological Survey Professional Paper 1551-B, T. L. Holzer, Ed., U.S. Gov. Printing Office, Washington, D.C., pp. B165-B180.

Joh S.-H. (1996). "Advances in Interpretation and Analysis Techniques for Spectral-Analysis-of-Surface-Wave (SASW) Measurements," Ph.D. Dissertation, Univ. of Texas at Austin.

Kayen, R. E., Mitchell, J. K., Seed, R. B., Lodge, A., Nishio, S., and Coutinho, R. (1992). "Evaluation of SPT-, CPT-, and Shear Wave-Based Methods for Liquefaction Potential Assessment Using Loma Prieta Data," Proceedings, Fourth Japan-U.S. Workshop on Earthquake Resistant Design of Lifeline Facilities and Countermeasures for Soil Liquefaction, Technical Report NCEER-92-0019, M. Hamada and T. D. O'Rourke, Eds., National Center for Earthquake Engineering Research, Buffalo, NY, Vol. 1, pp. 177-204.

Liao, S. S. C., and Whitman, R. V. (1986). "Overburden Correction Factors for SPT in Sand," Journal of Geotechnical Engineering, ASCE, New York, N.Y., Vol. 112, No. 3, pp. 373-377.

Lodge, A. L. (1994). "Shear Wave Velocity Measurements for Subsurface Characterization," Ph.D. Dissertation, Univ. of California at Berkeley.

Mitchell, J. K. and Wentz, F. J., Jr. (1991). "Performance of Improved Ground During the Loma Prieta Earthquake," Report No. UCB/EERC-91/12, Earthquake Engineering Research Center, Univ. of California at Berkeley, 93 p.

Mitchell, J. K. and Wentz, F. J., Jr. (1998). "Improved-Ground Performance During the Earthquake," The Loma Prieta, California Earthquake of October 17, 1989--Liquefaction, U.S. Geological Survey Professional Paper 1551-B, T. L. Holzer, Ed., U.S. Gov. Printing Office, Washington, D.C., pp. B241-B272.

Nazarian, S., Stokoe, K. H., II, and Hudson, W. R. (1983), "Use of Spectral Analysis of Surface Waves Method for Determination of Moduli and Thickness of Pavement Systems," Transportation Research Record, No. 930, Washington, D.C., pp. 38-45.

Nazarian, S., Yuan, D., and Baker, M. R. (1994). "Automation of Spectral Analysis of Surface Waves Method," Dynamic Geotechnical Testing II, STP 1213, R. J. Ebelhar, V. P. Drnevich, B. L. Kutter, Eds., ASTM, Philadelphia, Pa., pp. 88-100.

Nazarian, S., Yuan, D., and Baker, M. R. (1995), "Rapid Determination of Pavement Moduli with Spectral-Analysis-of-Surface-Waves Method," Research Report 1243-1, Center for Geotechnical and Highway Materials Research, Univ. of Texas at El Paso, 76 p.

Olsen, R. S. (1997). "Cyclic Liquefaction Based on the Cone Penetrometer Test," NCEER Workshop on Evaluation of Liquefaction Resistance of Soils, Technical Report NCEER-97-0022, T. L. Youd and I. M. Idriss, Eds., National Center for Earthquake Engineering Research, Buffalo, N.Y., pp. 225-276.

Power, M. S., Egan, J. A., Shewbridge, S. E., deBecker, J., and Faris, J. R. (1998). "Analysis of Liquefaction-Induced Damage on Treasure Island," The Loma Prieta, California Earthquake of October 17, 1989--Liquefaction, U.S. Geological Survey Professional Paper 1551-B, T. L. Holzer, ed., U.S. Gov. Printing Office, Washington, D.C., pp. B87-B119.

Richart, F. E., Jr., Hall, J. R., Jr., and Woods, R. D. (1970). Vibrations of Soils and Foundations, Prentice-Hall, Inc., Englewood Cliffs, N.J., 414 p.

Rix, G. J., and Leipski, E. A. (1991). "Accuracy and Resolution of Surface Wave Inversion," Recent Advances in Instrumentation, Data Acquisition and Testing in Soil Dynamics, Geotechnical Special Publication No. 29, ASCE, New York, N.Y., pp. 17-32.

Rix, G. J. Rix and Stokoe, K. H., II (1989). "Stiffness Profiling of Pavement Subgrades," Transportation Research Board Annual Meeting, Washington, D.C.

Robertson, P. K., Woeller, D. J., and Finn, W. D. L. (1992). "Seismic Cone Penetration Test for Evaluating Liquefaction Potential Under Cyclic Loading," Canadian Geotechnical Journal, Ottawa, Canada, Vol. 29, pp. 686-695.

Robertson, P. K., and Wride, C. E. (1997). "Cyclic Liquefaction and its Evaluation Based on the SPT and CPT," NCEER Workshop on Evaluation of Liquefaction Resistance of Soils, Technical Report NCEER-97-0022, T. L. Youd and I. M. Idriss, Eds., National Center for Earthquake Engineering Research, Buffalo, N.Y.

Roësset, J. M., Chang, D. W., and Stokoe, K. H., II (1991), "Comparison of 2-D and 3-D Models for Analysis of Surface Wave Tests," Proceedings, Fifth International Conference on Soil Dynamics and Earthquake Engineering, Karlsruhe, Germany, pp. 111-126.

Seed, H. B., and Idriss, I. M. (1971). "Simplified Procedure for Evaluating Soil Liquefaction Potential," Journal of the Soil Mechanics and Foundation Division, ASCE, New York, NY, Vol. 97, SM9, pp. 1249-1273.

Seed, H. B., and Idriss, I. M. (1982). Ground Motions and Soil Liquefaction During Earthquakes, monograph series, Earthquake Engineering Research Institute, Berkeley, California, 134 p.

Seed, H. B., Idriss, I. M., and Arango, I. (1983). "Evaluation of Liquefaction Potential Using Field Performance Data," Journal of Geotechnical Engineering Division, ASCE, New York, NY, Vol. 109, No. 3, pp. 458-482.

Seed, H. B., Tokimatsu, K., Harder, L. F., and Chung, R. M. (1985). "Influence of SPT Procedures in Soil Liquefaction Resistance Evaluations," Journal of Geotechnical Engineering Division, ASCE, Vol. 111, No. 12, pp. 1425-1445.

Stokoe, K. H., II, and Nazarian, S. (1985). "Use of Rayleigh Waves in Liquefaction Studies," Proceedings, Measurement and Use of Shear Wave Velocity for Evaluating Dynamic Soil Properties, held in Denver, Colorado, R. D. Woods, Ed., ASCE, New York, NY, pp. 1-17.

Stokoe, K. H., II, Nazarian, S., Rix, G. J., Sanchez-Salinero, I., Sheu, J. C., and Mok, Y. J. (1988a), "In Situ Testing of Hard-to-Sample Soils by Surface Wave Method," Earthquake Engineering and Soil Dynamics II, Geotechnical Special Publication No. 20, J. L. Von Thun, Ed., ASCE, pp. 264-278.

Stokoe, K. H., II, Roësset, J. M., Bierschwale, J. G. and Aouad, M. (1988b). "Liquefaction Potential of Sands from Shear Wave Velocity," Proceeding, 9th World Conference on Earthquake Engineering, Vol. III, Tokyo, Japan, Nissei Kogyo Co., Ltd., pp. 213-218.

Stokoe, K. H., II, and Rix, G. J. (1987). "Evaluation of Compaction Treatment of Foundation Soils at Jackson Lake Dam, Wyoming, by Surface Wave (SASW) method," Geotechnical Engineering Center Report GR87-8, Univ. of Texas at Austin, 51 p.

Stokoe, K. H., II, Wright, S. G., Bay, J. A. and Roësset, J. M. (1994). "Characterization of Geotechnical Sites by SASW Method," Geophysical Characterization of Sites, R. D. Woods, Ed., A. A. Balkeman, Rotterdam, The Netherlands, pp. 15-25.

Tokimatsu, K., Kuwayama, S., and Tamura, S. (1991). "Liquefaction Potential Evaluation Based on Rayleigh Wave Investigation and Its Comparison with Field Behavior," Proceedings, Second International Conference on Recent Advances in Geotechnical Earthquake Engineering and Soil Dynamics, S. Prakash, Ed., Univ. of Missouri-Rolla, Vol. I, pp. 357-364.

Youd, T. L. and Noble, S. K. (1997). "Liquefaction Criteria Based on Statistical and Probabilistic Analyses," NCEER Workshop on Evaluation of Liquefaction Resistance of Soils, Technical Report NCEER-97-0022, T. L. Youd and I. M. Idriss, Eds., National Center for Earthquake Engineering Research, Buffalo, N.Y, pp. 201-215.

Youd, T. L., Idriss, I. M., Andrus, R. D., Arango, I., Castro, G., Christian, J. T., Dobry, R., Finn, W. D. L., Harder, L. F., Jr., Hynes, M. E., Ishihara, K., Koester, J. P., Liao, S. S. C., Marcuson, W. F., III, Martin, G. R., Mitchell, J. K., Moriwaki, Y., Power, M. S., Robertson, P. K., Seed, R. B., Stokoe, K. H., II (1997). "Summary Report," NCEER Workshop on Evaluation of Liquefaction Resistance of Soils, Technical Report NCEER-97-0022, National Center for Earthquake Engineering Research, Buffalo, N.Y., pp. 1-40.